

Expanding the Anti-cancer Toolbox with Glycan- and Thiol-binding Nanobodies

Inaugural-Dissertation

to obtain the academic degree

Doctor rerum naturalium (Dr. rer. nat.)

submitted to the Department of Biology, Chemistry, Pharmacy
of Freie Universität Berlin

by

Felix Tobias Reinhard Goerdeler

2022

The presented work was performed between January 2019 and August 2022 under the guidance of Dr. Oren Moscovitz and Prof. Dr. Peter H. Seeberger in the Department of Biomolecular Systems, Max Planck Institute of Colloids and Interfaces, and the Institute of Chemistry and Biochemistry, Freie Universität Berlin.

1st reviewer: Prof. Dr. Peter H. Seeberger

2nd reviewer: Prof. Dr. Helge Ewers

Date of defense: 30.11.2022

Acknowledgements

I would like to express my deepest gratitude to the following people who have supported me during the last three-and-a-half years and without whom this work would not have been possible:

First and foremost, I would like to thank my supervisors Dr. Oren Moscovitz and Prof. Dr. Peter H. Seeberger for giving me the opportunity to work on this project and for their invaluable and continuing support.

Oren, your perpetual flow of new ideas and many inspirational (sometimes heated) discussions with you shaped not only this work but also my way of scientific thinking. Thank you for always keeping an open ear for my ideas and concerns and for always staying excited about the project, even during months of disappointing results.

Prof. Seeberger, thank you for teaching me not to lose sight of the bigger picture and for reminding me to always think of the next step. Your experienced opinion and career guidance have been extremely valuable.

Prof. Dr. Helge Ewers for kindly agreeing to review this thesis and for sharing his expertise and useful materials for nanobody-sortase reactions.

Prof. Dr. Susanne Hartmann and Dr. Toni Aebischer for providing their unique perspectives as part of my thesis advisory committee, and for helping me to question my results in frequent and fruitful discussions.

Sana Khan Khilji for proofreading this thesis as well as for her relentless efforts to complete the glycan-binding nanobodies project with me.

Emelie Reuber and Jost Lühle for their invaluable help during their time as student assistants and beyond as well as for going through the ups and downs of the CB2 project together with me.

Sabrina Leichnitz for synthesizing all rhamnose compounds needed for this study, for staying hopeful after not-so-promising initial results and for always finding fast and elegant synthetic solutions to my experimental requirements.

Dr. Maria Bräutigam for patiently answering all my chemistry questions and for providing invaluable help with chemical conjugations and mass spectrometry.

Dr. Christian Roth for useful discussions of biochemistry results and for his tireless efforts to keep the lab well-resourced, all machines well-maintained and everybody safe.

Dr. Eric Sletten for helping me with glycopeptide purifications.

Prof. Dr. Heiko Möller, Dr. Ruslan Nedieltkov, and Anika Freitag for NMR data of CB2.

Katrin Sellrie, Dorothee Böhme, and Eva Settels for organizational and technical support.

Dr. Uta Höpken and Dr. Armin Rehm for sharing their NHL cell lines with me.

Sharareh Salehi Hossainy and Dr. Toni Aebischer for providing *L. major* slides.

Anita Selig-Smith and Sultan, the alpaca, for enabling the immunization study.

All colleagues and friends of the Glycan-targeted Therapeutics group: Anika Freitag, Jost Lühle, Magdalena Zastona, and Sana Khan Khilji.

Former and current colleagues and friends from the “mainland and crystal island”: Dr. Bruna Mara Silva Seco, Dr. Chandradhish Ghosh, Dr. Christian Roth, Emelie Reuber, Fabienne Weber, Dr. Jonnel Anthony Jaurigue, Dr. Ling Yao, Michael Krummhaar, Patricia Priegue Piñeiro, Dr. Paulina Kaplonek, and Ruben Ananian.

Thank you all for making the lab a joyful workplace. I will miss lunch, coffee, and ice cream breaks with you!

The German Research Foundation (DFG, RTG2046 “parasite infections”), the Center of Infection Biology and Immunity (ZIBI), and the Dahlem Research School (DRS, Biomedical Sciences) for funding, a fantastic network, and useful workshops.

Finally, I would like to express my deepest gratitude to the people outside the lab who accompanied me during the last three-and-a-half years and before. My family for their unlimited support and affection – you made me the person I am now, and I would have never gotten this far without you. My friends for enriching my life with their empathy, laughs, thoughts, and countless wonderful non-work-related memories. My boyfriend for his unconditional love, for being my calm anchor and most ardent supporter.

Declaration of Independence

Herewith I certify that I have prepared and written my thesis independently and that I have not used any sources and aids other than those indicated by me.

Date, Place

Signature

Contents

List of Abbreviations.....	13
List of Tables	19
List of Figures.....	19
Summary.....	23
Zusammenfassung.....	25
1. Introduction.....	27
1.1. Cancer.....	27
1.1.1. Prevalence	27
1.1.2. Non-Hodgkin lymphoma	27
1.1.3. Therapeutic strategies.....	28
1.2. Tumor biomarkers	29
1.2.1. Tumor-associated carbohydrate antigens.....	29
1.2.2. Development of TACA-specific antibodies.....	32
1.2.3. Extracellular tumor redox microenvironment.....	34
1.2.4. Thiol-binding molecules	35
1.3. Nanobodies.....	36
1.3.1. Camelid heavy-chain antibodies.....	36
1.3.2. Nanobody structure and properties	37
1.3.3. Strategies for nanobody development	38
1.4. Nanobody functionalization.....	39
1.4.1. Multivalency and multispecificity	40
1.4.2. Fluorescence.....	41
1.4.3. Antibody recruitment.....	41
1.4.4. Internalization and drug delivery	42

1.4.5.	Strategies for nanobody functionalization	43
1.5.	Aims of this study	45
2.	Materials and Methods.....	47
2.1.	Induction of hcAbs in alpaca.....	47
2.1.1.	Conjugation of glycans to CRM ₁₉₇	47
2.1.2.	Alpaca immunization.....	49
2.1.3.	IgG subtype fractionation.....	50
2.1.4.	Sodium dodecyl sulfate-polyacrylamide gel electrophoresis	51
2.1.5.	Western blot.....	52
2.1.6.	Glycan array	52
2.2.	Cell culture	53
2.2.1.	Lymphoma cell lines.....	53
2.2.2.	PBMC isolation	53
2.2.3.	<i>Plasmodium falciparum</i>	54
2.2.4.	Breast cell lines	54
2.3.	Surface thiol quantification.....	54
2.4.	CB2 characterization	55
2.4.1.	Nanobody expression and purification.....	55
2.4.2.	Site-directed mutagenesis.....	56
2.4.3.	Nuclear magnetic resonance measurements of CB2 and C ^{105S} CB2.....	57
2.4.4.	Flow cytometry binding assay	57
2.4.5.	Confocal microscopy binding assay	59
2.4.6.	Inhibition assay with dithiothreitol	59
2.4.7.	Inhibition assay with N-ethylmaleimide	60
2.5.	CB2 functionalization	60
2.5.1.	Synthesis of Rha ₃	60
2.5.2.	Synthesis of GG-Rha ₃	61
2.5.3.	Conjugation of GG-Rha ₃ and CB2.....	62

2.5.4.	Conjugation of Rha ₃ and thFF03.....	62
2.5.5.	Conjugation of CB2 and Rha-thFF03.....	63
2.5.6.	Ab purification from human serum.....	63
2.5.7.	Complement activation assay.....	64
2.5.8.	Cy3 conjugation.....	64
2.5.9.	Internalization assay.....	66
2.5.10.	MMAE conjugation.....	67
2.5.11.	Drug delivery assay.....	67
3.	Results and Discussion.....	69
3.1.	Inducing TACA-binding hcAbs in alpaca.....	69
3.1.1.	Generation of glycoconjugates for alpaca immunization.....	69
3.1.2.	Glycoconjugates induce anti-TACA Abs in alpaca.....	70
3.1.3.	Anti-TACA Abs show varying degrees of cross-reactivity.....	72
3.1.4.	Anti-TACA Abs are induced across all IgG subtypes.....	74
3.2.	Elucidating the thiol-dependent nature of CB2 binding.....	75
3.2.1.	CB2 specifically recognizes several subtypes of B cell lymphoma.....	75
3.2.2.	B cell lymphoma cells display higher levels of reduced, accessible thiol groups on the surface than healthy lymphocytes.....	76
3.2.3.	CB2 binding is based on thiol-thiol interactions.....	78
3.2.4.	Cysteine 105 is indispensable for CB2 binding.....	79
3.3.	Functionalizing CB2 for complement activation.....	81
3.3.1.	Human serum shows higher Ab titers against Rha ₃ than Rha.....	81
3.3.2.	Pure CB2-Rha ₃ conjugates can be generated by srtA-mediated conjugation and fully retain binding activity.....	82
3.3.3.	CB2-Rha ₃ fails to activate complement against B cell lymphoma.....	83
3.3.4.	CB2-Rha-thFF03 can be generated in a two-step reaction and fully retains binding activity.....	85

3.3.5.	Multivalent Rha ₃ display of CB2-Rha-thFF03 facilitates Ab recruitment and complement activation against cancer cells.....	88
3.4.	Examining and exploiting CB2 internalization for drug delivery.....	90
3.4.1.	CB2-Cy3 and ^{C105S} CB2-Cy3 can be generated in a two-step reaction and directly detected on cells.....	90
3.4.2.	CB2-Cy3 is endocytosed by B cell lymphoma	92
3.4.3.	CB2-MMAE and ^{C105S} CB2-MMAE can be generated by srtA-mediated conjugation and fully retain binding activity.....	94
3.4.4.	CB2-MMAE shows higher cytotoxicity against B cell lymphoma than ^{C105S} CB2-MMAE	96
3.5.	Exploring additional CB2 targets	99
3.5.1.	CB2 specifically recognizes breast cancer cells.....	99
3.5.2.	CB2 binds to the parasites <i>P. falciparum</i> and <i>L. major</i>	100
4.	Conclusions and Outlook.....	102
5.	References.....	105
6.	Scientific Publications.....	121
7.	Scientific Conferences and Prizes	122
8.	Appendix	123
8.1.	Spectroscopic characterization of rhamnose compounds.....	123
8.2.	Biochemical characterization of CB2 and ^{C105S} CB2	125
8.4.	Control experiments for CB2 conjugation to Rha ₃ and Rha-thFF03	127
8.5.	Purification of human Abs	128
8.6.	Control experiment for endocytosis inhibition	128

List of Abbreviations

α Gal	Gal(α 1-3)Gal(β 1-4)GalNAc
7-AAD	7-aminoactinomycin D
A ₂₁₄	Absorbance at 214 nm
A ₂₈₀	Absorbance at 280 nm
A ₄₆₀	Absorbance at 460 nm
Ab	Antibody
ADC	Ab-drug conjugate
ADCC	Ab-dependent cellular cytotoxicity
APC-A	Amplitude of the allophycocyanin fluorescence
ARM	Ab-recruiting molecule
BCR	B cell receptor
BSA	Bovine serum albumin
C ^{105S} CB2	CB2 with a cysteine-to-serine mutation at position 105
CAR	Chimeric antigen receptor
CB2	Cancer-binding Nb 2
CD	Cluster of differentiation
CDC	Complement-dependent cytotoxicity
cDNA	Complementary DNA
CDR	Complementarity-determining region
CH1/2/3	Constant domain 1/2/3 of the heavy chain of Abs
CL	Constant domain of the light chain of conventional Abs
CRM ₁₉₇	Cross-reactive material 197, G52E mutant of diphtheria toxin
CS	Chondroitin sulfate
Cy3	Cyanine 3 dye
DAPI	4',6-Diamidino-2-phenylindole
DBCO	Dibenzocyclooctyne
DMEM	Dulbecco's modified Eagle's medium

DMSO	Dimethyl sulfoxide
DNA	Deoxyribonucleic acid
DNP	<i>p</i> -Dinitrophenol
DoHH-2	Follicular lymphoma cell line
DOL	Degree of loading
DSS	Sodium trimethylsilylpropanesulfonate
DTT	Dithiothreitol
<i>E. coli</i>	<i>Escherichia coli</i>
EDTA	Ethylenediaminetetraacetic acid
EGFRvIII	Epidermal growth factor receptor variant III
Eq.	Equivalent(s)
F12	Ham's F12 medium
FACS	Fluorescent-activated cell sorting
Fc	Fragment crystallizable
FCS	Fetal calf serum
FITC	Fluorescein isothiocyanate
FR	Framework region
FSC-A	Forward scatter amplitude
Fuc	Fucose
Gal	Galactose
GalNAc	N-Acetylgalactosamine
GG-Rha ₃	Glycyl-N-[1-[(Rha(α1-2)Rha(α1-2)Rha)oxy]pentyl]glycinamide
Glc	Glucose
GlcA	Glucuronic acid
GlcNAc	N-Acetylglucosamine
hcAb	Heavy-chain Ab
HEPES	4-(2-Hydroxyethyl)-1-piperazineethanesulfonic acid
HER2	Human epidermal growth receptor 2
HPLC	High-performance liquid chromatography

HRP	Horse radish peroxidase
HS	Heparan sulfate
HSQC	Heteronuclear single quantum coherence
IC50	Half maximal inhibitory concentration
IdoA	Iduronic acid
IgG	Immunoglobulin G
IgM	Immunoglobulin M
IPTG	Isopropyl β -D-thiogalactopyranoside
JeKo-1	Mantle cell lymphoma cell line
KH-1	Dimer of Le ^X -Le ^Y
<i>L. major</i>	<i>Leishmania major</i>
LB	Lysogeny broth
Le ^{X/Y/a/b}	Lewis X/Y/a/b antigen
m/z	Mass/charge
mAb	Monoclonal Ab
MALDI-TOF	Matrix-assisted laser desorption/ionization with time of flight
Man	Mannose
MCF-10A	Non-tumorigenic, epithelial breast cell line
MCF-7	Non-metastatic, epithelial breast cancer cell line
MDA-MB-231	Metastatic, epithelial breast cancer cell line
MFI	Mean fluorescence intensity
MHCII	Major histocompatibility complex II
MMAE	Monomethyl auristatin E
MWCO	Molecular weight cut-off
Nb	Nanobody (i.e. recombinantly expressed VHH domain)
NDC	Nb-drug conjugate
NEM	N-Ethylmaleimide
Neu5Ac	N-Acetylneuraminic acid (sialic acid type synthesized by humans)
NHL	Non-Hodgkin lymphoma

NMR	Nuclear magnetic resonance
o/n	Overnight
OD ₆₀₀	Optical density at 600 nm
<i>P. falciparum</i>	<i>Plasmodium falciparum</i>
PBMCs	Peripheral blood mononuclear cells
PBS	Phosphate buffered saline
PBS-T	PBS + 0.1 % Tween-20
PCR	Polymerase chain reaction
PDI	Protein disulfide isomerase
PVDF	Polyvinylidene fluoride
Raji	Burkitt's lymphoma cell line
RBC	Red blood cell
Rha	L-Rhamnose
Rha ₃	Rha(α1-2)Rha(α1-2)Rha-aminopentanol
Rha-thFF03	thFF03 functionalized with Rha ₃
RNA	Ribonucleic acid
RPMI	Roswell Park Memorial Institute medium
RT	Room temperature
SC-1	Follicular lymphoma cell line
SDS-PAGE	Sodium dodecyl sulfate-polyacrylamide gel electrophoresis
SEC	Size exclusion chromatography
SEM	Standard error of the mean
SrtA	Sortase A
SSC-A	Sideward scatter amplitude
SSEA	Stage-specific embryonic antigen
STF	Sialyl-TF antigen
STn	Sialyl-Tn antigen
SU-DHL-4	Diffuse large B cell lymphoma cell line

TAA	Tumor-associated antigen
TACA	Tumor-associated carbohydrate antigen
TB	Terrific broth
TBS	Tris buffered saline
TBST	TBS + 0.1 % Tween-20
t-BuOH	Tert-butyl alcohol
TCR	T cell receptor
TEA	Triethylamine
TF	Thomsen-Friedenreich antigen
TFA	Trifluoroacetic acid
thFF03	Truncated, glycyated hFF03 peptide
Tn	Thomsen nouveau antigen
Tris	Tris(hydroxymethyl)aminomethane
TSA	Tumor-specific antigen
VH	Variable domain of the heavy chain of a conventional Ab
VHH	Variable domain of a hcAb
VL	Variable domain of the light chain of a conventional Ab
Xyl	Xylose

List of Tables

Table 1. Degree of loading and glycan dose/injection for the different CRM ₁₉₇ glycoconjugates.	49
Table 2. Primers used for site-directed mutagenesis to generate C ^{105S} CB2.....	57
Table 3 TACAs examined in this study.	69

List of Figures

Figure 1 Non-Hodgkin lymphoma.....	27
Figure 2 Important types of tumor-associated carbohydrate antigens.	31
Figure 3 Immune response induced by glycans and glycoconjugates.....	33
Figure 4 PDI overexpression causes aberrant surface thiols in cancer and is linked to tumor progression.	35
Figure 5 IgG subtypes in humans and camelids.....	36
Figure 6 Nanobodies have a conserved structure.....	37
Figure 7 Nanobodies can be endowed with additional properties through functionalization.	40
Figure 8 The srtA reaction cycle for Nb functionalization.	44
Figure 9 Aims of this study.....	46
Figure 10 Conjugation of STn to CRM ₁₉₇	48
Figure 11 Immunization regime.	50
Figure 12 Fractionation of alpaca IgG subtypes.	51
Figure 13 Gating strategy for NHL cell lines in flow cytometry.....	58

Figure 14. General workflow for the synthesis of Rha ₃	61
Figure 15 Synthesis of GG-Rha ₃	62
Figure 16 Generation of CB2-Rha-thFF03.	63
Figure 17 Conjugation of CB2 and Cy3.	65
Figure 18 TACAs were successfully conjugated to CRM ₁₉₇	70
Figure 19 The serum Ab titer against the four injected TACAs increases over the course of immunization.....	71
Figure 20 Induced anti-TACA Abs exhibit different levels of cross-reactivity.	73
Figure 21 Immunization induced Abs in all IgG subclasses.	74
Figure 22 CB2 binding to several B cell lymphoma subtypes.	76
Figure 23 Levels of reduced thiol groups are increased on the surface of lymphoma cells compared to healthy lymphocytes.....	77
Figure 24 CB2 binding to SC-1 cells is abolished in the presence of DTT.	78
Figure 25 CB2 pre-incubation with NEM causes a complete loss of binding to SC-1 cells.	79
Figure 26 The C105S mutation completely abolishes SC-1 cell binding.	80
Figure 27 Loss-of-binding with ^{C105S} CB2 is confirmed by confocal microscopy.	80
Figure 28 Rha ₃ -binding IgGs are significantly more abundant in human serum than Rha-binding IgGs.....	82
Figure 29 CB2-Rha ₃ was successfully generated and still recognizes SC-1 cells.....	83
Figure 30 CB2-Rha ₃ does not induce complement activity against SC-1 cells.....	84

Figure 31 Chemical conjugation yields rhamnosylated thFF03 with varying DOLs....	86
Figure 32 SrtA-mediated conjugation yields CB2-Rha-thFF03 but also hydrolyzed CB2.	86
Figure 33 CB2-Rha-thFF03 retains full binding activity to SC-1 cells.	87
Figure 34 CB2-Rha-thFF03 induces complement activity against SC-1 cells.	88
Figure 35 Proposed model for complement activation by CB2-Rha-thFF03.	89
Figure 36 CB2-Cy3 and ^{C105S} CB2-Cy3 were successfully generated.	91
Figure 37 Cy3 conjugation does not affect the binding activity of CB2 and ^{C105S} CB2...	91
Figure 38 CB2-Cy3 is internalized by SC-1 cells, presumably via clathrin-mediated endocytosis.	93
Figure 39 Structure and hypothesized mechanism of action of CB2-MMAE.	94
Figure 40 CB2 and ^{C105S} CB2 were successfully conjugated to MMAE.	95
Figure 41 MMAE conjugation does not affect the binding activity of CB2 and ^{C105S} CB2.	96
Figure 42 CB2-MMAE can be used for drug delivery to lymphoma cells.	97
Figure 43 Time-dependent MMAE release from ^{C105S} CB2-MMAE in solution.	98
Figure 44 CB2 binds to different breast cancer cell lines but not to non-tumorigenic breast cells.	100
Figure 45 CB2 recognizes <i>L. major</i> and <i>P. falciparum</i>	101

Appendix

Figure S 1 ^{13}C - ^1H HSQC spectrum of Rha ₃	123
Figure S 2 ^{13}C - ^1H HSQC spectrum of GG-Rha ₃	124
Figure S 3 Purification of CB2 and $^{13}\text{C}^{105\text{S}}$ CB2.	125
Figure S 4 Comparison of ^{15}N - ^1H HSQC spectra of CB2 and $^{13}\text{C}^{105\text{S}}$ CB2.	126
Figure S 5 Western blot of CB2 and CB2-Rha ₃ with Abs from human serum.	127
Figure S 6 Conjugation of CB2 and non-rhamnosylated thFF03.	127
Figure S 7 Ab purification from human serum.	128
Figure S 8 Inhibition of transferrin endocytosis.	128

Summary

Cancer is the second-most common cause of death for humans and engendered by malignant human cells dividing uncontrollably due to the failure of cell growth control mechanisms. A major bottleneck for the development of new diagnostics and therapeutics is the identification of specific tumor biomarkers and the generation of suitable tools to target these biomarkers. Tumor-associated carbohydrate antigens (TACAs) and aberrant surface thiol groups are promising classes of tumor biomarkers. However, the number of available tools to study them is very limited.

I established an approach to generate heavy-chain antibodies targeting TACAs by immunization of an alpaca, thereby expanding the toolbox against TACAs. Conjugates of TACAs and carrier proteins were produced and injected into an alpaca, inducing the formation of glycan-specific conventional and heavy-chain antibodies in the animal. These heavy-chain antibodies formed the basis for the generation of nanobodies binding to the tumor-associated glycan Globo-H.

By serendipity, I discovered a new tool for targeting thiol groups on cancer cells, as nanobody CB2 specifically binds to several subtypes of B cell lymphoma and breast cancer via thiol-thiol interactions. I demonstrated that CB2 binding is linked to increased thiol levels on lymphoma cells and requires the presence of an unusual cysteine in the antigen-binding region of the nanobody. CB2 was endowed with additional properties through functionalization, using a combination of chemical and enzymatic conjugation methods. On one hand, I showed that CB2 modified with a rhamnosylated glycopeptide can recruit antibodies to lymphoma cells, resulting in complement activation and cancer cell death. On the other hand, using fluorophore-coupled CB2, I proved that thiol-mediated CB2 binding is followed by internalization into lymphoma cells. Finally, I demonstrated that CB2 internalization can be exploited for the delivery of cytotoxic agents to cancer cells, again leading to cancer cell death.

In summary, the results of my work illustrate the potential of combining thiol-binding, internalizing nanobodies with further functionalization, thereby laying the foundation for numerous applications in cancer diagnostics and therapeutics.

Zusammenfassung

Krebs ist die zweithäufigste Todesursache für Menschen und wird verursacht durch maligne menschliche Zellen, die sich unkontrolliert teilen, da Kontrollmechanismen des Zellwachstums versagen. Ein bedeutendes Nadelöhr bei der Entwicklung neuer Diagnostika und Therapeutika ist die Identifizierung spezifischer Tumorbiomarker und die Generierung geeigneter Werkzeuge, die diese Biomarker zum Ziel haben. Tumorassoziierte Kohlenhydratantigene (TACAs) und aberrante Oberflächenthiole sind vielversprechende Klassen von Tumorbiomarkern. Allerdings sind zu deren Untersuchung nur wenige Werkzeuge verfügbar.

Ich habe eine Methode etabliert, mit der durch Immunisierung eines Alpakas TACA-bindende Schwere-Ketten-Antikörper generiert werden können, um die Anzahl auf TACAs abzielender Werkzeuge zu erhöhen. Dazu wurden Konjugate von TACAs und Trägerproteinen produziert und in ein Alpaka injiziert, was die Bildung von glykanspezifischen konventionellen Antikörpern und Schwere-Ketten-Antikörpern induzierte. Die Schwere-Ketten-Antikörper bildeten die Grundlage für die Entwicklung von Nanokörpern, welche das tumorassoziierte Glykan Globo-H binden.

Durch Zufall habe ich ein neues Werkzeug für die Untersuchung von Thiolgruppen auf Krebszellen entdeckt, da der Nanokörper CB2 spezifisch an verschiedene Subtypen von B-Zelllymphomen und Brustkrebs über Thiol-Thiol-Interaktionen bindet. Ich konnte zeigen, dass das spezifische Bindeverhalten von CB2 mit erhöhten Thioldmengen auf Lymphomazellen zusammenhängt und die Anwesenheit eines ungewöhnlichen Cysteins in der antigenbindenden Region des Nanokörpers voraussetzt. Durch Funktionalisierung wurde CB2 mit zusätzlichen Eigenschaften ausgestattet unter Verwendung einer Kombination chemischer und enzymatischer Konjugationsmethoden. Einerseits demonstrierte ich, dass CB2 durch Modifizierung mit einem rhamnosylierten Glykopeptid die Fähigkeit erlangt, Antikörper zu Lymphomzellen zu rekrutieren, gefolgt von der Aktivierung des Komplementsystems und dem Tod der Krebszellen. Andererseits konnte ich unter Verwendung von an einen

Fluorophor gekoppeltem CB2 beweisen, dass die thiolvermittelte Bindung zur Internalisierung von CB2 durch Lymphomzellen führt. Schließlich zeigte ich, dass die Internalisierung von CB2 ausgenutzt werden kann für die Lieferung cytotoxischer Stoffe an Krebszellen, was zum Tod der Krebszellen führt.

Zusammengefasst verdeutlichen die Ergebnisse meiner Arbeit das Potenzial von thiolbindenden, internalisierenden Nanokörpern kombiniert mit weiterer Funktionalisierung und legen den Grundstein für zahlreiche Anwendungen in der Krebsdiagnostik und Krebstherapie.

1. Introduction

1.1. Cancer

1.1.1. Prevalence

Cancer is a non-infectious disease characterized by aberrant cell proliferation and invasion of malignant cells into healthy tissue. In total, every year around 19 million new patients develop cancer and approx. 10 million patients succumb to the disease, rendering cancer the second-most common cause of death for humans¹. Cancer can affect any organ of the human body, the most prevalent solid tumors being lung cancer, colorectal cancer, breast cancer (for women) and prostate cancer (for men). In addition, cancer can occur in the blood and lymphatic system as non-solid tumor^{2,3}.

1.1.2. Non-Hodgkin lymphoma

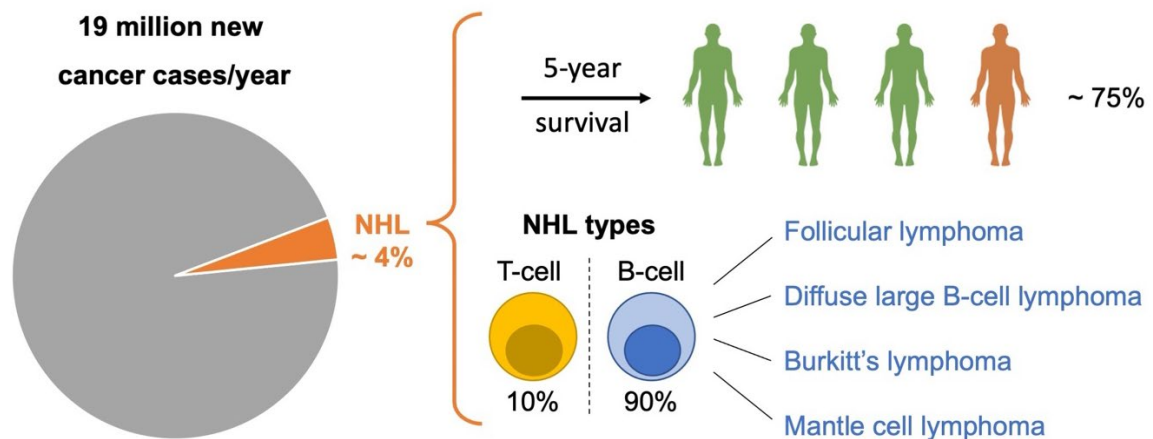


Figure 1 Non-Hodgkin lymphoma. Approx. 4 % of 19 million annual new cancer cases are Non-Hodgkin lymphoma (NHL), and one out of four patients succumbs to the disease within 5 years. NHL can affect T or B cells and several subtypes of B cell NHL have been described^{4,5}.

Non-Hodgkin lymphoma (NHL) is a type of non-solid tumor, developing from lymphocytes. Most cases (85-90 %) originate from B lymphocytes⁴ and approx. 2 % of humans develop NHL during their lifetime, making NHL the 7th-most common cancer type⁵. Within five years after the diagnosis, every fourth patient dies from NHL (Figure 1). Different subtypes of B cell NHL can be distinguished, including follicular

lymphoma, diffuse large B cell lymphoma, Burkitt's lymphoma, and mantle cell lymphoma. These subtypes vary in growth rate, and some can also transform into one another over time⁴.

1.1.3. Therapeutic strategies

Traditionally, cancer has been treated mainly by surgery, radiation therapy, and/or chemotherapy^{6,7}. While some tumors can be manually removed by surgery, radiation therapy destroys the tumor locally by applying ionizing radiation to damage the DNA of cancer cells beyond repair. In contrast, chemotherapy capitalizes on the faster proliferation of cancer cells compared to healthy tissues and involves the systemic administration of cytotoxic drugs that usually inhibit cell division⁸. These methods are often used in combination and show success in the treatment of some cancer types, but they suffer from low efficiency or high off-target toxicity in other cases, highlighting the need for more targeted therapies⁹. The main bottleneck for the development of targeted therapies is the identification of tumor biomarkers, so-called tumor-specific antigens (TSAs) or tumor-associated antigens (TAAs). TAAs and TSAs express at a high level on cancer cells but show lower or no expression on healthy cells, respectively^{10,11}.

Over recent years, several tumor-targeting monoclonal antibodies (mAbs) have been developed and approved, initiating a paradigm shift for cancer therapy^{12,13}. If the biomarker targeted by the respective mAb is expressed by the cancer, mAb treatment shows high efficiency and specificity. For instance, breast cancer cells expressing the TAA HER2 (human epidermal growth factor receptor 2) can be successfully treated with the mAb trastuzumab¹⁴. However, not the same biomarkers are expressed in every case of a certain cancer type; for instance, only 15 % of breast cancer cases are HER2-positive¹⁵. Another example is the TSA EGFRvIII (epidermal growth factor receptor variant III), which is highly specific for glioblastoma but only found in < 12 % of patients¹⁶. In case of brain tumors such as glioblastoma, even if a TSA is expressed, mAbs are still of limited use as they cannot cross the blood-brain barrier¹⁷.

While mAb therapies are more targeted than conventional cancer treatments, off-target effects can still occur when targeting TAAs, as low levels of a given TAA are found on healthy cells as well. Cancers may also develop resistance to targeted treatments, for instance by altering the gene expression of the targeted biomarker or by mutating the mAb's binding epitope¹⁸.

1.2. Tumor biomarkers

1.2.1. Tumor-associated carbohydrate antigens

To date, the vast majority of identified TSAs or TAAs are protein antigens. However, glycans are also emerging as attractive tumor biomarkers, forming the group of tumor-associated carbohydrate antigens (TACAs)¹⁹. Most TACAs identified so far can be grouped into the following categories: *N*-glycans, *O*-glycans, glycosphingolipids, glycosaminoglycans, and Lewis glycans (Figure 2). While *N*-glycans tend to become longer and more branched on cancer cells²⁰, *O*-glycan structures appear more truncated²¹. Two well-studied examples of tumor-associated truncated *O*-glycans are the Thomsen nouveau (Tn) antigen and its sialylated version, the STn antigen. Both contain a GalNAc moiety, which is sialylated at the 6-position in case of STn (Figure 2). Tn and STn are abundantly found on a variety of cancer types, including gastric, colon, breast, lung, bladder, and prostate cancer. Tn and STn overexpression also promote metastasis, leading to a poor prognosis for patients²²⁻²⁵. A different example from the group of TACA *O*-glycans is the Thomsen-Friedenreich (TF) antigen which consists of a GalNAc extended by a single Gal. The TF antigen also exists in mono- and disialylated form and is overexpressed in the vast majority of cancers²⁶.

Another group of important TACAs is the Globo series of glycosphingolipids, including the glycans GB5 (also known as SSEA-3), SSEA-4, and Globo-H (also known as SSEA-3b). These three glycosphingolipids share a pentasaccharide core of Gal(β1-3)GalNAc(α1-3)Gal(β1-4)Gal(α1-4)Glc (GB5) which is sialylated or fucosylated at the non-reducing end in SSEA-4 or Globo-H, respectively (Figure 2). Globo series glycans

are highly expressed on the surface of many cancers, such as prostate, breast, lung or pancreas cancer but hardly expressed on healthy tissues²⁷⁻²⁹. In addition, their expression has been linked to poor prognosis and metastasis^{27,28,30}. SSEA-4 expression, for instance, renders tumor cells less adhesive and more invasive, enabling migration into adjacent tissues³⁰. Globo-H, in turn, contributes to angiogenesis and tumor progression in the form of Globo-H-containing microvesicles which are shed by tumor cells and absorbed by the surrounding endothelium³¹. Due to Globo-H's specific expression on cancer cells and critical role in cancer signaling, Globo-H-binding mAbs and Globo-H-based vaccines have been recently investigated in clinical trials³²⁻³⁶. While only half of the patients with metastatic breast cancer developed an Ab response against the Globo-H vaccine in a recent phase III trial, the responding patients showed significantly prolonged survival, suggesting a substantial benefit of such a glycovaccine for a subgroup of patients³⁶. An ongoing phase III trial investigates the specific effect of a Globo-H vaccine on patients with triple-negative breast cancer which is notoriously difficult to treat³⁷.

Glycans from the Lewis family are found on proteins and lipids and play important roles for healthy cells, e.g. as blood group antigens and in cell-cell recognition³⁸. However, many Lewis glycans are overexpressed in cancer, such as Lewis a, Sialyl-Lewis a, Lewis X, Sialyl-Lewis X or dimers of Lewis X-Lewis Y (termed KH-1)³⁹⁻⁴¹. Particularly, KH-1 has so far not been detected on healthy tissues, rendering it an excellent tumor biomarker⁴². Sialyl-Lewis a (SLe^a) is also of high clinical relevance as it is currently the only FDA-approved biomarker for pancreatic ductal adenocarcinoma⁴³.

Glycosaminoglycans form the glycan part of proteoglycans which are a major component of the extracellular matrix. They contribute to various aspects of tumorigenesis, from angiogenesis over tumor proliferation to metastasis. Furthermore, altered glycosaminoglycan expression on cancer cells has a severe impact on the tumor microenvironment and has been linked to poor prognosis^{44,45}.

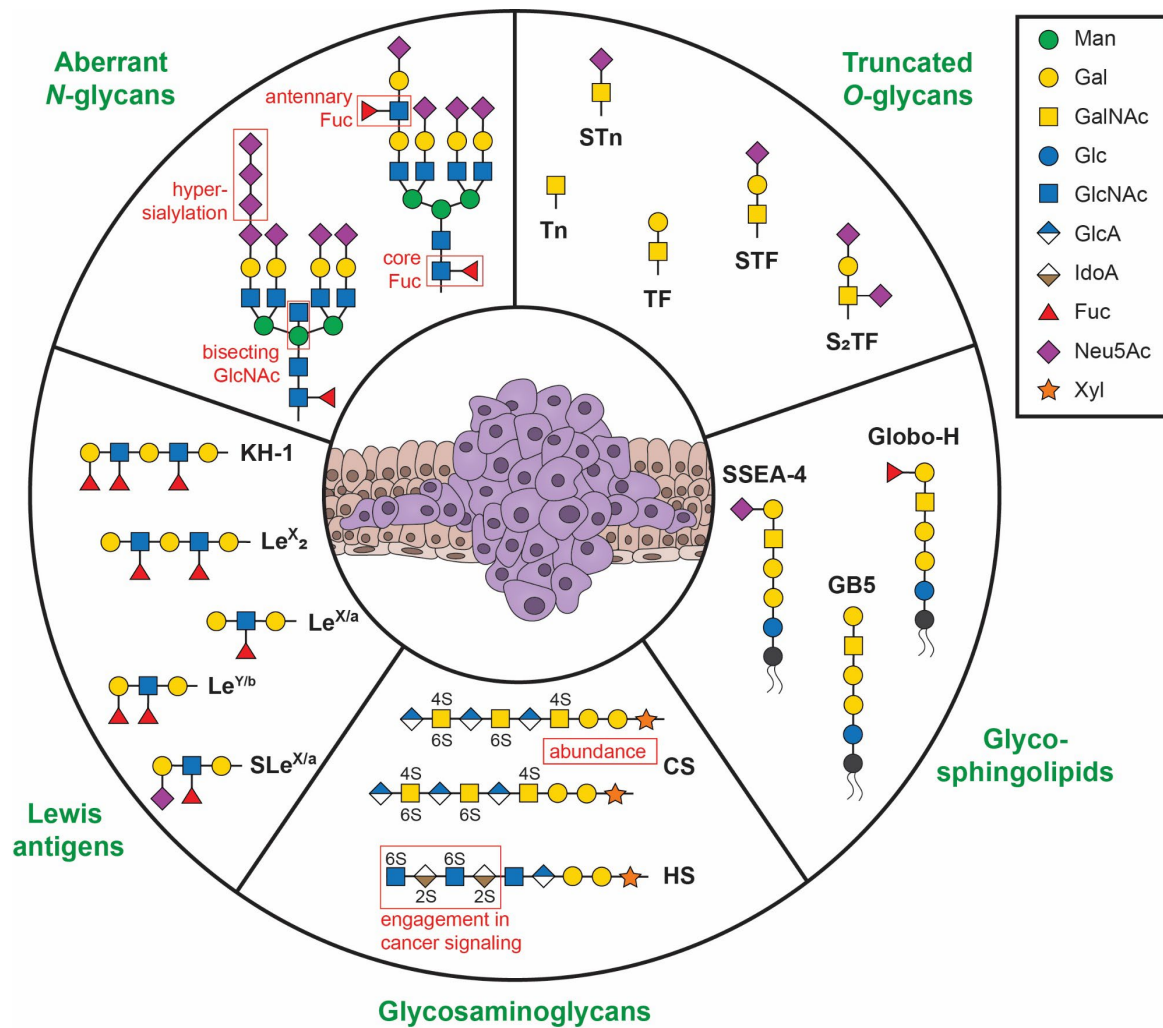


Figure 2 Important types of tumor-associated carbohydrate antigens. Glycans on cancer cells significantly differ from glycans on healthy cells. *N*-glycans often display increased complexity and branching on cancer cells and examples for such modifications are marked by red frames in the figure. In contrast, truncated *O*-glycans appear on tumor cells such as the Tn or STn antigens. Lewis antigens are also overexpressed on many cancers and the more complex structures KH-1 and Le^X₂ have not been identified on healthy cells so far. Glycosphingolipids are directly displayed on cancer cells as part of the membrane lipids and are not connected to surface proteins. They play important roles in cancer signaling and many glycosphingolipids are currently investigated as cancer vaccine candidates or mAb targets in clinical trials. Glycosaminoglycans form part of the extracellular matrix's proteoglycans. Higher glycosaminoglycan levels in tumors contribute to the dense tumor microenvironment, and specific glycan sulfation patterns have been linked to cancer cell signaling (red frames). CS = chondroitin sulfate, HS = heparan sulfate, SSEA-4 = stage-specific embryonic antigen 4. Other glycan abbreviations are explained in the main text and in the list of abbreviations.

TACAs harbor great potential as tumor biomarkers not only due to their specific expression on cancer cells but also due to their complex biosynthesis. Cancers can evade targeting of their protein antigens by reducing protein expression or by mutating the drug's binding epitope, thereby growing resistant to treatment¹⁸. However, TACA expression is not the result of a single enzyme but controlled by many enzymes in a multi-step process which decreases the likelihood for resistance to treatment when targeting TACAs¹⁹.

While many tumor-associated protein antigens are only expressed in a small fraction of cancer cases, some TACAs show a very high incidence for certain cancer types. For instance, the protein HER2 is only expressed in approx. 15 % of breast cancer cases¹⁵ but STn is found on > 90 % of colorectal cancers⁴⁶.

1.2.2. Development of TACA-specific antibodies

Due to the immense potential of TACAs as tumor biomarkers, several TACA-binding mAbs have been developed over the past decades and approved for diagnostic use. Compared to Abs against protein antigens, however, the number of TACA-binding mAbs remains meager⁴⁷. In the past, one of the main bottlenecks in the development of new TACA-binding Abs was the scarcity of well-defined TACAs for immunization as organic synthesis of sufficient amounts remained challenging. Therefore, the majority of anti-TACA mAbs has been derived by immunization of animals with crude, heterogeneous glycoprotein extracts or whole cancer cells¹⁹, or by mAb purification from human patients⁴⁸. In both cases, the identification of TACA-specific mAbs becomes an unpredictable enterprise. Even though existing TACA-specific mAbs often suffer from low (micromolar) affinity, some of them have high clinical relevance, such as the SLe^a-targeting mAb 116-NS-19-9 which is currently the most sensitive diagnostic tool for pancreatic cancer^{43,49}.

Due to recent advances in automated-glycan assembly⁵⁰⁻⁵², sufficient amounts of synthetic TACAs can now be generated and used for immunization with well-defined, homogeneous samples. However, the inherently low immunogenicity of glycans still poses a major challenge in anti-TACA mAb development⁵³.

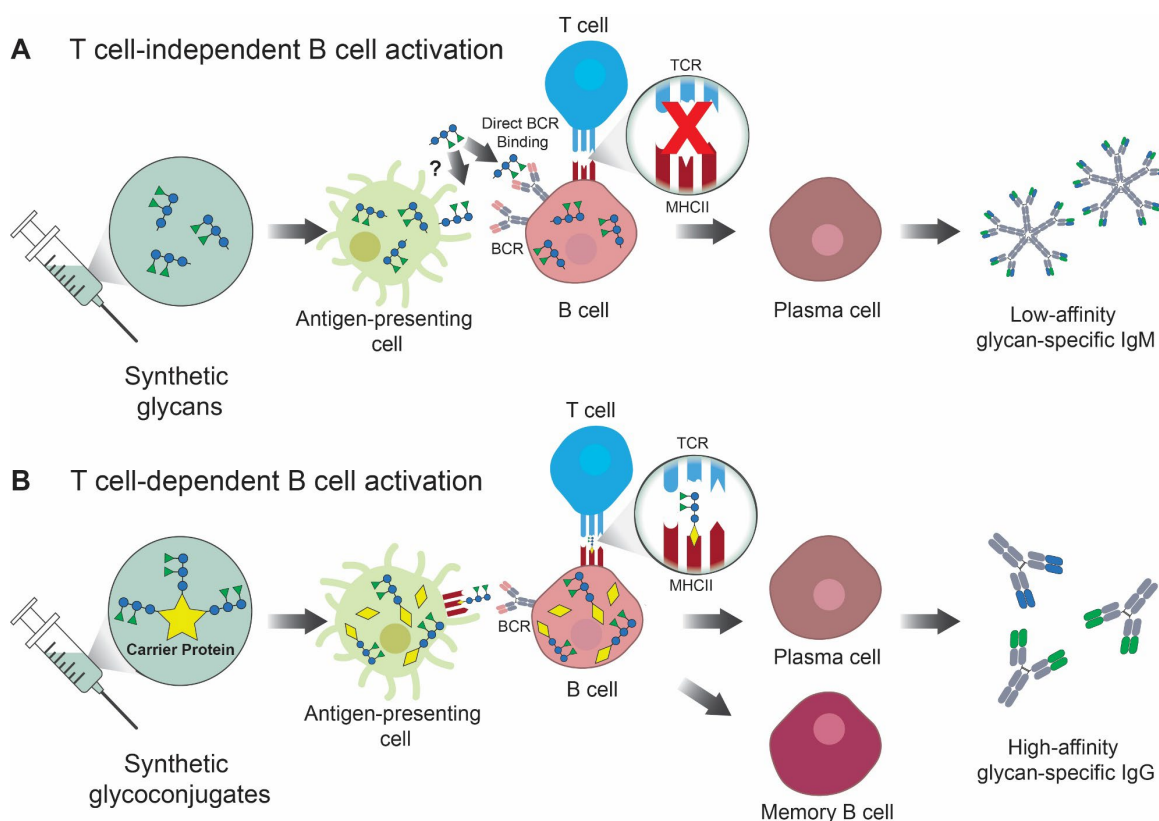


Figure 3 Immune response induced by glycans and glycoconjugates. Immunization with synthetic glycans predominantly results in a T cell-independent response. The glycan is recognized by BCRs, inducing the transition to plasma B cells which mainly produce low-affinity glycan-binding IgM Abs. **(B)** In contrast, synthetic glycoconjugates are processed to glycopeptides by antigen-presenting cells which present the glycopeptides on their surface MHCII. Glycopeptide-loaded MHCII can recruit T cell help via interaction with TCRs, resulting in class switching and affinity maturation and thereby in high-affinity glycan-binding IgG Abs. In addition, memory B cells are formed which convey immunological memory in case of antigen re-exposure. IgG = immunoglobulin G, IgM = immunoglobulin M, MHCII = major histocompatibility complex II, BCR = B cell receptor, TCR = T cell receptor. Figure adapted from Zastona *et al.*⁵⁴.

Immunization with glycans usually leads to a T cell-independent immune response, yielding mostly plasma cells that produce low-affinity immunoglobulin M (IgM)

Abs^{55,56} (Figure 3). As a result, the number of circulating anti-glycan antibodies and glycan-specific B cells remains relatively low. The low immunogenicity can be circumvented by conjugating glycans to immunogenic carrier proteins⁵⁵ and by selecting a suitable adjuvant for immunization⁵⁷. Common carrier proteins are keyhole limpet hemocyanin (KLH) and cross-reactive material 197 (CRM₁₉₇). CRM₁₉₇ is a non-toxic G52E mutant of diphtheria toxin⁵⁸ and already approved for use in humans as part of the pneumococcal glycoconjugate vaccine PREVNAR13⁵⁹. Immunization with glycoconjugates is believed to enable the presentation of processed glycopeptides by major histocompatibility complex II (MHCII) on the surface of antigen-presenting cells and B cells. MHCII presentation leads to a T cell-dependent immune response, involving affinity maturation and memory B cell formation, and, hence, high-affinity immunoglobulin G (IgG) Abs can be obtained⁵⁵ (Figure 3).

1.2.3. Extracellular tumor redox microenvironment

Accumulating evidence from recent years suggests that the extracellular redox state of many cancers is significantly altered compared to healthy tissues⁶⁰⁻⁶². Redox-controlling proteins, such as protein disulfide isomerases (PDIs) or the thioredoxin system, show high expression levels in various tumors^{60,63,64}. Thioredoxin and PDIs catalyze thiol-disulfide exchange reactions of cysteine residues, leading to altered levels of reduced or oxidized protein disulfide bridges (Figure 4). Free thiol groups on the surface of breast cancer cells promote cell adhesion and metastasis⁶¹, linking the extracellular redox state to cancer progression. This is further validated by the observation that PDI inhibition reduces cancer proliferation (Figure 4), rendering PDIs promising therapeutic targets⁶³⁻⁶⁵. Due to their implication in cancer proliferation and metastasis, aberrant surface thiols also harbor potential as tumor biomarkers. However, no quantitative information about the levels of free thiol groups on healthy and tumorigenic cells is currently available, leaving the question whether altered surface thiols would provide sufficient tumor specificity so far unanswered.

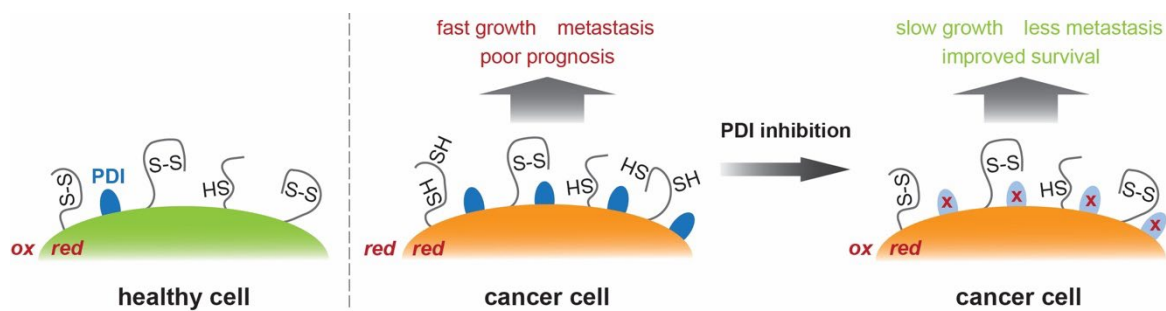


Figure 4 PDI overexpression causes aberrant surface thiols in cancer and is linked to tumor progression. Healthy cells (green, left) generally possess an oxidative (ox) extracellular microenvironment and reducing (red) conditions in the cytosol with protein disulfide isomerase (PDI) and other surface enzymes maintaining a cell surface equilibrium between disulfide bonds and reduced thiol groups. Due to PDI overexpression in cancer cells (orange, center), increasing amounts of surface disulfide bonds are becoming re-shuffled, potentially leading to a more reducing tumor microenvironment. Aberrant surface thiols are associated with fast tumor growth, increased metastasis, and poor prognosis. PDI inhibition restores the healthy redox microenvironment (orange, right), leading to a decrease in tumor growth and metastasis as well as longer survival.

1.2.4. Thiol-binding molecules

The presence of surface thiols on the cell surface can be exploited as a vantage point for thiol-functionalized small molecules, peptides or even liposomes, binding these surface thiols. Importantly, thiol-thiol interactions often trigger cellular uptake, either by endocytosis, direct translocation or fusion⁶⁶⁻⁶⁹. Common examples of molecules exhibiting thiol-mediated uptake include maleimide probes and cell-penetrating disulfides⁷⁰. Various studies already highlighted how thiol-based internalization can be exploited for the intracellular delivery of diverse cargoes, ranging from small molecules to whole enzymes^{69,71-73}. For instance, activated disulfides have been successfully used to deliver Gd(III) complexes into leukemic lymphoblast cells as contrast agents for magnetic resonance imaging⁷³. Cell-penetrating disulfides were employed to transport quantum dots and GFP-binding peptides into the cytosol, e.g. for single-molecule imaging⁷². Finally, thiol-functionalized nanoparticles have been generated as drug carriers to target bladder cancer cells but also pathogens such as *Plasmodium*^{74,75}.

1.3. Nanobodies

1.3.1. Camelid heavy-chain antibodies

IgG Abs found in humans and most other mammals conventionally consist of a heavy and a light chain (Figure 5). The antigen-binding region of the Ab is formed by the variable domains of heavy and light chain, VH and VL respectively. In 1993, experiments with camel serum led to the surprising finding that camelids such as camels, llamas or alpacas also possess so-called heavy-chain antibodies (hcAbs) devoid of light chains⁷⁶. Specifically, camelid serum was found to contain three IgG subtypes: 50 % IgG1 (conventional Abs), 30 % IgG2 and 20 % IgG3 (both hcAbs)^{76,77} (Figure 5). Due to the lack of a light chain, the antigen-binding region of hcAbs is formed by a single domain, designated VHH, which can be recombinantly expressed as so-called nanobody (Nb).

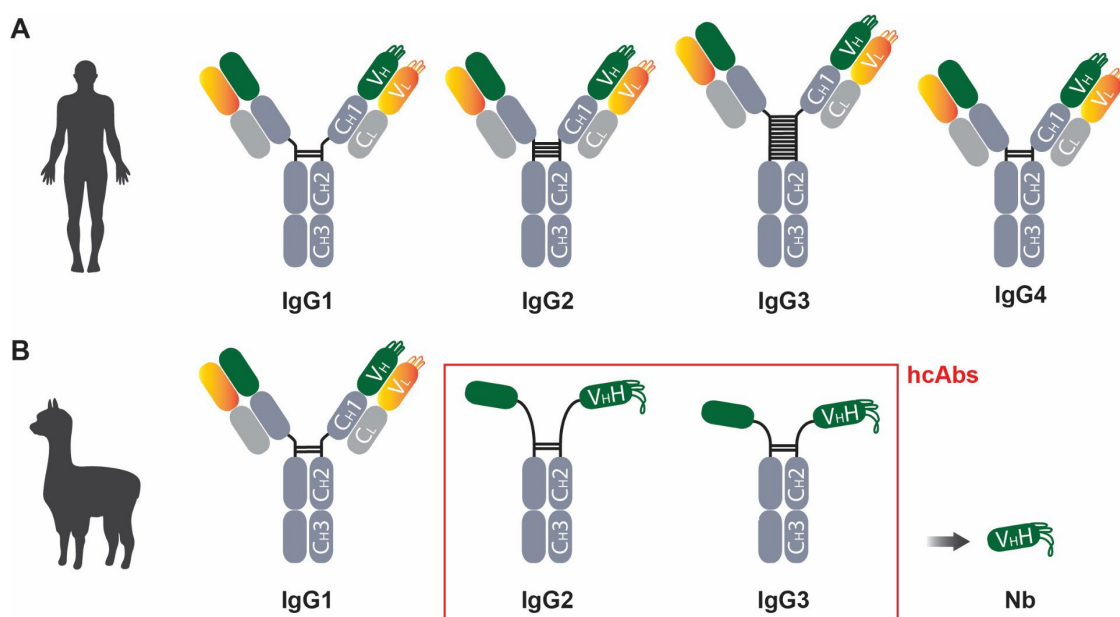


Figure 5 IgG subtypes in humans and camelids. (A) Humans possess four different IgG subtypes, IgG1-4, which all consist of a heavy and a light chain and differ mainly in the hinge regions of the heavy chain. The antigen-binding regions are formed by VH and VL domains. **(B)** Camelids, e.g. alpacas, possess conventional Abs of the IgG1 subtype as well. However, their serum also contains heavy-chain Abs (hcAbs, red frame), IgG2 and IgG3, lacking the light chain and the CH1 domain. In hcAbs, the antigen-binding region is formed by a single VHH domain, called Nanobody (Nb) upon recombinant expression.

1.3.2. Nanobody structure and properties

Nbs are only around 15 kDa in size which is 10 % of the size of a conventional IgG. Their single-domain nature enables straightforward recombinant expression in bacteria, yielding high amounts of protein at a low cost. Most Nbs are highly stable and soluble across a wide range of pH, salt, and temperature⁷⁸. Nbs have a conserved structure (Figure 6) consisting of four framework regions (FR1-4) interspaced by three complementarity-determining regions (CDR1-3)⁷⁹. As the sequences of FR1-4 are highly conserved, the antigen is recognized by the non-conserved CDRs which protrude as flexible loops from the barrel-like core. On average, the CDR3 loop of Nbs tends to be longer than of conventional Abs with a mean CDR3 length of 15 amino acids for VHH vs. 12 amino acids for VH, respectively^{80,81}. The longer CDR3 enables Nbs to recognize less accessible, cryptic epitopes^{80,82}.

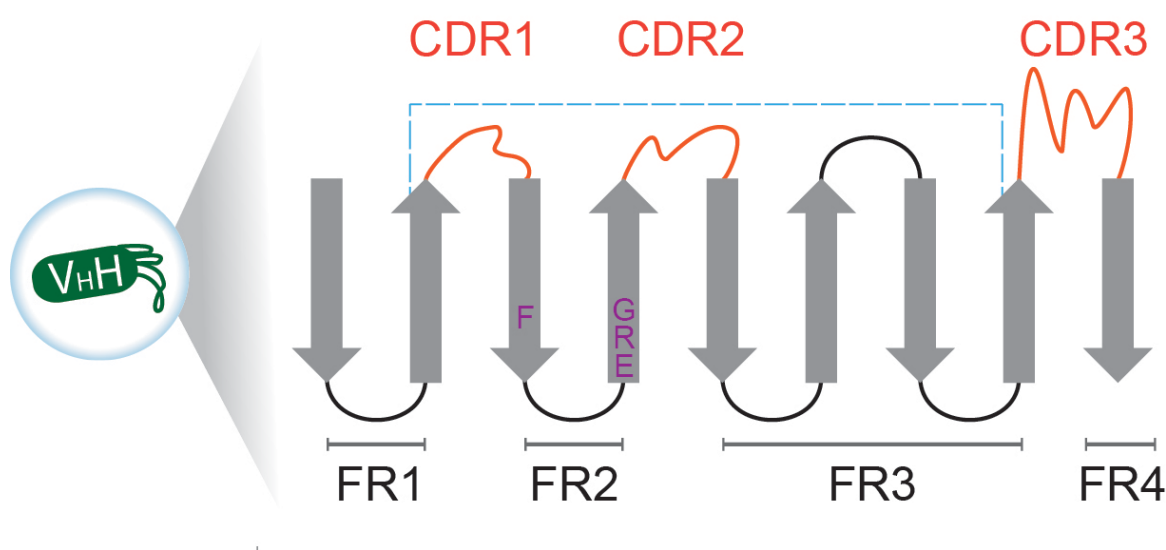


Figure 6 Nanobodies have a conserved structure. Nine β sheets in the framework regions (FRs, grey) form a barrel-like core from which the antigen-binding loops of the three complementarity-determining regions (CDRs, orange) protrude. The CDR3 of Nbs is usually longer than the CDR3 of conventional Abs, allowing the binding to less accessible surface antigens. In VHH sequences, several hydrophobic amino acids in FR2 are frequently swapped out for more hydrophilic residues (purple) to increase stability. In addition, Nbs are stabilized by a disulfide bond between FR1 and FR3 (blue dashed line).

While the surface of VH domains in conventional Abs is partially covered by the VL domain of the light chain, the Nb surface is completely exposed to the surrounding solvent⁸⁰. Therefore, VHH and VH frequently differ in so-called hallmark amino acids. For instance, the FR2 of VH carries V42, G49, L50 and W52, whereas VHH sequences often contain F42, E49, R50 and G52 (Figure 6), constituting a shift from hydrophobic towards polar and hydrophilic surface residues⁸⁰. Although these mutations can convey higher stability to the Nb, stable Nbs also exist which possess no or only some VHH hallmark amino acids^{83,84}. Nbs are further stabilized through disulfide bonds: FR1 and FR3 are connected through a conserved disulfide bond, and an additional bond between CDR1 and CDR3 may also be present in some cases to rigidify the longer CDR3^{79,85}.

Due to their small size, Nbs have interesting properties for *in vivo* applications. On one hand, Nbs are rapidly cleared from the blood stream through the kidneys which is desirable for diagnostic use but can be a challenge for therapeutic application⁸⁶. On the other hand, Nbs overwhelmingly exhibit low immunogenicity in humans, rendering humanization of the sequence expendable for most Nbs⁸⁷. Finally, Nbs can penetrate the dense tissue of solid tumors more efficiently than conventional Abs, leading to a more homogeneous tissue distribution which can be advantageous both for diagnostic and therapeutic use^{88,89}.

1.3.3. Strategies for nanobody development

Similar to conventional Abs, Nb development usually starts with immunization of a camelid with the antigen(s) of choice. To generate conventional Abs, immunization is followed by isolation of the spleen and fusion of B cells to myeloma cells, yielding immortal, Ab-producing hybridoma cells which are selected for binding to the antigen⁹⁰. While this workflow is very well established, it is time-consuming and costly. For Nb development, in contrast, a Nb sequence library can be directly generated by isolation of the animal's peripheral blood mononuclear cells (PBMCs), followed by RNA extraction and reverse transcription into complementary DNA (cDNA)⁷⁹. Therefore,

only a sustainable amount of blood is needed from the animal and isolation of the spleen can be omitted, making Nb development less harmful and more ethical than Ab development. Recently, naïve or synthetic Nb sequence libraries have been generated and successfully used for Nb development as well, obviating the need for animal immunization^{91,92}.

Based on the Nb sequence library, different techniques can be employed to select Nbs binding to the antigen(s) of interest. Display on phages, bacteria, yeast or ribosomes combined with selection of high-affinity binders in multiple so-called biopanning rounds has been extensively used to enrich high-affinity Nbs⁹²⁻⁹⁵. Alternatively, hcAbs in the serum of the immunized camelid can be sequenced by mass spectrometry, matched to the cDNA library, and ranked by peptide coverage to select abundant, likely affinity-matured hcAbs for Nb development⁹⁶.

The generation of glycan-binding Nbs is hampered by the same obstacles as the generation of glycan-binding conventional Abs: low immunogenicity of glycans and limited availability of homogeneous compounds for immunization. Hence, the few existing glycan-binding Nbs were derived from immunization with native glycoproteins or whole cells and recognize mostly heterogeneous, uncharacterized polysaccharides or glycoproteins rather than pure glycan epitopes^{82,97,98}.

1.4. Nanobody functionalization

Due to their single-domain nature and high chemical stability, Nbs are rapidly functionalized during or post expression. Since Nbs by themselves do not possess other functions than antigen binding, functionalization has been used to convey additional desired properties to Nbs. Selected types of Nb functionalization are summarized in Figure 7 and presented subsequently in more detail.

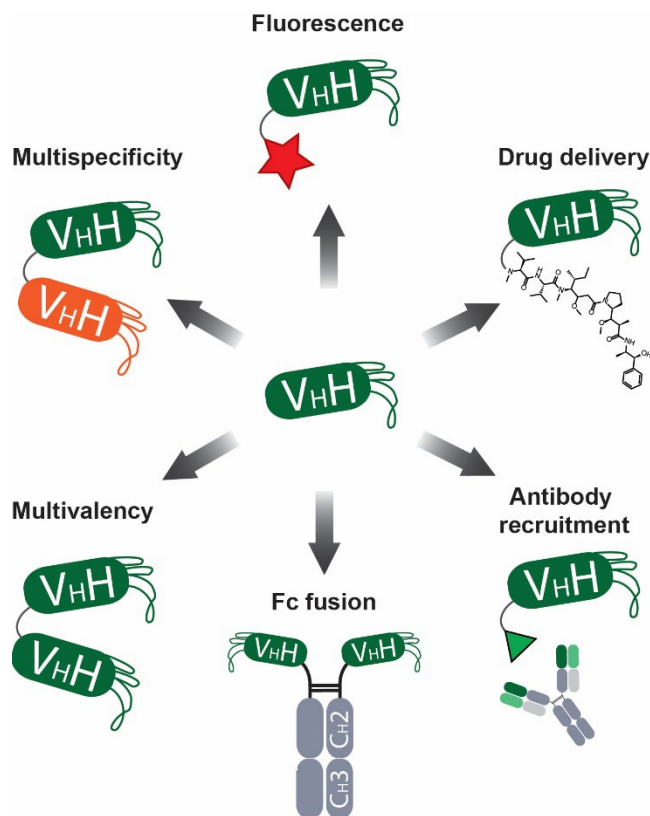


Figure 7 Nanobodies can be endowed with additional properties through functionalization. Clockwise from the top: By attaching a fluorophore, Nbs become fluorescent tools which can be used for imaging and diagnostics. Conjugation to cytotoxic agents enables therapeutic use for drug delivery in case of internalizing Nbs. Non-internalizing Nbs can be therapeutically employed by coupling to antibody-recruiting molecules (ARMs) such as rhamnose. By expressing Nbs as human Fc fusions, immune signaling can be restored. Homodimers and heterodimers are designed to achieve multivalency or multispecificity, respectively.

1.4.1. Multivalency and multispecificity

Multivalency can be easily achieved by expression of Nb homodimers or even higher multimers. Nb head-to-tail fusions separated by short flexible linkers are expressible from the same plasmid and provide avidity, while maintaining a relatively small size compared to full-length Abs^{88,99}. If size is not relevant for the application, Nb domains can also be expressed as fusions to human Fc domains of a hcAb, thereby restoring the capability of downstream signaling via the Fc¹⁰⁰.

Multispecific Nbs are also attractive for many applications. Nb heterodimers were successfully used to improve cell recognition by combining two distinct biomarkers to increase the binding specificity to cancer cells¹⁰¹. Fusing a Nb targeting serum albumin to any other Nb can significantly increase the serum half-life of that Nb⁸⁶, a useful property for therapeutic application.

1.4.2. Fluorescence

Co-expression of Nbs with fluorescent proteins or attachment of fluorophores to Nbs post expression transforms Nbs into powerful tools for visualization and diagnostics. For instance, Nbs form excellent probes for super resolution microscopy as they can reduce the distance between dye and target (so-called “linkage error”) due to their small size, allowing higher resolution¹⁰². In addition, fluorescent Nbs are used to study intracellular dynamics in living cells¹⁰³ and also show great potential for *in vivo* tumor imaging where they can be employed in fluorescence-guided surgery^{104,105}.

1.4.3. Antibody recruitment

Since Nbs lack the Fc domain, they do not recruit further downstream effector molecules of the immune system, such as Fc receptors or complement factors, to their target. To trigger an immune response against Nb-targeted cells, Nbs can be fused to antibody-recruiting molecules (ARMs). Suitable ARMs are antigens themselves, against which high titers of endogenous Abs are present in human serum. Well-studied examples of ARMs are *p*-dinitrophenol (DNP), the trisaccharide Gal(α 1-3)Gal(β 1-4)GalNac (α Gal), and rhamnose (Rha)¹⁰⁶⁻¹⁰⁹. Both α Gal and Rha are glycan antigens that are abundantly found in other organisms: α Gal in almost all other mammals and Rha in the surface polysaccharides of many bacteria and plants¹¹⁰⁻¹¹². However, α Gal cannot be produced by humans due to the absence of alpha-1,3-galactosyltransferase¹¹³, and Rha is not found in the human glycome. Therefore, the immune system considers these glycans as foreign, resulting in a high number of α Gal- and Rha-binding Abs in human serum. The reason for the presence of anti-DNP Abs in human serum is yet to be found but it has been suggested that anti-DNP Abs could be cross-reactive to another antigen that humans are in contact with¹⁰⁷. Strikingly, of all IgGs in human serum, up to 1 % are directed against DNP, around 2 % are directed against α Gal and more than 2 % bind to Rha^{106,107,109,114}.

ARM-mediated Ab recruitment mainly triggers the activation of two immune defense mechanisms: antibody-dependent cellular cytotoxicity (ADCC) and complement-dependent cytotoxicity (CDC)¹¹⁵. In the ADCC pathway, Abs can be recognized by Fc γ receptors on natural killer cells which release granzymes to kill the Ab-targeted cell¹¹⁵. In the classical pathway of CDC, Abs recruit complement factor C1q which activates the complement cascade, a multi-step process involving several proteins. At the end of the cascade, membrane attack complexes are formed which create pores in the target cell membrane, thereby leading to cell lysis¹¹⁵.

Previous work revealed that Nb-DNP conjugates can efficiently recruit Abs to cancer cells followed by ADCC and CDC activation¹¹⁶. Since anti-Rha Abs are even more abundant in human serum than anti-DNP Abs, recent studies demonstrated that Rha conjugates to Abs or bispecific Nbs as well as Rha-functionalized liposomes reliably induce ADCC and CDC against cancer cells, underscoring the potential of Rha-mediated Ab recruitment for cancer therapy¹¹⁷⁻¹¹⁹.

1.4.4. Internalization and drug delivery

Current strategies to enable cellular uptake of Nbs either rely on receptor-mediated endocytosis or direct translocation by introducing positive charges into the protein sequence¹²⁰. Surface receptors may undergo endocytosis upon Nb binding and this effect can be exploited, for instance to disrupt signaling pathways of proliferating tumors¹²¹. However, endocytosed Nbs are located inside vesicles and eventually enter the lysosomal pathway which prevents Nb binding to cytosolic targets¹²⁰. This can be achieved through endocytosis-independent, direct Nb translocation. Either the whole Nbs is subjected to cationic resurfacing by grafting arginine residues into solvent-exposed parts of the Nb framework regions¹²², or a cyclic polycationic peptide is added to the C-terminus of the Nb¹²³. Both approaches cause efficient cell penetration of the Nb into the cytosol and enable Nb binding to cytosolic targets.

Recent years have witnessed the development of a variety of antibody-drug conjugates (ADCs) to specifically deliver drugs into cancer cells¹²⁴. Whereas several ADCs are already approved for use in humans and on the market, the development of nanobody-drug conjugates (NDCs) lagged behind with the result that no NDCs have been approved so far¹²⁵. Since Nbs show better penetration of solid tumors than conventional Abs due to their small size⁸⁸, NDCs are particularly promising for homogeneous drug delivery into cancer cells.

1.4.5. Strategies for nanobody functionalization

Generally, functionalization strategies can be grouped into random and site-directed conjugation methods, with the choice of strategy depending on the desired application¹²⁰. Random conjugation usually relies on chemical attachment of the functional groups to accessible lysine side chains throughout the Nb sequence. This harbors the advantage that a high degree of loading (DOL) can be achieved in a fast and straightforward manner, but the resulting product will be a heterogeneous mixture with undefined stoichiometry, and conjugation close to or inside the CDRs may interfere with Nb binding¹²⁰. Therefore, several site-directed approaches have been developed for Nb functionalization which attach just one functional group, i.e. max. DOL = 1, to a specific site in the Nb sequence, most often the C-terminus. Some site-directed approaches use similar chemistry as the random ones, for instance, by introducing a C-terminal cysteine residue which is amenable to thiol-maleimide reactions¹²⁶. However, most site-directed approaches involve enzymes due to the high sequence and substrate specificity that can be achieved.

One of the most established enzymatic conjugation methods is the sortase A (srtA) reaction^{127,128} (Figure 8). SrtA was originally discovered in *Staphylococcus aureus* where it links surface proteins to the bacterial cell wall¹²⁹. SrtA recognizes proteins with a sortag of the sequence LPXTG (for X, any amino acid but proline is allowed). If a glycine-functionalized substrate is available in excess, the enzyme will replace the

protein sequence after the sortag with the substrate. For Nb conjugation, the sortag is typically placed close to the C-terminus and followed by a His-tag for affinity chromatography¹³⁰. This enables straightforward purification of the desired conjugation product as the His-tag is then replaced by the substrate during the srtA reaction, allowing the separation of unconjugated and conjugated Nb (Figure 8). Since the reaction is reversible, it is usually forced towards the desired product by an excess of substrate, and the reaction time is optimized to prevent the backreaction. Excess of substrate also prevents the formation of hydrolyzed Nb which is observed if too little or no substrate is available^{131,132} (Figure 8).

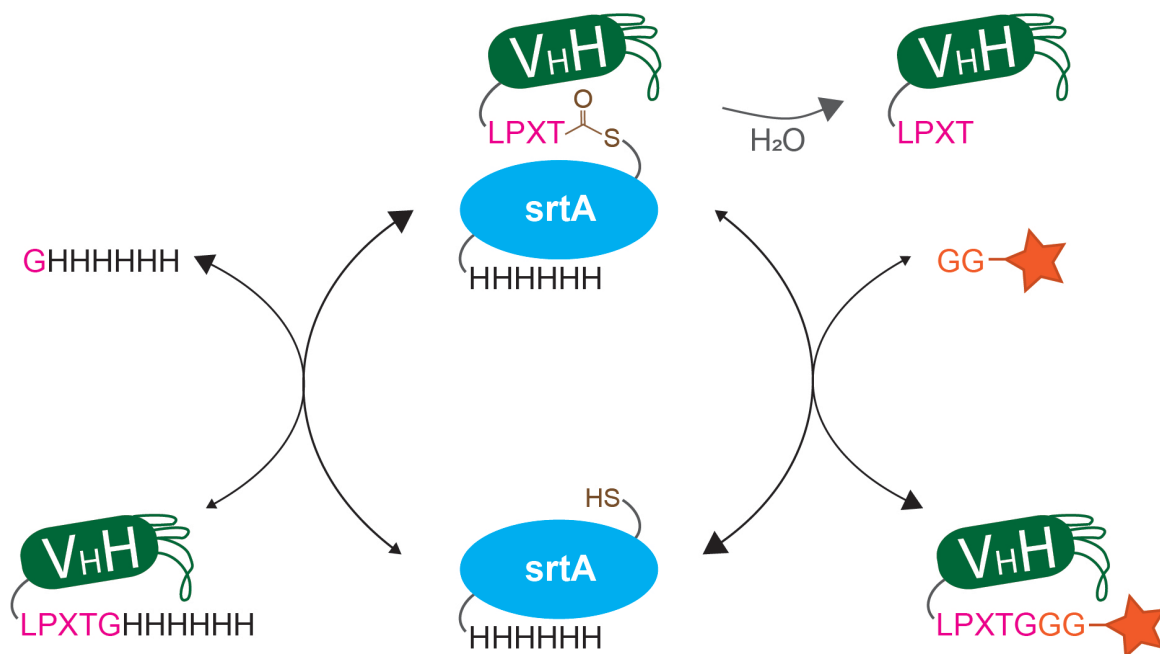


Figure 8 The srtA reaction cycle for Nb functionalization. SrtA reacts with the sortag (pink) close to the C-terminus of the Nb, resulting in the formation of a Nb-srtA thioester intermediate and the loss of the Nb's C-terminal His-tag (left side). A glycosylated substrate (orange) serves as the nucleophile and is conjugated by srtA to the sortag, leading to the release of the enzyme which is ready to enter the next cycle (right side). If too little substrate is available, water can act as a nucleophile, yielding hydrolyzed Nb as a side product. Note that both the unconjugated Nb and srtA carry C-terminal His-tags but the Nb conjugate does not, allowing straightforward purification of the desired product via affinity chromatography. As the reaction is reversible, an excess of unconjugated Nb and substrate is required to facilitate the desired (clockwise) reaction direction yielding functionalized Nb.

1.5. Aims of this study

Both TACAs and aberrant surface thiols are promising classes of tumor biomarkers. Although they play important roles in tumor proliferation and metastasis, the tools to study these biomarkers are meager and insufficient. Due to the challenges in anti-TACA Ab development, Abs against defined glycan structures are still rare. Nbs show great potential for tumor diagnostics and therapeutics due to their small size and deeper tumor penetration but methods to specifically develop glycan-binding Nbs are not available so far. With this work, I aimed to **establish a general workflow for immunization with TACA glycoconjugates to raise TACA-binding hcAbs in alpaca** (Figure 9). Therefore, I developed the following subgoals:

- Generating TACA glycoconjugates for alpaca immunization (A1)
- Proving the induction of TACA-specific hcAbs in the serum of the immunized alpaca (A2)

Anti-glycan hcAbs were the basis for the development of Nbs binding to the TACA Globo-H, proving the feasibility of the workflow.

While screening Nb candidates for cancer cell binding, I identified an unusual Nb, called CB2, which recognized B cell lymphoma cancer cells with high specificity but none of the TACAs used for alpaca immunization. Surprisingly, I found that CB2 binds cancer cells in a thiol-dependent manner. Due to the important role of surface thiols in cancer biology, my main goal was to **show the applicability of thiol-binding CB2 for targeting B cell lymphoma by generating functionalized versions of CB2** (Figure 9). Specifically, I wanted to address the following key questions:

- Can CB2 be used for Ab recruitment? (B1)
- Is CB2 capable of thiol-mediated internalization? (B2)
- If CB2 internalizes, can internalization be exploited for drug delivery? (B3)
- Can CB2 also be used to target other thiol-rich cell surfaces, for instance, breast cancer cells or the protozoan parasites *Plasmodium* and *Leishmania*? (B4)

Ultimately, this thesis aimed to expand the toolbox for targeting TACAs and surface thiols on cancer cells. By establishing a workflow for glycoconjugate immunization of alpacas, this work forms the basis for Nb development against a variety of TACAs. Introducing the first thiol-binding Nb CB2, I demonstrated the applicability of thiol-binding proteins in cancer therapy and identified a novel internalization mode for Nbs, paving the way for the exploitation of surface thiols for diagnostics and therapeutics.

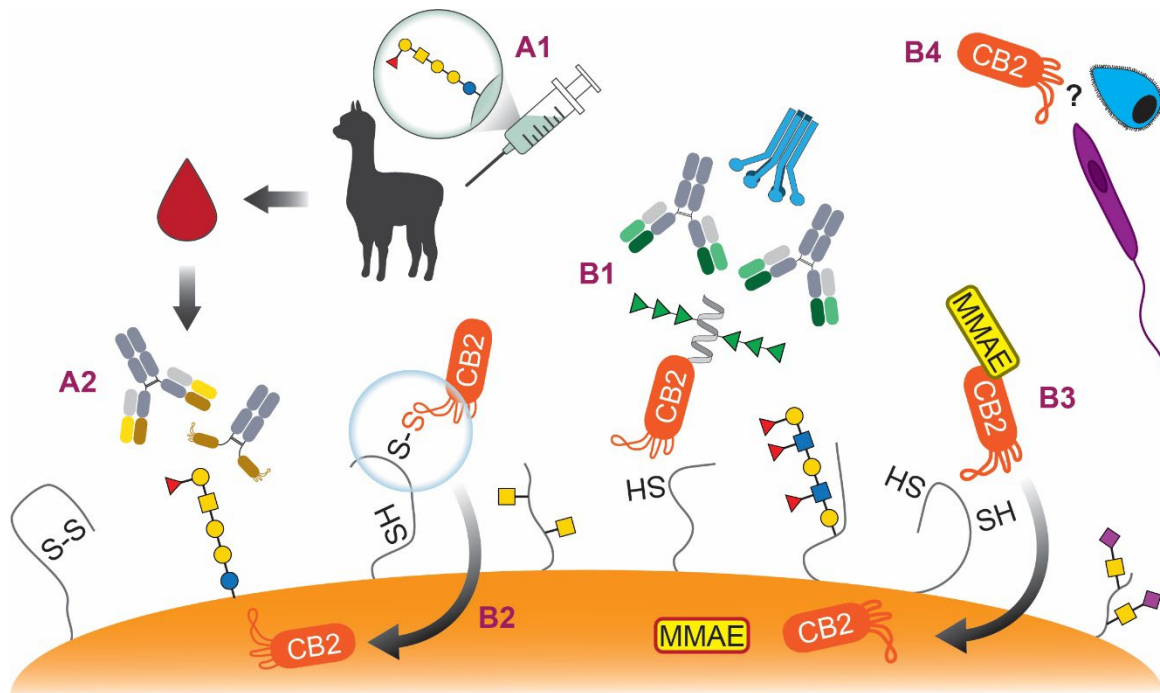


Figure 9 Aims of this study. TACAs and aberrant surface thiols both represent biomarkers on the surface of cancer cells. They have in common that available tools targeting them are rare. This thesis aimed to establish a general workflow for immunization with TACA glycoconjugates (A1) to raise TACA-binding conventional Abs and hcAbs in alpacas (A2). As part of this work, I also discovered and characterized an unusual Nb called CB2 which binds to cancer cells in a thiol-dependent manner. Here, my key aim was to show the applicability of CB2 and thiol-binding Nbs by generating differently functionalized versions of CB2. First, I set out to examine a potential use of rhamnosylated CB2 in Ab recruitment and complement activation (B1). In addition, I aimed to investigate whether CB2 is capable of thiol-mediated internalization (B2) and whether internalizing CB2 can be employed to deliver drugs such as monomethyl auristatin E (MMAE) to cancer cells (B3). Finally, I explored CB2 recognition of other cancer types and protozoan parasites with thiol-rich surfaces (B4).

2. Materials and Methods

2.1. Induction of hcAbs in alpaca

2.1.1. Conjugation of glycans to CRM₁₉₇

All synthetic glycans selected for immunization were previously synthesized in our department using established solution-phase protocols or automated glycan assembly^{133–135}. All compounds carried an aminopentanol linker at the reducing end which was used for conjugation to CRM₁₉₇ following established protocols^{136,137}. Briefly, one eq. of glycan was mixed with 10 eq. of homobifunctional bis(*p*-nitrophenyl) adipate in 300 μ L dimethyl sulfoxide (DMSO) + 25 μ L pyridine + 10 μ L triethylamine (TEA) and stirred for 3 h at 300 rpm, RT (Figure 10). After lyophilization, the glycan half ester was washed thrice with chloroform and thrice with dichloromethane until uncoupled linker was no longer detected in the wash fractions by UV light. For that purpose, all wash fractions were spotted onto a silica plate. After UV analysis, the absence of glycan in the wash fractions was also confirmed by incubating the silica plate with staining solution (3.7 mL of *p*-anisaldehyde in 140 mL of 3.5 % H₂SO₄ in ethanol) and then drying the plate with a heat gun.

Meanwhile, 1 mg of CRM₁₉₇ (Reagent Proteins) was brought into conjugation buffer (0.1 M sodium phosphate pH 8) on an Amicon® Ultra centrifugal filter unit (MWCO = 10 kDa). Then, 70 eq. of washed glycan half ester were mixed with one eq. of CRM₁₉₇ in 140 μ L conjugation buffer and stirred for 24 h at 70 rpm, RT (Figure 10). The buffer of the glycoconjugates was changed to sterile PBS (PAN-Biotech) on an Amicon® Ultra centrifugal filter units (MWCO = 10 kDa) and the protein concentration was measured at 280 nm by NanoDrop® ND-1000.

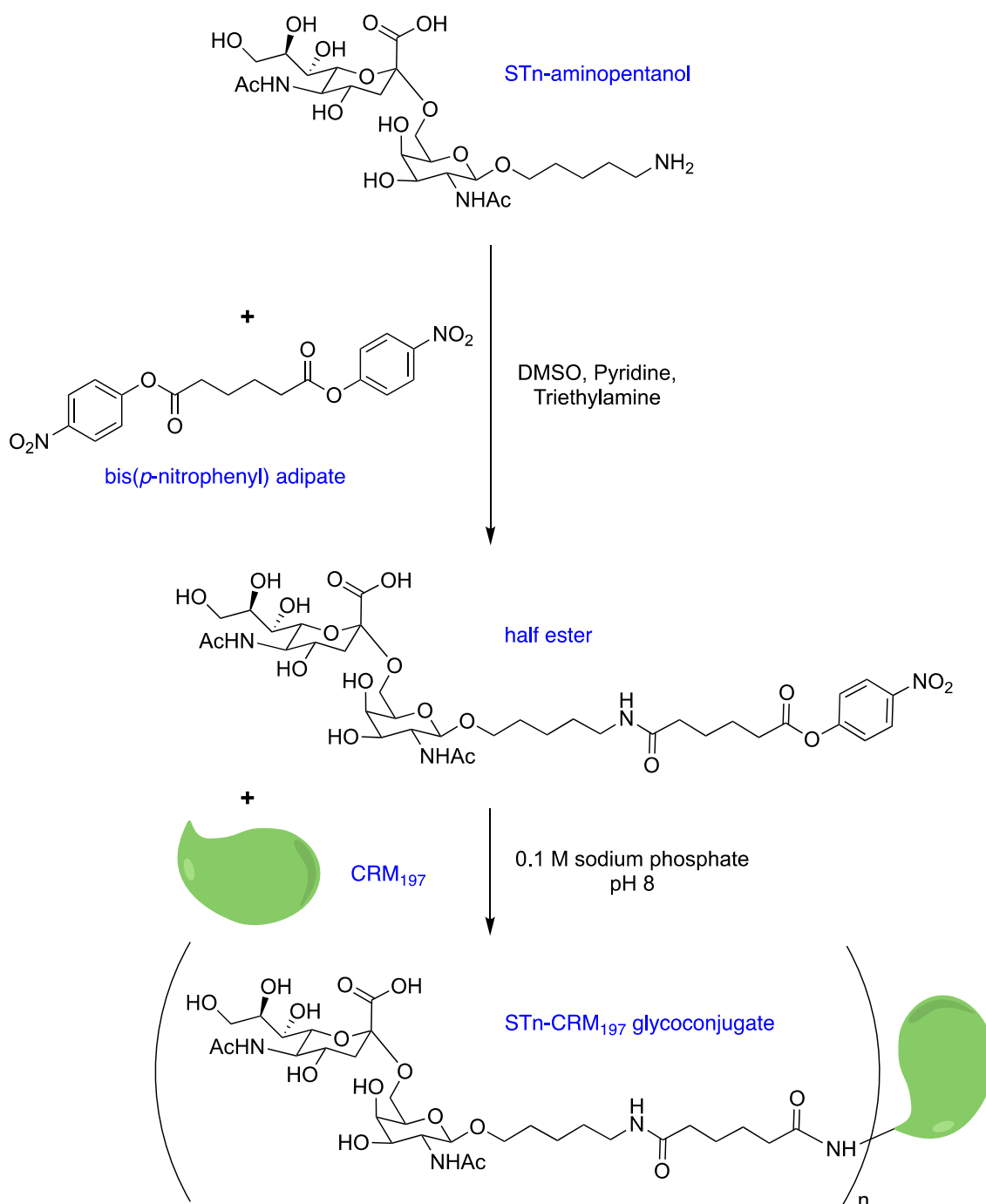


Figure 10 Conjugation of STn to CRM₁₉₇. First, STn-aminopentanol was coupled to bis(*p*-nitrophenyl) adipate. Next, the resulting “half ester” was conjugated to lysine side chains of CRM₁₉₇ under basic conditions, yielding STn-CRM₁₉₇ glycoconjugates. The same workflow was used to generate CRM₁₉₇ conjugates of Globo-H, KH-1, and Tn. DMSO = dimethyl sulfoxide, CRM₁₉₇ = cross-reactive material 197.

The degree of loading (DOL) was assessed by matrix-assisted laser desorption/ionization time of flight (MALDI-TOF) mass spectrometry, comparing unconjugated and glycan-conjugated CRM₁₉₇. Briefly, protein was mixed with 2,5-dihydroxyacetophenone and spotted onto an MTP 384 steel plate. Spectra were recorded on an Autoflex Speed (Bruker Daltonics) with the help of Dr. Maria Bräutigam in linear positive ion mode between 25,000 and 210,000 m/z. The DOL was calculated using the following equation (1):

$$DOL = \frac{m(\text{glycoconjugate}) - m(\text{unconjugated CRM})}{m(\text{adipic linker} + \text{glycan})} \quad (1)$$

2.1.2. Alpaca immunization

The alpaca was treated strictly according to German and European Law and the experiment was approved by the Office for Health and Social Affairs Potsdam, Brandenburg (LAVG) (Permit 2347-A-30-1-2018). One day before immunization, the different glycoconjugates were mixed and added 1:1 (v:v) to aluminum hydroxide Al(OH)₃ (Alhydrogel). To allow adsorption to the Al(OH)₃ adjuvant, samples were rotated o/n at 4 °C. Since the DOL varied between glycans, different doses were injected for each glycan (Table 1).

Table 1. Degree of loading and glycan dose/injection for the different CRM₁₉₇ glycoconjugates. The DOL and glycoconjugate yield determined the available glycan dose/injection.

Glycan	DOL	Glycan dose (µg)/injection
Globo-H	3.5	4
KH-1	12	16
STn	6.3	7.8
Tn	4.2	12.8

An adult male alpaca at the age of 10 was injected subcutaneously along the base of the neck for a total of six consecutive immunization rounds on days 0, 7, 14, 28, 37 and 45 (Figure 11). Whole blood (300 mL) was extracted for serum and PBMC isolation eight

days after the last immunization, on day 53. Before each immunization, 10 mL of blood were drawn for serum isolation (Figure 11). Briefly, whole blood was incubated at RT for 1 h to allow clotting and centrifuged at 2,000 g for 10 min at RT, yielding the serum in the supernatant. Serum was aliquoted and flash-frozen for long-term storage at -80 °C.

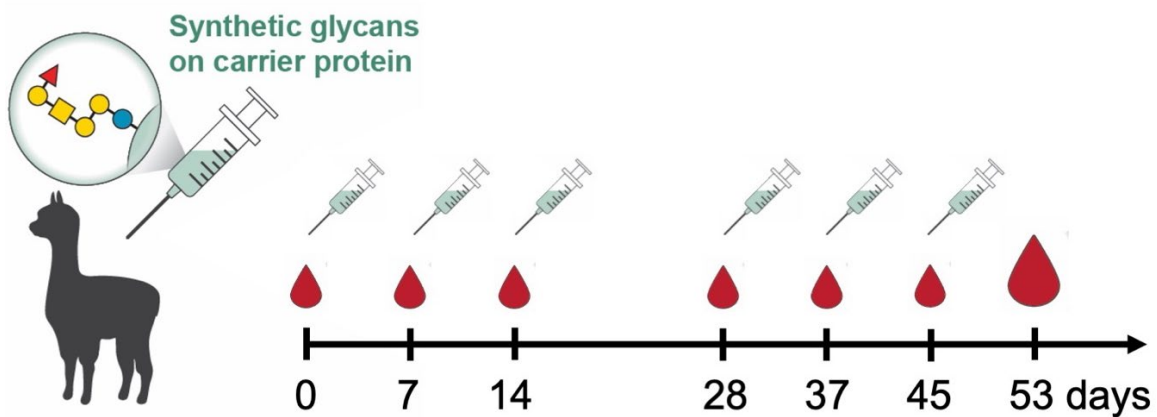


Figure 11 Immunization regime. The alpaca was immunized with the glycoconjugate mixture adsorbed onto an aluminum hydroxide matrix six times over the course of six weeks. Each injection is indicated by a syringe symbol. Each time, 10 mL of blood were also extracted (small blood drops) to assess serum Ab titers. After 53 days, 300 mL of blood were taken (big blood drop) for PBMC isolation.

2.1.3. IgG subtype fractionation

Six mL of glycan-immunized alpaca serum were mixed in a 1:1 ratio with 20 mM sodium phosphate buffer and fractionated by differential absorption on Protein A and Protein G columns (Pierce) as described elsewhere¹³⁸ (Figure 12). First, serum is adsorbed onto the Protein G column and IgG3 is eluted with 0.15 M NaCl, 0.58 % acetic acid at pH 3.5. Then, IgG1 is eluted with 0.1 M glycine-HCl at pH 2.7. Finally, the flow-through of the Protein G column is adsorbed onto the Protein A column and IgG2 is eluted with 0.15 M NaCl, 0.58 % acetic acid at pH 4.5 (Figure 12). The individual IgG subtypes were brought into PBS by size exclusion chromatography with a Superdex 200 10/300 column (Cytiva).

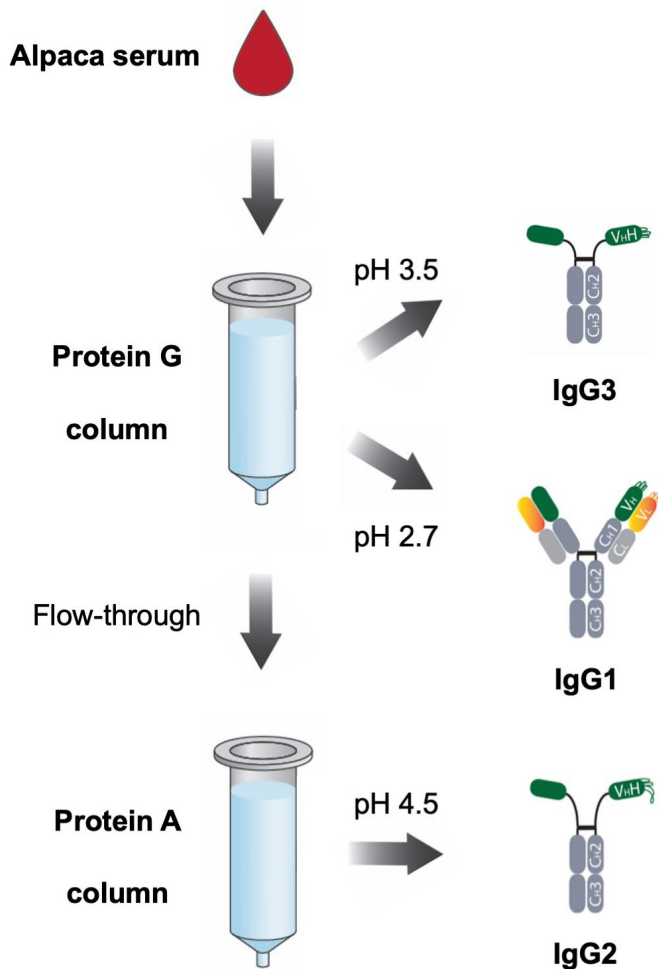


Figure 12 Fractionation of alpaca IgG subtypes. Alpaca serum is first passed over a Protein G affinity column, and IgG3 and IgG1 Abs are sequentially eluted at a pH of 3.5 and 2.7, respectively. The flow-through of the Protein G column is then added onto a Protein A affinity column and IgG2 Abs are eluted at a pH of 4.5.

2.1.4. Sodium dodecyl sulfate-polyacrylamide gel electrophoresis

Successful IgG subtype purification was confirmed by sodium dodecyl sulfate-polyacrylamide gel electrophoresis (SDS-PAGE)¹³⁹ and Western Blot using a MiniProtean system (Bio-Rad). Briefly, a separating gel (375 mM Tris-HCl pH 8.8, 10 % or 15 % of 37.5:1 acrylamide:bisacrylamide, 0.1 % sodium dodecyl sulfate, 0.1 % ammonium persulfate, 0.04 % tetramethylethylenediamine) and a stacking gel (125 mM Tris-HCl pH 6.8, 5 % of 37.5:1 acrylamide:bisacrylamide, 0.1 % sodium dodecyl sulfate, 0.1 % ammonium persulfate, 0.1 % tetramethylethylenediamine) were consecutively poured into an assembled glass chamber (spacing = 1 mm). Two μg of each IgG subtype were mixed with 5x SDS-loading buffer (250 mM Tris-HCl pH 6.8, 5 % β -mercaptoethanol, 50 % glycerol, 10 % SDS), boiled for 5 min at 95 °C and loaded into different wells of the stacking gel. Four μL of PageRuler Plus Prestained Protein Ladder (ThermoFisher) were included as a size marker. The gel and running chamber

were filled with running buffer (25 mM Tris-HCl pH 8.3, 192 mM glycine, 1 % SDS) and the proteins were separated at 120 V, 25 mA until the dye front reached the bottom of the gel. The gel was then either used for western blot (2.1.5) or direct protein staining. The latter was achieved by incubating the gel with Coomassie Brilliant Blue G250 (70 μ M Coomassie in 40 mM HCl) and boiling it for 5 s followed by 5 min shaking at RT. Excess dye was removed by washing the gel thrice with water, boiling it once more and incubating it on the shaker for another 30 min. The gel was analyzed on a Gel Doc EZ imaging system (BioRad).

2.1.5. Western blot

Alternatively, proteins were transferred after SDS-PAGE from the gel onto a ready-to-use Trans-Blot Turbo Mini 0.2 μ m PVDF membrane (Bio-Rad) using a Trans-Blot Turbo Transfer System (Bio-Rad). The membrane was blocked for 1 h with 5 % milk powder in TBST and then incubated with goat anti-llama IgG (H+L) HRP Ab (Invitrogen, diluted 1:5000 into 5 % milk powder in TBST) for 1 h. After washing thrice with TBST, the membrane was developed with AmershamTM ECL solution (Cytiva), following the manufacturer's protocol, and imaged using a LAS-4000 mini Image Reader (Fujifilm) with incremental acquisition every 10 s in chemiluminescence mode.

2.1.6. Glycan array

Synthetic glycans (0.2 mM) were dissolved in 50 mM sodium phosphate buffer (pH 8.5) and printed by Katrin Sellrie on glass slides coated with epoxy for amine/thiol-functionalized glycans or *N*-hydroxyl succinimide ester for amine-functionalized glycans (Codelink®, SurModics Inc, USA), using a piezoelectric spotting device (S3, Scienion)¹⁴⁰. After 24 h in a humid chamber at room temperature, slides were quenched with 50 mM ethanolamine solution (pH 9) for 1 h at 50 °C. Ab titers in alpaca serum were measured by glycan array as described previously¹⁴¹: The slides were assembled onto microplate holders, and wells were blocked in PBS + 1 % BSA for 1 h. Blocked wells were incubated with 50 μ L of alpaca serum (1:50) or PBS for 1 h at RT. Alternatively, for examination of IgG subclasses, wells were incubated with 25 μ L of

IgG1, 2 and 3 (0.2 mg/mL) in duplicates in three independent experiments. Wells were washed thrice with PBS and incubated with 25 μ L of anti-llama FITC Ab (1:200, Invitrogen) for 1 h at RT in the dark. Wells were washed thrice with PBST, once with ddH₂O, and dried by centrifugation (100 g, 2 min). After removal of the multi-well grid, the slide was scanned with an Axon GenePix[®] 4300A scanner (Molecular Devices) and results were analyzed using GenePix Pro 7 (Molecular Devices).

2.2. Cell culture

All cell lines were tested for mycoplasma contamination on a monthly basis.

2.2.1. Lymphoma cell lines

All B cell lymphoma cell lines, except for SC-1, were a kind gift by Dr. Uta Hoepken and Dr. Armin Rehm (MDC Berlin). SC-1 cells were acquired from DSMZ. B cell lymphoma cell lines were cultured in RPMI + 10 % FCS + 2 mM glutamine + 1 mM sodium pyruvate + 1x penicillin/streptomycin (all reagents from PAN-Biotech) at 37 °C, 5 % CO₂. Cells were diluted into fresh medium every 2-3 days.

2.2.2. PBMC isolation

Human PBMCs were isolated from whole blood from healthy donors¹⁴² (DRK Nordost). Therefore, blood was mixed 1:1 with pre-warmed RPMI and carefully layered onto 15 mL of Pancoll separating solution (PAN-Biotech) in a 50 mL conical tube. After centrifugation at 800 g, RT for 25 min without brake, the mononuclear cell layer was transferred into a new conical tube. Cells were washed thrice with RPMI at 300 g, 4 °C for 10 min, each time discarding the supernatant. Remaining erythrocytes were removed by resuspension of the cell pellet in RBC lysis buffer (eBioscience, Invitrogen) and incubation for 5 min. After one more wash with RPMI, cells were counted and either directly used for binding assays or frozen in 90 % FCS + 10 % DMSO using a Mr. Frosty[™] freezing container (ThermoFisher).

2.2.3. *Plasmodium falciparum*

Blood stages of *P. falciparum* were cultured as described elsewhere¹⁴³. Briefly, parasites were maintained at 1-10 % parasitemia and 1 % hematocrit in growth medium (RPMI + 25 mM HEPES + 0.5 % AlbuMAX + 100 μ M hypoxanthine + 2 mM glutamine + 12.5 μ g/mL gentamicin sulfate) at 5 % CO₂, 37 °C. Parasitemia was assessed every 2-3 days by blood smears: 5 μ L of sedimented blood cells were smeared onto a microscope glass slide using a second glass slide at an angle of approx. 30°. After fixation with methanol for 30 s, the blood smear was stained with 6 % Giemsa stain (PanReac AppliChem) for 15 min. Then, the glass slide was washed with H₂O, air-dried and parasites were counted manually under the microscope. The culture was split by pelleting the parasitized blood at 300 g for 5 min, diluting with uninfected erythrocytes from healthy donors (blood factor 0+, DRK Nordost) and resuspending in fresh growth medium.

2.2.4. Breast cell lines

MCF-7 cells and HEK cells were cultured in DMEM + 10 % FCS + 2 mM glutamine + 1x penicillin/streptomycin at 37 °C, 5 % CO₂. MCF-10A cells were cultured in DMEM/F12 (1:1) + 5 % horse serum + 20 ng/mL EGF + 0.5 mg/mL hydrocortisone + 100 ng/mL cholera toxin + 10 μ g/mL insulin + 2 mM glutamine + 1x penicillin/streptomycin at 37 °C, 5 % CO₂. Cell lines were passaged and diluted every 3-4 days when confluent using trypsin/EDTA (PAN-Biotech).

2.3. Surface thiol quantification

One million PBMCs or SC-1 cells were pelleted and incubated with AF647-maleimide (1:1,000, Jena Bioscience) or PBS for 15 min in the dark on ice to prevent cellular uptake⁶². Cells were washed thrice with PBS and analyzed by flow cytometry. An additional sample was prepared the same way and mounted on a microscopy slide to confirm that AF647-maleimide only stains the cell membrane but not intracellular compartments. The mean fluorescence intensity (MFI) from three independent FACS

experiments was quantified and normalized to the MFI of SC-1 cells (100 %) via equation (2). Differences between healthy lymphocytes and SC-1 cells from three independent experiments were tested for significance using student's t-test in OriginPro (version 2021b).

$$\text{Normalized MFI} = \frac{\text{MFI}(x)}{\text{MFI}(\text{SC-1})} \cdot 100 \quad (2)$$

2.4. CB2 characterization

2.4.1. Nanobody expression and purification

The DNA sequence of CB2 was synthesized by Synbio Technologies with a C-terminal section encoding a glycine-serine linker ([G4S]₃) followed by a sortag (LPETG) and a His₆ tag, and provided in a pET-28b(+) vector. The plasmid, carrying a kanamycin resistance gene, was transformed via heat-shock for 30 s at 42 °C into chemically competent *E. coli* SHuffle cells (NEB) which facilitate disulfide bond formation despite cytosolic expression. In the evening, 10 mL of lysogeny broth (LB) + 50 µg/mL kanamycin were inoculated with transformed *E. coli* and incubated at 37 °C o/n. The next day, the LB starter was diluted into 1 L of terrific broth (TB) + 50 µg/mL kanamycin and the culture was incubated at 37 °C, monitoring the optical density at 600 nm (OD₆₀₀) every 30 min. At OD₆₀₀ = 1.2-1.5, protein expression was induced by addition of 0.5 mM IPTG and incubation at 16°C o/n. After pelleting the bacteria at 6,000 g, 4 °C for 15 min, the pellet was resuspended in 20 mL sample buffer (40 mM sodium phosphate pH 8, 150 mM NaCl, 10 mM imidazole, 0.75 mM DTT, 1:100 SERVA protease inhibitor mix HP) and lysed by passing the suspension twice through the French press (Emulsiflex C3) at 10,000-15,000 psi. After centrifugation at 42,000 g, 4 °C for 45 min, the supernatant containing soluble CB2 was filtered through a 0.22 µm filter onto 1 mL of equilibrated HisPur Ni-NTA agarose (Pierce) beads and rotated for 1 h at 4 °C. Beads were washed with 20 mL sample buffer, 20 mL wash buffer 1 (40 mM sodium phosphate pH 8, 1 M NaCl, 10 mM imidazole, 0.75 mM DTT) and 20 mL wash buffer 2 (40 mM sodium phosphate pH 8, 150 mM NaCl, 30 mM imidazole, 0.75 mM DTT). CB2 was

eluted by incubation for 15 min with 20 mL elution buffer (40 mM sodium phosphate pH 8, 150 mM NaCl, 300 mM imidazole, 0.75 mM DTT) and further purified by size exclusion chromatography (SEC) on an ÄKTApurifier with a Superdex 75 16/600 column (Cytiva). All steps of the nanobody purification workflow and SEC fractions were examined by SDS-PAGE as described in 2.1.4. CB2-containing fractions were pooled, concentrated via Amicon® Ultra centrifugal filter units (MWCO = 3 kDa) and aliquoted for snap-freezing and long-term storage at -80 °C.

2.4.2. Site-directed mutagenesis

The C^{105S}CB2 mutant was generated in-lab via overlap extension polymerase chain reaction (PCR) as described elsewhere¹⁴⁴. First, two separate PCRs were performed with T7 forward + C105S reverse and C105S forward + T7 reverse primers (Table 2), using the wildtype CB2 plasmid as a template. The two PCR products were then combined by overlap extension in a third PCR¹⁴⁴. Both the overlap extension PCR product and the wildtype CB2-containing pET28b(+) plasmid were digested for 1 h at 37 °C with XbaI and XhoI (NEB) to create sticky ends for ligation. In addition, the plasmid was digested for 1 h at 37 °C with Antarctic phosphatase (NEB) to prevent re-ligation of the linearized plasmid. Digested products were purified by agarose gel electrophoresis followed by gel extraction with a NucleoSpin Gel and PCR clean-up kit (Macherey-Nagel). Using a fivefold molar excess of the insert, the sequence of the C^{105S}CB2 mutant was ligated into the pET28b(+) backbone by T4 ligase (NEB) for 1 h at RT, and the ligated plasmid was directly transformed via heat-shock into chemically competent DH5α *E. coli*. After o/n incubation at 37 °C on kanamycin-containing LB-agar plates, several colonies were used for inoculation of 10 mL LB + 50 µg/mL kanamycin. After o/n incubation of the liquid cultures at 37 °C, plasmid DNA was extracted with a NucleoSpin Plasmid kit (Macherey-Nagel) and sent for sequencing (LGC genomics) with T7 forward and T7 reverse primers to confirm successful mutagenesis.

Table 2. Primers used for site-directed mutagenesis to generate ^{C105S}CB2. DNA sequences are displayed 5' → 3'. All primers were ordered from IDT.

Name	Sequence
T7 forward	TAATACGACTCACTATAG
T7 reverse	GCTAGTTATTGCTCAGCGG
C105S forward	GCCGCCTTGAATCGCTACAGCGGAAATGAG
C105S reverse	CATATTCATACTCATTTCGGCTGTAGCGAT

2.4.3. Nuclear magnetic resonance measurements of CB2 and ^{C105S}CB2

Both proteins were expressed in labelled M9 minimal medium (1 g/L ¹⁵N-NH₄Cl (Merck), 1 g/L NaCl, 3 g/L KH₂PO₄, 6 g/L Na₂HPO₄, pH 7.4, 2 mM MgSO₄, 100 μM CaCl₂, vitamin mix and 100 mg/L ¹⁵N-Celtone (Cambridge Isotope Laboratories)) via induction with 0.5 mM IPTG at 16 °C o/n. The proteins were purified as described in 2.4.1 and diluted into PBS buffer supplemented with 0.75 mM DTT, 8 mM NaN₃, 0.5 mM DSS and 5 % D₂O to a concentration of [CB2] = 160 μM and [^{C105S}CB2] = 70 μM.

¹H-¹⁵N HSQC spectra were acquired by Anika Freitag and Dr. Ruslan Nediellkov on a NEO 500 MHz nuclear magnetic resonance (NMR) spectrometer (Bruker) equipped with a TCI cryogenic probe head with Z gradient, using a standard pulse sequence with an acquisition time of 140 ms and 256 increments with 16 scans for CB2 and 160 scans for ^{C105S}CB2. All measurements were performed at 298 K, and total measurement time was 1 h 20 min and 13 h 30 min for CB2 and ^{C105S}CB2, respectively. The spectra were processed and analyzed using Topspin (version 4.1.4, Bruker).

2.4.4. Flow cytometry binding assay

One million cells per sample of the respective cell line or healthy PBMCs were incubated with 50 μL of nanobody solution (24 μM) or PBS for 1 h at RT, 400 rpm. After washing the cells thrice with PBS (300 g, 5 min), they were resuspended in 50 μL of

anti-6X His Tag ATTO 647N conjugated Ab (1:750, Rockland Inc.) and incubated for 1 h at RT, 400 rpm in the dark. After another three washes with PBS, stained cells were measured on a FACSCanto™ II device (BD Biosciences). The main cell population was selected via forward and sideward scatter amplitude (FSC-A and SSC-A) and events were gated for single cells via FSC-A and FSC height using the software FlowJo (V10.8.1). For qualitative data analysis, histograms of the allophycocyanin (APC) channel were generated (Figure 13). For quantification, the MFI of the APC-A signal was exported for three independent experiments and compared to examine differences in cell binding.

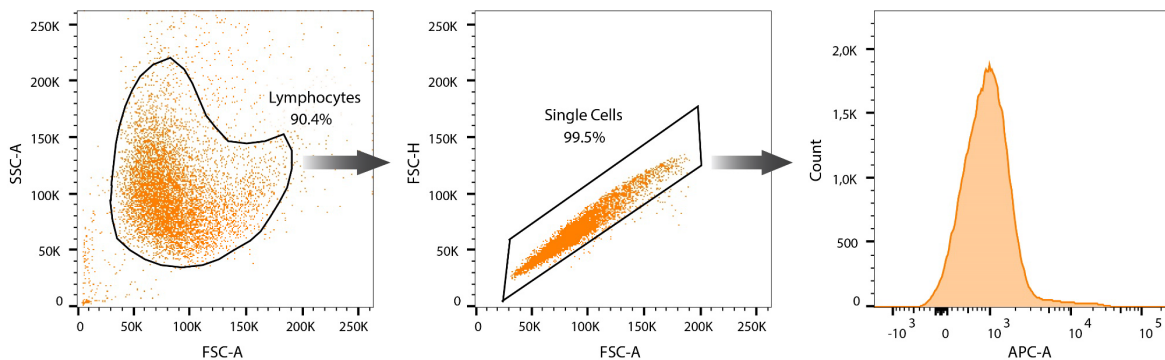


Figure 13 Gating strategy for NHL cell lines in flow cytometry. First, cell debris and small contaminants are removed by selecting the main cell population in SSC-A over FSC-A dot plots (left). Then, aggregated cells are filtered out in FSC-H over FSC-A dot plots (center). The resulting cell population is displayed as histogram of the APC-A signal (right) or used for MFI quantification. Secondary Abs with emission at 647 nm were used to examine CB2 binding which are detected in the APC channel in flow cytometry.

For binding assays with *P. falciparum*, parasites at the schizont stage were isolated by lysing infected erythrocytes for 5 min on ice with a 0.15 % saponin solution. Parasites were pelleted for 5 min at 2,000 g, 4 °C and washed thrice with PBS. The volume of the pellet was estimated, and the pellet was resuspended in 150x the volume of PBS. Of this suspension, 120 µL were used per sample and stained for flow cytometry as described above. Raw data for CB2 binding to breast cell lines were generated with the help of Zeinab Fandi and Anika Freitag using the same protocol as for lymphoma cell lines and then processed and analyzed by me.

2.4.5. Confocal microscopy binding assay

Two million cells per sample were washed once with PBS and incubated with 50 μ L of nanobody solution (24 μ M) or PBS for 1 h at RT, 400 rpm. After three washes with PBS, cells were incubated with 50 μ L anti-6X His Tag Atto 647N conjugated Ab (1:750, Rockland Inc.) for 1 h at RT, 400 rpm in the dark. Cells were washed thrice with PBS, resuspended in 1 mL PBS, and settled on 25 mm coverslips in 6-well plates for 30 min in the dark at RT. After careful aspiration of the supernatant, 750 μ L of fixative (4 % paraformaldehyde + 0.2 % glutaraldehyde in PBS) were added to each well, and cells were fixed at RT for 15 min in the dark. Coverslips were washed thrice with 1 mL PBS, flipped onto a microscopy glass slide prepared with 50 μ L of Roti®Mount FluorCare DAPI mounting solution (Carl Roth), and sealed with transparent nail polish. The slides were examined and imaged under an LSM700 laser scanning confocal microscope (Zeiss) at 63x magnification.

For quantification, the images were analyzed using Fiji (ImageJ) by manually selecting cells and then measuring their fluorescence intensity (mean grey value). The MFI was normalized to the maximum (incubation with CB2, 100 %) and minimum (incubation with PBS, 0 %) using the following equation (3):

$$\text{Normalized MFI } (x) = \frac{\text{MFI}(x) - \text{MFI}(\text{PBS})}{\text{MFI}(\text{CB2}) - \text{MFI}(\text{PBS})} \quad (3)$$

The statistical analysis was performed with the software GraphPad Prism 9.3.1 (GraphPad Software, Inc.).

To examine CB2 binding to *L. major*, fixed parasites at the promastigote stage were kindly provided by Sharareh Salehi Hossainy (Robert Koch Institute) and stained directly on cover slips with the nanobody as described above.

2.4.6. Inhibition assay with dithiothreitol

CB2 binding was generally examined as described in 2.4.4. However, incubation of SC-1 cells with CB2 was carried out in the presence or absence of 1 mM DTT and bound

Nb was detected with MonoRab™ Rabbit Anti-Camelid VHH Cocktail iFluor 647 (1:500, GenScript). Anti-CD19-PE Ab (1:100, BioLegend) was used as positive control because DTT should not affect binding of this Ab to B cells. For quantitative comparison, the fluorescence intensity was normalized to the positive control (CB2 without DTT, 100 %) via equation (4) and the normalized MFI from three independent experiments was used for significance testing in OriginPro (version 2021b).

$$\text{Normalized MFI} = \frac{\text{MFI}(x)}{\text{MFI}(\text{CB2 without DTT})} \cdot 100 \quad (4)$$

2.4.7. Inhibition assay with N-ethylmaleimide

CB2 was pre-incubated with 1.2 mM N-ethylmaleimide (NEM) for 2 h at RT followed by three washes with PBS to remove excess NEM using an Amicon® Ultra Centrifugal Filter Unit (MWCO = 10 kDa). Binding of CB2 or NEM-pre-treated CB2 was then examined as described in 2.4.4. Bound Nb was detected with MonoRab™ Rabbit Anti-Camelid VHH Cocktail iFluor 647 (1:500, GenScript). For quantitative comparison, the fluorescence intensity was normalized to the positive control (CB2 without NEM, 100 %) via equation (5) and the normalized MFI from three independent experiments was used for significance testing in OriginPro (version 2021b).

$$\text{Normalized MFI} = \frac{\text{MFI}(x)}{\text{MFI}(\text{CB2 without NEM})} \cdot 100 \quad (5)$$

2.5. CB2 functionalization

2.5.1. Synthesis of Rha₃

The automated synthesis of Rha(α1-2)Rha(α1-2)Rha-aminopentanol (Rha₃) was performed by Sabrina Lechnitz on a home-built synthesizer developed at the Max Planck Institute of Colloids and Interfaces using modules reported earlier⁵¹ (Figure 14). NMR spectra confirming the purity of the compound can be found in Figure S 1.

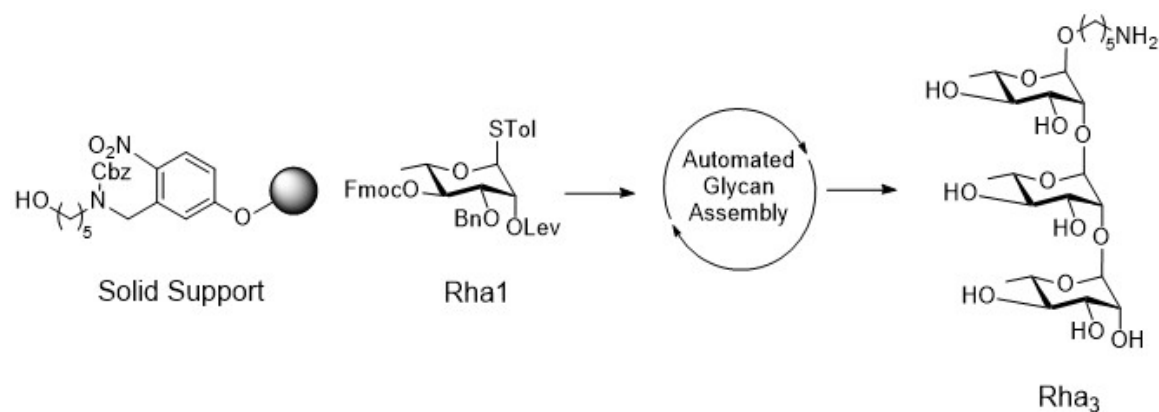


Figure 14. General workflow for the synthesis of Rha₃. Protected Rha1 is used as a building block for automated glycan assembly on a solid support. Photo-cleavage from the solid support yields the glycan with an aminopentanol linker at the reducing end which can be used for conjugation to proteins or peptides. Figure provided by Sabrina Lechnitz.

2.5.2. Synthesis of GG-Rha₃

Glycyl-N-[1-[(Rha(α1-2)Rha(α1-2)Rha)oxy]pentyl]glycinamide (hereon GG-Rha₃) was synthesized by Sabrina Lechnitz using the following protocol (Figure 15). TEA (10 μL, 0.07 mmol, 2 eq.) was dissolved in DMSO (2 mL). Rha₃ (20 mg, 0.04 mmol, 1 eq.) was dissolved in 1 mL of the TEA/DMSO mixture. NHS-activated N-Boc-glycylglycine¹⁴⁵ (18.2 mg, 0.06 mmol, 1.5 eq.) was dissolved in the remaining 1 mL of the TEA/DMSO mixture and then added dropwise to the glycan solution. The mixture was stirred for 18 h, followed by DMSO removal using a stream of nitrogen. The product was used without further purification. The residue was then dissolved at 0 °C in a mixture of TFA in CH₂Cl₂ (30 % TFA, 2 mL) and stirred for 2 h. Volatiles were removed under reduced pressure and purification by reverse-phase HPLC afforded deprotected GG-Rha₃ (6.7 mg, 0.01 mmol, 28 %) as a white solid after lyophilization. NMR spectra confirming the purity of the compound can be found in Figure S 2.

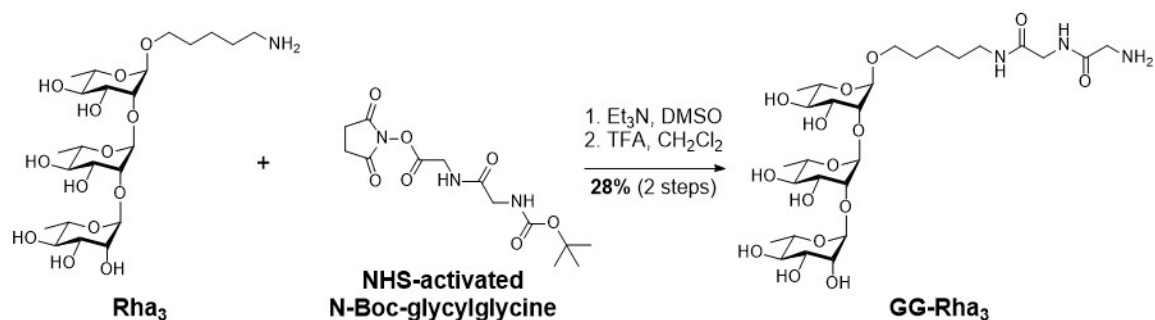


Figure 15 Synthesis of GG-Rha₃. Figure provided by Sabrina Lechnitz.

2.5.3. Conjugation of GG-Rha₃ and CB2

To conjugate GG-Rha₃ to CB2, 15 nmol of CB2, 3.75 nmol of srtA, 450 nmol of GG-Rha₃ and 40 μL of equilibrated HisPur Ni-NTA resin (ThermoFisher) were mixed in 300 μL of srtA buffer (150 mM NaCl, 10 mM CaCl₂, pH 7.5) and incubated rotating for 30 min at 4 °C. Resin was pelleted (700 g, 2 min) and the supernatant was checked for the presence of CB2-Rha₃ by SDS-PAGE and MALDI-TOF and brought into PBS via Amicon® Ultra centrifugal filter units (MWCO = 10 kDa).

2.5.4. Conjugation of Rha₃ and thFF03

To achieve multivalent display of Rha₃ while maintaining CB2 binding activity, a glycopeptide for conjugation to CB2 was generated. Specifically, Rha₃ was coupled to the synthetic peptide thFF03 (synthesized by ProteoGenix) with the sequence GGGLKKELAALKKELAALKK (Figure 16). The peptide thFF03 is a truncated, glycosylated version of the previously published hFF03¹⁴⁶ and was chosen because its many lysines allow for chemical conjugation, while the N-terminal glycines make it amenable to srtA conjugation. Rha₃ with an aminopentanol linker was conjugated to thFF03 following the protocol described in 2.1.1. Briefly, one eq. of Rha₃ was mixed with 10 eq. of homobifunctional bis(*p*-nitrophenyl) adipate in 300 μL DMSO + 25 μL pyridine + 10 μL triethylamine and stirred for 3 h at 300 rpm, RT. After lyophilization, Rha₃ half ester was washed thrice with a 1:1 mixture of diethyl ether and dichloromethane and thrice with a 1:4 mixture of the same solvents until uncoupled

linker was no longer detected in the wash fractions by UV light. Then, 6 eq. of Rha₃ half ester were mixed with one eq. of thFF03 in 140 µL conjugation buffer (0.1 M sodium phosphate pH 8) and stirred for 24 h at 70 rpm, RT. Successful conjugation and DOL was assessed by MALDI-TOF and the glycopeptide (hereon Rha-thFF03) was purified by HPLC on a C18 column (gradient from 90 %:10 % water:acetonitrile to 100 % acetonitrile). Peptide-containing fractions were identified by absorbance at 214 nm (A₂₁₄, peptide bonds), analyzed by MALDI-TOF, pooled, and lyophilized.

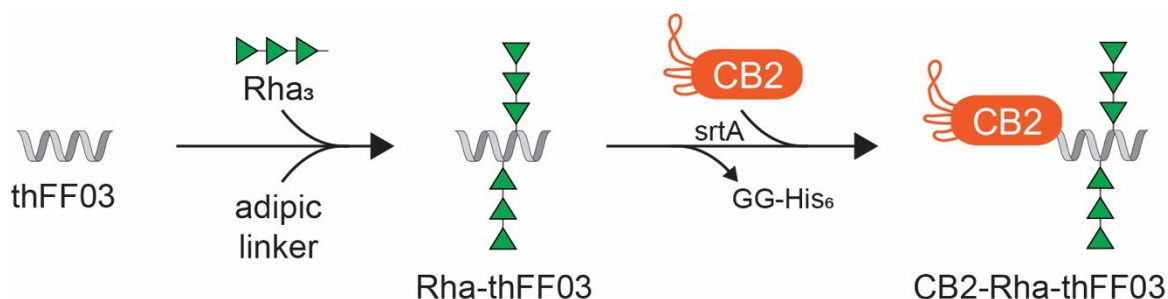


Figure 16 Generation of CB2-Rha-thFF03. First, several Rha₃ moieties are coupled to the synthetic thFF03 peptide via adipic linkers as described in 2.1.1. In a second step, the resulting Rha-thFF03 glycopeptide was coupled to CB2 in a srtA reaction, yielding CB2-Rha-thFF03.

2.5.5. Conjugation of CB2 and Rha-thFF03

In a second step, Rha-thFF03 was conjugated to CB2 via srtA coupling (Figure 16). Therefore, 15 nmol of CB2, 3.75 nmol of srtA, 406 nmol of Rha-thFF03 and 40 µL of equilibrated HisPur Ni-NTA resin (ThermoFisher) were mixed in 300 µL of srtA buffer (150 mM NaCl, 10 mM CaCl₂, pH 7.5) and incubated rotating for 30 min at 4 °C. Resin was pelleted (700 g, 2 min) and the supernatant was checked for the presence of CB2-Rha-thFF03 by SDS-PAGE and MALDI-TOF and brought into PBS via Amicon® Ultra centrifugal filter units (MWCO = 10 kDa).

2.5.6. Ab purification from human serum

Human IgG/IgM Abs were purified from human serum (Seraclot, PAN-Biotech) via Protein A/G column (ThermoFisher). Briefly, human serum was filtered through a 0.45 µm filter and diluted 1:1 with PBS. Diluted serum was loaded onto the column by circulation in a closed loop o/n at a flow rate of 0.5 mL/min. The next day, the column

was washed with PBS until absorbance at 280 nm (A_{280}) reached zero. Column-bound Abs were eluted with 0.1 M glycine (pH 2) into fraction collector plates prepared with sufficient amounts of 2 M Tris-HCl (pH 8) to directly neutralize the acidic glycine buffer. Abs were dialyzed o/n using 5 L of PBS and the concentration was measured via A_{280} . The presence of Rha-binding Abs was detected by glycan array (performed by Emelie Reuber as described in 2.1.5) using the purified Abs (1:100 in PBS + 1 % BSA) followed by goat anti-human IgG (H+L) AlexaFluor 647 (1:400, Invitrogen) and goat anti-human IgM (μ chain) AlexaFluor 488 (1:400, Invitrogen) for detection. Statistical analysis was performed with the software GraphPad Prism 9.3.1.

2.5.7. Complement activation assay

Human IgG/IgM Abs (0.2 mg/mL) were mixed with CB2, CB2-Rha3 or CB2-Rha-thFF03 (0.4 mg/mL) and incubated for 1 h at RT. Two aliquots of one million SC-1 cells each were incubated with the CB2, CB2-Rha3 or CB2-Rha-thFF03 Ab mixtures for 1 h at RT, 400 rpm. Two samples incubated with goat anti-human IgG Ab (0.24 mg/mL, Invitrogen) were included as positive controls because this Ab binds to the surface IgGs of B cell lymphoma. After 1 h incubation, cells were pelleted, resuspended in 50 μ L of active or heat-inactivated (30 min at 56 °C) rabbit complement (Cedarlane) and incubated for 2 h at 37 °C. Cells were again pelleted, resuspended in 200 μ L of 7-aminoactinomycin D (7-AAD, 1:100, BioLegend) and cell viability was measured on a FACSCanto II (BD Bioscience). To allow the comparison between individual experiments, the percentage of dead cells (p) was converted into normalized CDC (%) using equation (6) with negative control = unconjugated CB2 + heat-inactivated complement and positive control = anti-IgG Ab + active complement:

$$\text{Normalized CDC (\%)} = \frac{p(x) - p(\text{negative control})}{p(\text{positive control}) - p(\text{negative control})} \cdot 100 \quad (6)$$

2.5.8. Cy3 conjugation

Cyanine 3 (Cy3) conjugates were prepared by modifying a previously published protocol¹⁴⁷. First, 100 μ M CB2 or ^{C105S}CB2, 25 μ M srtA and 3 mM dibenzocyclooctyne-

amine (DBCO-NH₂) were mixed in 1.2 mL srtA buffer (150 mM NaCl, 10 mM CaCl₂, pH 7.5) for 30 min at 4° C with 180 µL Ni-NTA resin on a rotation wheel. This step functionalizes the sortagged Nb with DBCO (Figure 17). The supernatant containing CB2-DBCO or ^{C105S}CB2-DBCO was collected, and remaining DBCO-NH₂ was removed using a PD MidiTrap™ G-10 column (Cytiva). Meanwhile, the beads were incubated with srtA buffer + 300 mM imidazole to elute any remaining proteins. Nb-DBCO conjugate was concentrated via Amicon® Ultra centrifugal filter units (MWCO = 3 kDa) at 4 °C, 3,200 g and concentrations were determined by A280 with a NanoDrop® ND-1000. Supernatant before and after G-10 column as well as the eluate were analyzed via SDS-PAGE as described in 2.1.4 to validate the purity of the conjugate before proceeding with the click reaction.

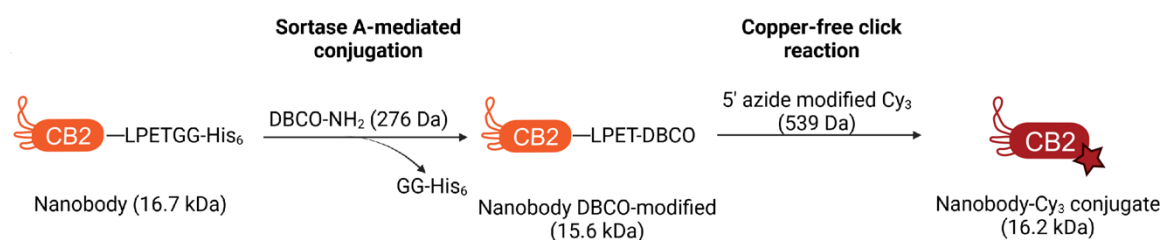


Figure 17 Conjugation of CB2 and Cy3. In the first step, sortagged CB2 is functionalized with DBCO using srtA-mediated conjugation. Note that although DBCO-NH₂ is not glycylylated, srtA is sufficiently promiscuous to accept this as substrate when used in large excess. In the second step, CB2-DBCO reacts with Cy3-azide via click chemistry, yielding the final product CB2-Cy3. The same workflow was used to generate ^{C105S}CB2-Cy3.

Next, 40 µM CB2-DBCO or ^{C105S}CB2-DBCO conjugate were incubated with 80 µM Cy3-azide (Jena Bioscience) in click reaction buffer (20 mM HEPES pH 7.5, 300 mM NaCl and 10 % glycerol) for 17 h in the dark to conjugate the dye to the Nb (Figure 17). Unbound Cy3-azide was removed using a PD MidiTrap™ G-10 column (Cytiva). Successful labeling was again verified by SDS-PAGE, examining the unstained and Coomassie-stained gel. The DOL was quantified based on the intensity of Coomassie-stained bands on the gel with ImageLab (version 6.1). Furthermore, binding of the conjugates was compared to unconjugated CB2 via flow cytometry as described in 2.4.4,

detecting bound Nb both via secondary Abs and via Cy3 fluorescence. After validating cell binding, the conjugates (CB2-Cy3 or ^{C105S}CB2-Cy3) were stored at 4°C and used for internalization assays within two weeks.

2.5.9. Internalization assay

To examine internalization, 1.5 million SC-1 cells were incubated with 100 µL of CB2-Cy3 or ^{C105S}CB2-Cy3 (30 µM) for 2 h at RT, 400 rpm in the dark. For endocytosis inhibition assays, cells were pre-treated for 30 min with 80 µM dynasore or chlorpromazine and then incubated with CB2-Cy3 in the presence of the respective inhibitor. Next, cells were pelleted, washed once with 1 mL ice-cold acidic wash buffer (100 mM glycine, 150 mM NaCl, pH 2.2) to remove surface-bound protein, and twice with PBS. Cell pellets were resuspended in 250 µL PBS and settled onto 12 mm coverslips for 30 min at RT in the dark. The suspension was carefully aspirated, and cells were fixed with 250 µL fixative (4 % paraformaldehyde + 0.2 % glutaraldehyde in PBS) for 15 min at RT in the dark. Coverslips were washed thrice with PBS, mounted onto a drop of Fluoromount G (ThermoFisher), sealed with nail polish, and stored in the dark till imaging.

For quantification of internalization, > 160 cells per condition from three independent experiments were manually selected and the mean grey value for each cell in the Cy3 channel was determined using Fiji (Image J). Fluorescence intensities were then normalized to CB2-Cy3 fluorescence (100 %) and ^{C105S}CB2-Cy3 fluorescence (0 %) for each independent experiment using the following equation (7).

$$\text{Normalized MFI (\%)} = \frac{\text{MFI}(x) - \text{MFI}(\text{C}^{105\text{S}}\text{CB2-Cy3})}{\text{MFI}(\text{CB2-Cy3}) - \text{MFI}(\text{C}^{105\text{S}}\text{CB2-Cy3})} \cdot 100 \quad (7)$$

Normalized fluorescence intensities were averaged to yield the normalized MFI from all experiments and were used to test for significant differences by one-way ANOVA followed by Tukey's *post-hoc* test in OriginPro (version 2021b).

2.5.10. MMAE conjugation

To conjugate MMAE to CB2, 30 nmol of CB2 or ^{105}S CB2, 7.5 nmol of srtA, 900 nmol of Gly³-Val-Cit-PAB-MMAE (MedChemExpress, dissolved in DMSO) and 80 μL of equilibrated HisPur Ni-NTA resin (ThermoFisher) were mixed in 600 μL of srtA buffer (150 mM NaCl, 10 mM CaCl₂, pH 7.5) and incubated rotating for 30 min at 4 °C. The resin was pelleted (700 g, 2 min) and the supernatant containing the MMAE conjugates was collected. Then, the resin was incubated with srtA buffer + 300 mM imidazole to elute any remaining proteins. Both supernatant and eluate were analyzed by SDS-PAGE and MALDI-TOF to determine the purity of MMAE conjugates. The supernatant was then dialyzed with 3x 2 L PBS (last dialysis o/n) to remove any uncoupled drug and concentrated via Amicon® Ultra centrifugal filter units (MWCO = 10 kDa). The protein concentration was determined via microBCA kit (ThermoFisher) following the manufacturer's instruction. To validate that conjugation does not interfere with CB2 binding, MMAE conjugates were compared to unconjugated CB2 regarding SC-1 cell binding via flow cytometry as described in 2.4.4. Finally, MMAE conjugates were filtered through a 0.22 μm filter (Merck), stored at 4 °C, and used for drug delivery assays within two weeks.

2.5.11. Drug delivery assay

In a 96-well plate, triplicates of CB2-MMAE, ^{105}S CB2-MMAE and MMAE were prepared adding 10 μL of varying MMAE concentrations per well. Wells with unconjugated CB2 and 0.1 % Triton-X100 were included as negative and positive controls, respectively. SC-1 cells were resuspended in complete medium without phenol red, and 30,000 cells in 180 μL medium were added to each well. Three additional empty wells were filled with medium without cells. The plate was incubated for 48 h at 37 °C, 5 % CO₂. Next, 10 μL of WST-8 reagent (from CCK8 kit, Abcam) were added to each well and the plate was incubated for 3 h at 37 °C, 5 % CO₂. The absorbance of the plate at 460 nm (A_{460}), correlating with cell proliferation, was

measured with an Infinite plate reader (Tecan). A_{460} data was plotted over MMAE concentration and fitted to a sigmoidal dose-response curve using OriginPro (version 2021b). The curves' inflection points yielded the half maximal inhibitory concentration (IC50).

The assay was then repeated twice at a fixed MMAE concentration of 10 nM, taking into account the slightly different DOLs of CB2-MMAE and C105S CB2-MMAE, and the A_{460} from all three independent experiments was converted into % dead cells and normalized to positive and negative controls using the following equation (8):

$$Dead\ cells\ (\%) = \frac{A_{460}(x) - A_{460}(TritonX100)}{A_{460}(unconjugated\ CB2) - A_{460}(TritonX100)} \cdot 100 \quad (8)$$

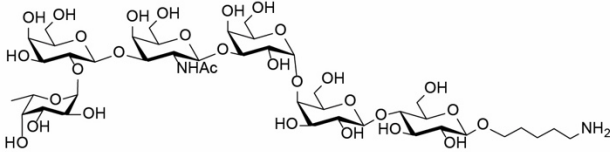
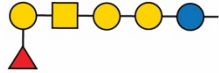
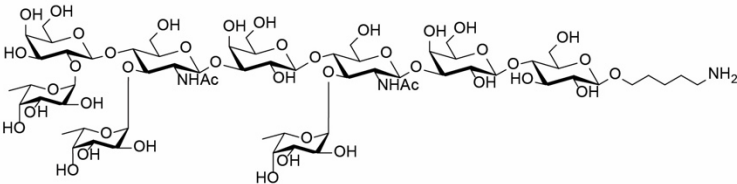
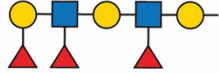
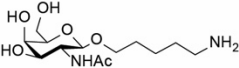

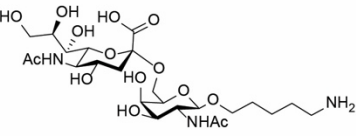
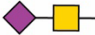
3. Results and Discussion

3.1. Inducing TACA-binding hcAbs in alpaca

3.1.1. Generation of glycoconjugates for alpaca immunization

Due to their high incidence in and clinical relevance for various cancer types, I chose the four TACAs Globo-H, KH-1, Tn, and STn for alpaca immunization (Table 3).

Table 3 TACAs examined in this study. All glycans were previously synthesized in our department with an aminopentanol linker that is depicted here at the reducing end of each glycan. All structures were drawn using ChemDraw (version 20). Symbol nomenclature follows the standard guidelines¹⁴⁸.

Structure	Symbol nomenclature	Name
		Globo-H
		KH-1
		Tn
		STn

Since glycans are predominantly weak immunogens, I surmised that directly injecting synthetic glycans into alpacas would also cause a T cell-independent response yielding mostly low-affinity IgM Abs⁵⁵ (Figure 3), as in other mammalian species. To circumvent this potential hurdle, I generated conjugates of Globo-H, KH-1, Tn, and STn to the

carrier protein CRM₁₉₇. For that purpose, the aminopentanol moieties of the synthetic glycans were connected to the lysine side chain amino groups of CRM₁₉₇ via short adipic linkers. MALDI-TOF spectra confirmed the successful conjugation to CRM₁₉₇ for all four TACAs of interest (Figure 18).

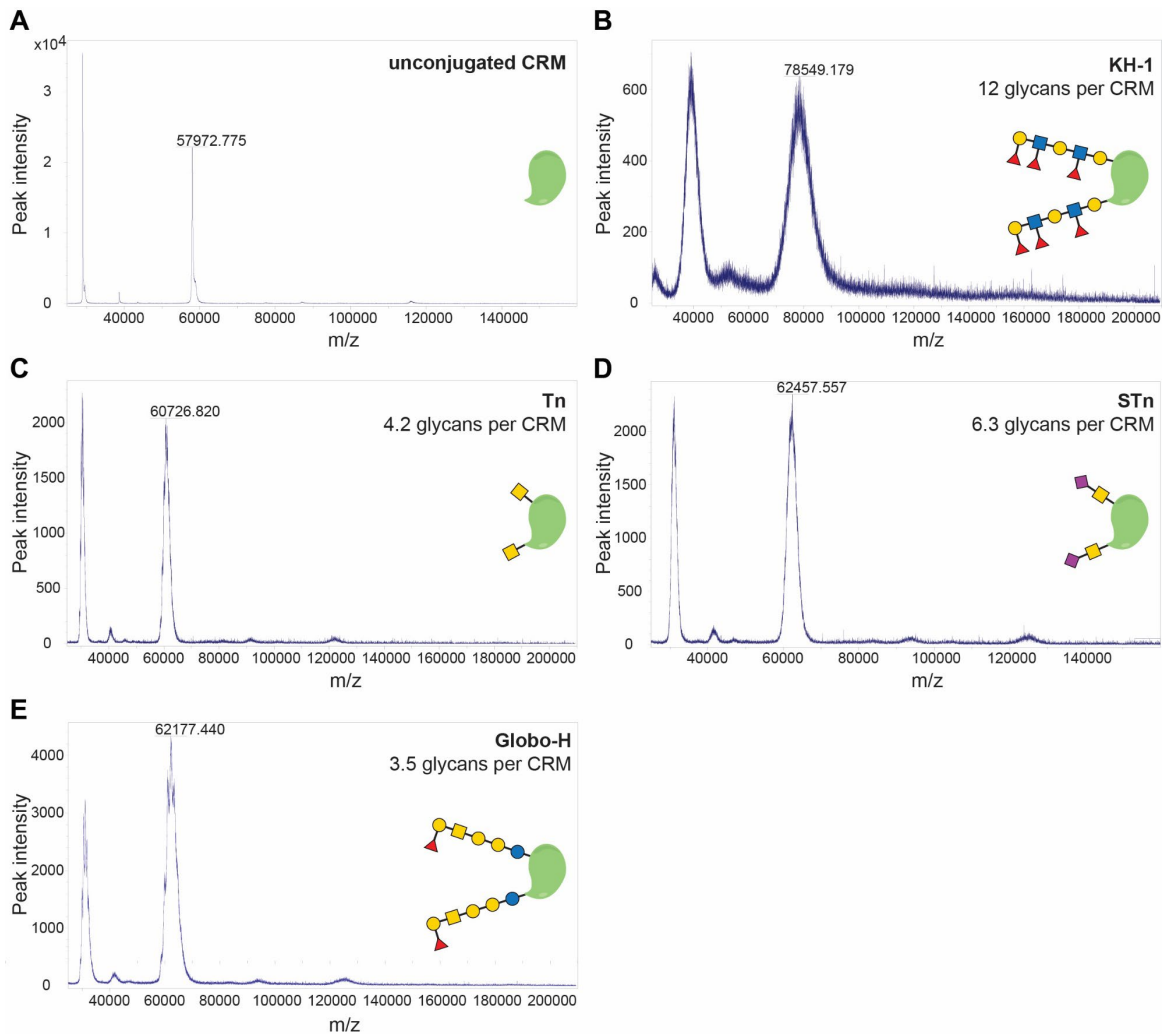


Figure 18 TACAs were successfully conjugated to CRM₁₉₇. MALDI-TOF spectra of unconjugated CRM₁₉₇ (A) and CRM₁₉₇ conjugates of KH-1 (B), Tn (C), STn (D), and Globo-H (E) are compared to calculate the DOL for each glycoconjugate based on the respective mass difference. Y axis: peak intensity, X axis: m/z.

3.1.2. Glycoconjugates induce anti-TACA Abs in alpaca

Over the course of six weeks, the alpaca received weekly injections of the four glycoconjugates mixed with aluminum adjuvant. To examine the formation of TACA-binding Abs in the alpaca, I collected small amounts of the animal's serum at each

injection time point and tested it on a glycan array containing the four glycans used for immunization (Globo-H, KH-1, Tn and STn) and a repeating unit of heparin (GlcNSO₃[6-OSO₃](α 1-4)IdoA[2-OSO₃](α 1-4)GlcNSO₃[6-OSO₃](α 1-4)IdoA[2-OSO₃](α 1-4)GlcNSO₃[6-OSO₃](α 1-4)IdoA[2-OSO₃]) as control glycan. Since the animal was not immunized with the heparin structure, the titer against this glycan reflects the pre-existing Ab repertoire of the naïve animal.

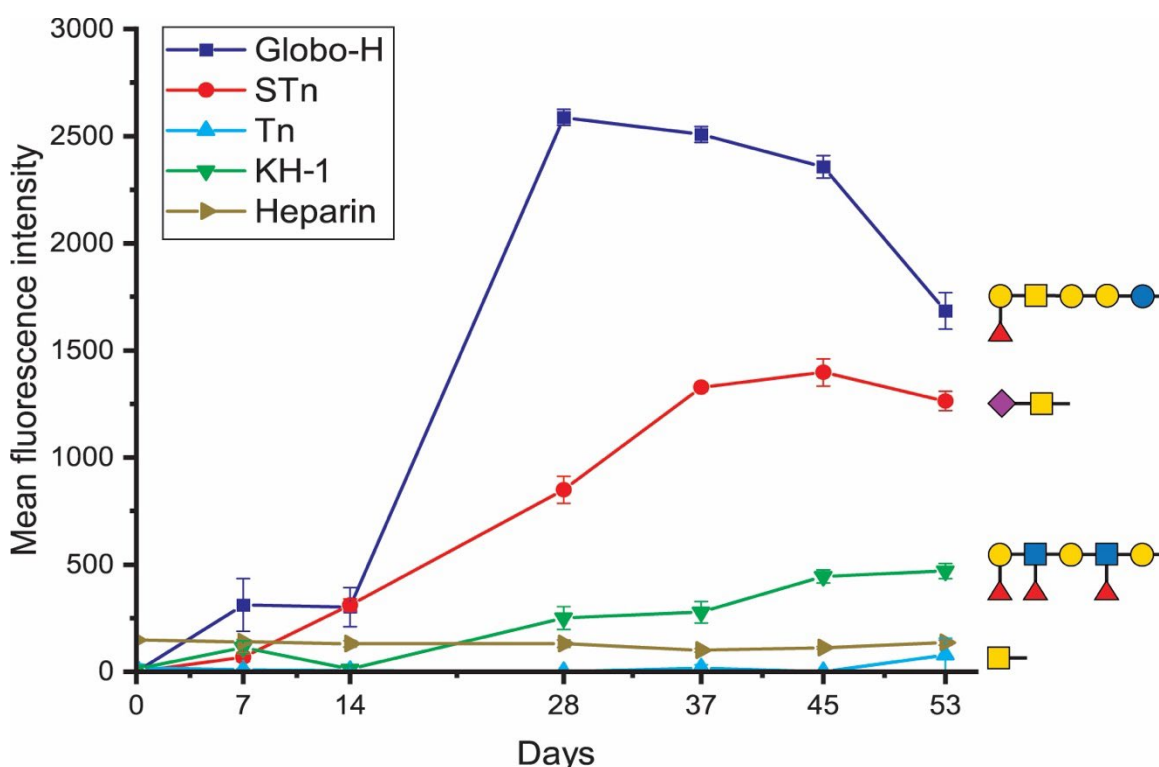


Figure 19 The serum Ab titer against the four injected TACAs increases over the course of immunization. Glycan array was used to determine the Ab titers for Globo-H, KH-1, Tn, and STn. Notably, while in general Ab titers show an increase with ongoing immunization, Ab levels for the different glycans diverge from each other, indicating the need for optimized immunization regimes for each glycan. Y axis: mean fluorescence intensity, X axis: time (d). Only those days are displayed on which serum samples were taken from the animal. Values represent mean \pm SEM from quadruplicates. A heparin substructure (brown) was included as negative control.

Comparing the sera from multiple time points, the Ab titer increased over time for the four injected glycans but not for heparin, suggesting the specific induction of anti-TACA Abs upon immunization (Figure 19). Three out of four glycans (Globo-H, KH-1 and STn) showed an Ab response above the Ab level against heparin, while Tn gave a

weaker response. The weak response against Tn could be related to the size of the antigen: A single GalNAc might be too small compared to the size of CRM₁₉₇ and the aminopentanol and adipic linkers. This notion is supported by a previous study demonstrating that a monomeric sialic acid conjugated to carrier proteins cannot be recognized by T cell receptors¹⁴⁹.

The titer profiles of Globo-H, KH-1, and STn also showed significant variation. While titers against Globo-H and STn rose quickly and reached a plateau within 4-6 weeks followed by a decline, KH-1 caused a slower, almost linear Ab response and no plateau was observed till the last time point (Figure 19). This finding suggests that even higher anti-KH-1 Ab levels could have been achieved at a later time point and that each glycan generally requires a different immunization regime. For future anti-glycan Ab development in alpacas, I would thus recommend an extended immunization regime with multiple time points for blood withdrawal to ensure that the anti-glycan Ab repertoire is collected at the peak titer.

Interestingly, the Ab titer did not correlate with the glycoconjugate's DOL as Globo-H-CRM₁₉₇ and Tn-CRM₁₉₇ both had a DOL of approx. 4 but triggered very different Ab responses in the alpaca (Table 1, Figure 19). Notably, higher glycan doses/injection did not improve Ab formation as the highest doses were injected for KH-1 and Tn glycoconjugates, which induced a comparably weak response. The examples of Globo-H and STn demonstrate that a moderate DOL between 4-6 and glycan doses of < 8 µg per injection can already be sufficient to induce high Ab titers in alpaca.

3.1.3. Anti-TACA Abs show varying degrees of cross-reactivity

To examine how specific induced Abs are for the injected TACAs, I performed additional glycan arrays exemplarily for Globo-H and KH-1, including several related structures from the Globo or Lewis family. Globo-H-binding Abs showed substantial cross-reactivity, increasing from GB3 over GB4 to GB5 (Figure 20). While GB3 and GB4 gave lower responses than Globo-H, the signal detected for GB5 was even higher than for Globo-H, suggesting that the additional fucose of Globo-H reduces antigenicity.

Therefore, when developing Nbs against Globo-H, cross-reactivity to GB5 must be excluded via thorough selection.

In contrast, anti-KH-1 Abs were more specific to KH-1 as responses against smaller Lewis glycans (Lewis X, Lewis X, Lewis A, Lewis B, SLe^x) were very low (Figure 20). The only structure to which anti-KH-1 Abs displayed cross-reactivity was a Lewis X dimer, only differing from KH-1 by the absence of one fucose at the reducing end. However, Lewis X dimers also represent an attractive TACA as they are specifically overexpressed in adenocarcinoma¹⁵⁰, and Nbs recognizing these glycans are thus in principal interesting as well. Nevertheless, the overall lower immunogenicity of KH-1 compared to Globo-H limits the probability for successfully obtaining KH-1-specific Nbs.

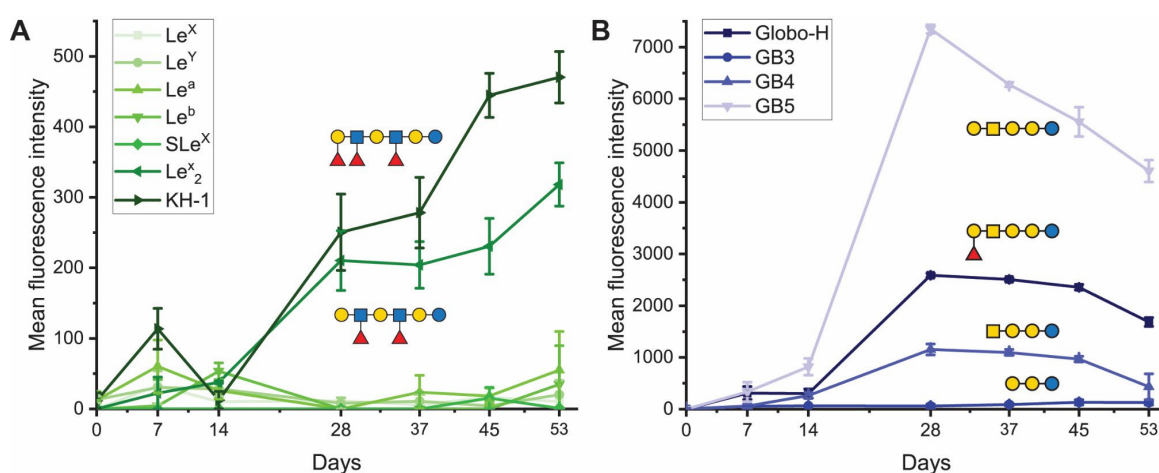


Figure 20 Induced anti-TACA Abs exhibit different levels of cross-reactivity. Glycan arrays were used to determine the cross-reactivity of induced Abs against glycans which are structurally similar or are substructures of KH-1 and Globo-H. **(A)** Cross-reactivity of anti-KH-1 Abs. Note that none of the other Lewis antigens is recognized by the induced Abs except for Le^x₂. **(B)** Cross-reactivity of anti-Globo-H Abs. Abs become more cross-reactive with increasing length of the Globo family glycans. Interestingly, the additional Fuc on Globo-H leads to a decrease in antigenicity compared to GB5. Y axis: mean fluorescence intensity, X axis: time (d). Only those days are displayed on which serum samples were taken from the animal. Values represent mean ± SEM from quadruplicates.

3.1.4. Anti-TACA Abs are induced across all IgG subtypes

Only hcAbs from the IgG2 and IgG3 subtypes can be used as a basis for Nb development, and the formation of these subtypes in alpaca upon immunization has not been investigated so far. Therefore, I aimed to determine the specific Ab titer for each IgG subtype. As detection Abs against the individual alpaca IgG subtypes are not commercially available, I purified the three different alpaca IgG subtypes (Figure 21) from serum collected at day 37 via sequential affinity chromatography with Protein A/G columns (described in 2.1.3). After confirming the purity of each subclass via SDS-PAGE and western blot based on the expected mass differences and absence/presence of the light chain (Figure 21), glycan arrays with the individual IgG subtypes were performed.

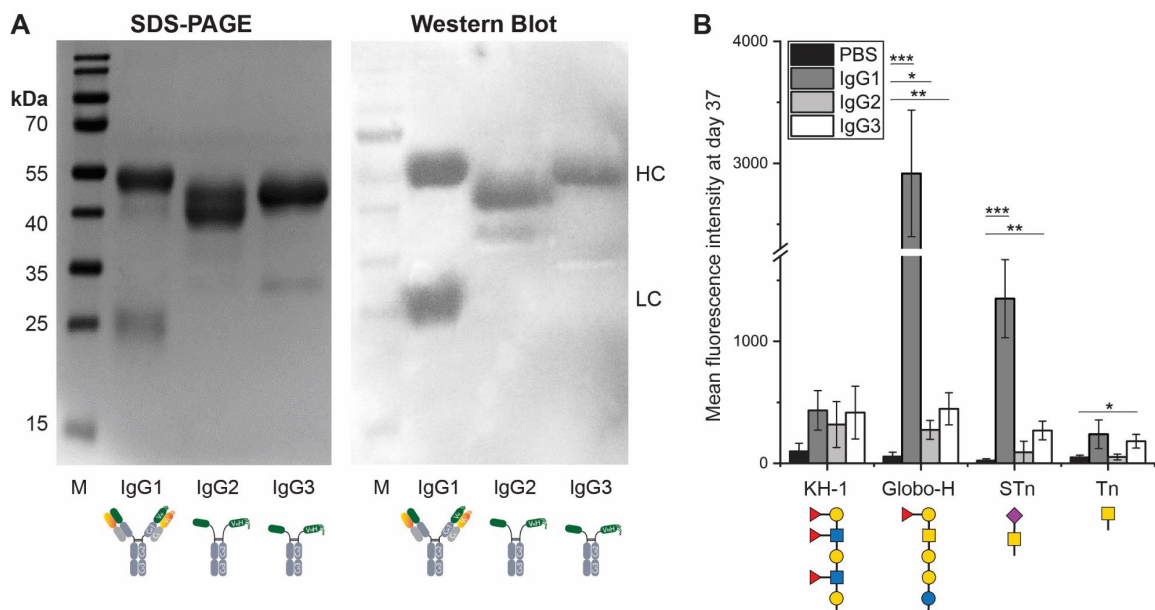


Figure 21 Immunization induced Abs in all IgG subclasses. (A) Purification of the individual IgG subtypes was confirmed by SDS-PAGE and western blot using anti-llama IgG HRP-conjugated Ab for detection. Note the presence of heavy chain (HC) and light chain (LC) for IgG1, whereas IgG2 and IgG3 lack the light chain. **(B)** The anti-TACA Ab level per subclass was quantified using glycan array. PBS was included as a negative control. Compared to the negative control, the different subclasses were induced at varying degrees, depending on the glycan, but all subtypes were generally detected, indicating successful formation of TACA-targeting hcAbs. Means from three independent experiments were compared by two-sample t-test with (*) $p < 0.05$, (**) $p < 0.01$, (***) $p < 0.001$. Error bars represent SEM.

In general, anti-TACA Ab levels were increased across all IgG subtypes but varying distributions between the three subtypes were observed depending on the glycan. The more immunogenic glycans Globo-H and STn induced predominantly IgG1 Abs but also, to a smaller extent, IgG2 and IgG3 (Figure 21). This is in good agreement with the literature as generally around 50 % of Abs in alpaca serum are of the IgG1 type⁷⁷. KH-1 and Tn induced a more balanced distribution of IgG subtypes with Ab levels in the same range as anti-Globo-H and anti-STn IgG2/3. Since the Ab response triggered by KH-1 and Tn was generally lower and more delayed, purifying the different IgG subclasses also from serum collected at a later time point might be advisable.

In conclusion, these data demonstrate that alpaca immunization with glycoconjugates can be used to induce TACA-binding hcAbs in alpaca, forming the basis for Nb development against a variety of clinically relevant glycan targets.

3.2. Elucidating the thiol-dependent nature of CB2 binding

3.2.1. CB2 specifically recognizes several subtypes of B cell lymphoma

Based on hcAbs derived from the TACA-immunized animal described in 3.1, several Nbs were developed in our group and screened for binding to TACAs and B cell lymphoma¹⁴¹. During the screening process, I identified by serendipity an unusual Nb, termed CB2 (cancer-binding Nb 2), which did not bind to any of the glycans used for immunization but reliably recognized different B cell lymphoma cell lines (Figure 22). Incubation with CB2 yielded significant shifts in flow cytometry histograms representing binding for the B cell NHL subtypes of follicular lymphoma (SC-1 and DoHH-2), diffuse large B cell lymphoma (SU-DHL-4), mantle cell lymphoma (JeKo-1), and Burkitt's lymphoma (Raji). In contrast, no CB2 binding was observed with healthy human PBMCs (Figure 22), indicating specific binding to NHL.

These findings sparked my interest in the molecular basis for CB2 specificity, and I therefore sought to characterize CB2 in more detail. Since flow cytometry showed the

largest shift for CB2 binding to follicular lymphoma cell line SC-1, I decided to focus on this cell line for further CB2 characterization.

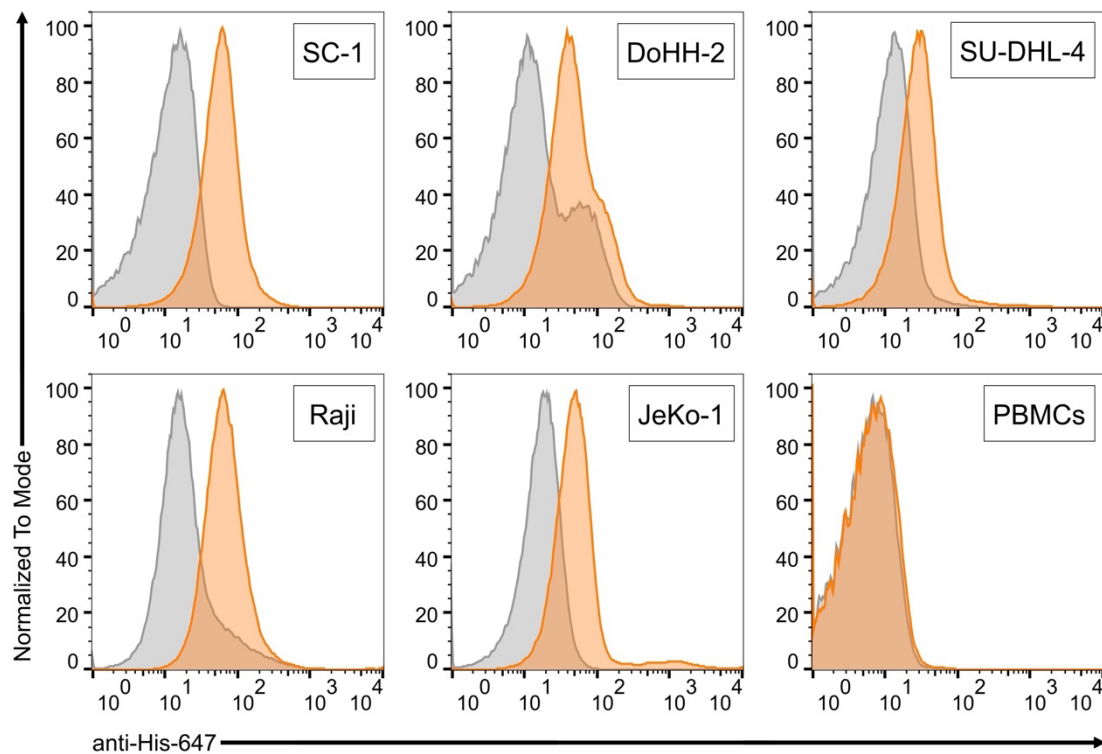


Figure 22 CB2 binding to several B cell lymphoma subtypes. Flow cytometry binding assay with CB2 and the B cell NHL cell lines SC-1, DoHH-2, SU-DHL-4, Raji, JeKo-1 (from left to right, top to bottom). CB2 recognized all cell lines as indicated by a shift in fluorescence. In contrast, CB2 did not bind to healthy PBMCs (bottom right). Y axis: cell count normalized to mode, X axis: fluorescence intensity. Grey: SC-1 cell staining only with anti-His-647 secondary Ab but without CB2. Orange: SC-1 cell staining with CB2 and anti-His-647 secondary Ab.

3.2.2. B cell lymphoma cells display higher levels of reduced, accessible thiol groups on the surface than healthy lymphocytes

While purifying CB2, I noticed that a significant part of the Nb formed dimers which was prevented in the presence of the reducing agents DTT or β -mercaptoethanol (Figure S 3). Subsequently, I identified a non-conserved cysteine at position 105 in CB2's CDR3 region (Figure S 3), prompting the hypothesis that CB2 binding to cells requires thiol-thiol interactions. Previous work unveiled that surface thiols undergo significant changes in the tumor microenvironment, for example, due to the

overexpression of PDI and the thioredoxin system^{60,61,63,64}. However, a quantitative comparison of surface-accessible thiol groups on lymphoma and healthy lymphocytes does not exist so far. To close this gap, I determined the level of free thiol groups on B cell lymphoma and healthy lymphocytes with the thiol probe Alexa647-maleimide. First, I validated by confocal microscopy that Alexa647-maleimide is not internalized by SC-1 cells and stays on the cell surface. Indeed, the thiol probe shows a ring-like staining around the edges of SC-1 cells, suggesting that the employed thiol staining protocol is surface-specific as previously proposed⁶² (Figure 23). Next, I quantified the surface thiol levels of SC-1 cells and healthy lymphocytes by flow cytometry. After staining with Alexa647-maleimide, the B cell lymphoma showed approx. fivefold fluorescence intensity compared to healthy lymphocytes (Figure 23), indicating that surface thiol levels on SC-1 lymphoma cells are significantly higher than on healthy lymphocytes.

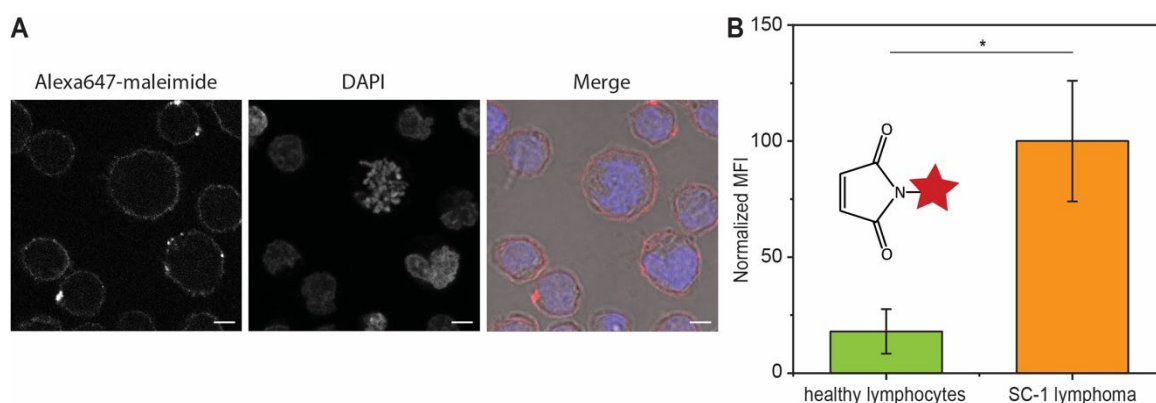


Figure 23 Levels of reduced thiol groups are increased on the surface of lymphoma cells compared to healthy lymphocytes. (A) Specific staining of the cell surface with Alexa647-maleimide was confirmed by confocal microscopy. Scale bar = 5 μm . Colors in merge: red = Alexa647-maleimide, blue = DAPI, greyscale = transmission light. **(B)** Surface thiol levels were quantified via flow cytometry and found to be elevated on SC-1 cells. Y axis: normalized MFI. Values represent mean \pm SEM from three independent experiments. Differences were tested for significance using a two-sample t-test with (*) $p < 0.05$.

3.2.3. CB2 binding is based on thiol-thiol interactions

To probe the hypothesis that CB2 binding requires thiol-thiol interactions, I designed and performed several inhibition assays. First, I tested CB2 binding in the presence of DTT, anticipating that this would prevent thiol-mediated binding. Indeed, CB2 entirely lost binding to SC-1 cells in the presence of DTT (Figure 24). In contrast, binding of the B cell-targeting anti-CD19 control Ab was not affected, demonstrating that only CB2 is susceptible to mildly reducing conditions.

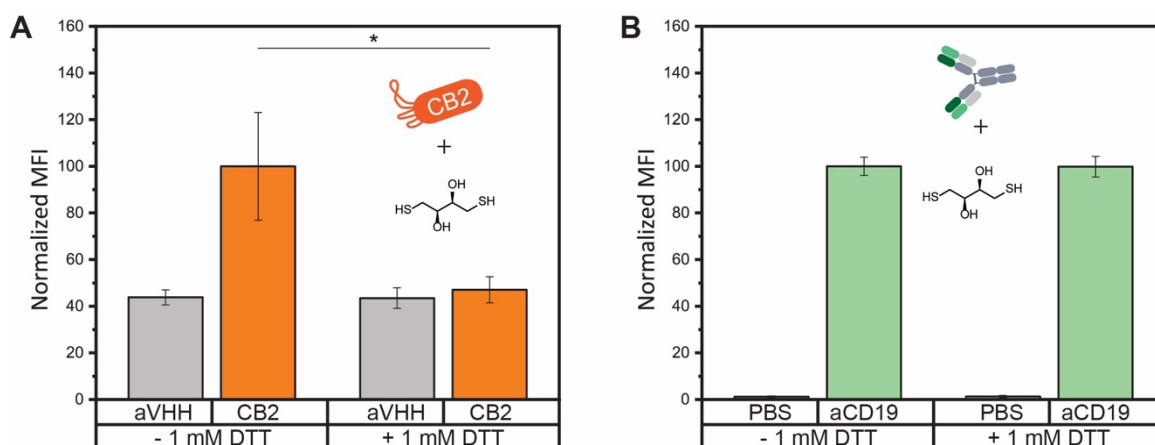


Figure 24 CB2 binding to SC-1 cells is abolished in the presence of DTT. (A) Comparison of CB2 binding (orange) via flow cytometry in the absence or presence of 1 mM DTT. Cells stained only with the detection Ab anti-VHH-647 were included as negative control (grey). Note that CB2 only binds in the absence of DTT. Differences were tested for significance by one-way ANOVA followed by Tukey's *post-hoc* analysis with (*) $p < 0.05$. **(B)** Comparison of anti-CD19-PE Ab binding (green) via flow cytometry in the absence or presence of 1 mM DTT. Cells incubated with PBS were included as negative control (grey). Notably, anti-CD19-PE binding is not affected by DTT. Y axis: normalized MFI. Values represent mean \pm SEM from three independent experiments.

Additionally, I prepared quenched CB2 by pre-incubation with the thiol-blocking compound N-ethylmaleimide (NEM) and tested binding to SC-1 cells. CB2 binding to SC-1 cells was completely abolished after NEM treatment (Figure 25), further corroborating the essential role of thiol-thiol interactions for CB2 binding.

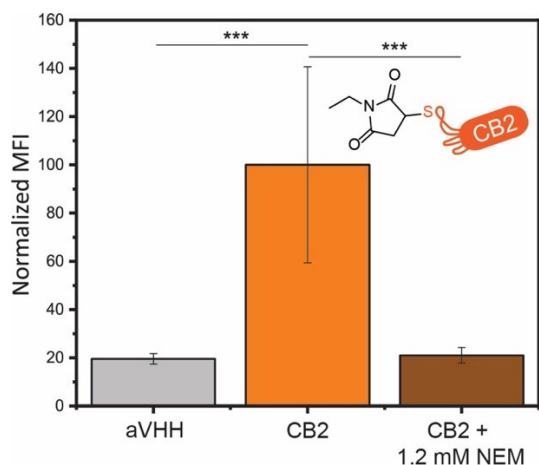


Figure 25 CB2 pre-incubation with NEM causes a complete loss of binding to SC-1 cells. Binding of CB2 (orange), NEM-quenched CB2 (brown) or only detection Ab anti-VHH-647 (grey) was compared by flow cytometry. Note that no binding is observed after NEM treatment. Y axis: normalized MFI. Values represent mean \pm SEM from three independent experiments. Differences were tested for significance by one-way ANOVA followed by Tukey's *post-hoc* analysis with (***) $p < 0.001$.

3.2.4. Cysteine 105 is indispensable for CB2 binding

Motivated by the results of the inhibition assays, I designed a C105S mutant of CB2 (^{C105S}CB2) to determine the role of cysteine 105 for CB2 binding unequivocally. First, it was confirmed that ^{C105S}CB2 maintains the same structure and folding by recording NMR spectra of CB2 wildtype and mutant which only differed in slight signal shifts (Figure S 4). Next, I compared SC-1 cell binding of CB2 and ^{C105S}CB2 via flow cytometry (Figure 26). Strikingly, a complete loss of binding to SC-1 cells was observed for ^{C105S}CB2. This observation was recapitulated when staining SC-1 cells with CB2 or ^{C105S}CB2 for confocal microscopy (Figure 27); again, only CB2 could be detected on SC-1 cells but not ^{C105S}CB2, substantiating that cysteine 105 is indispensable for CB2's binding mode.

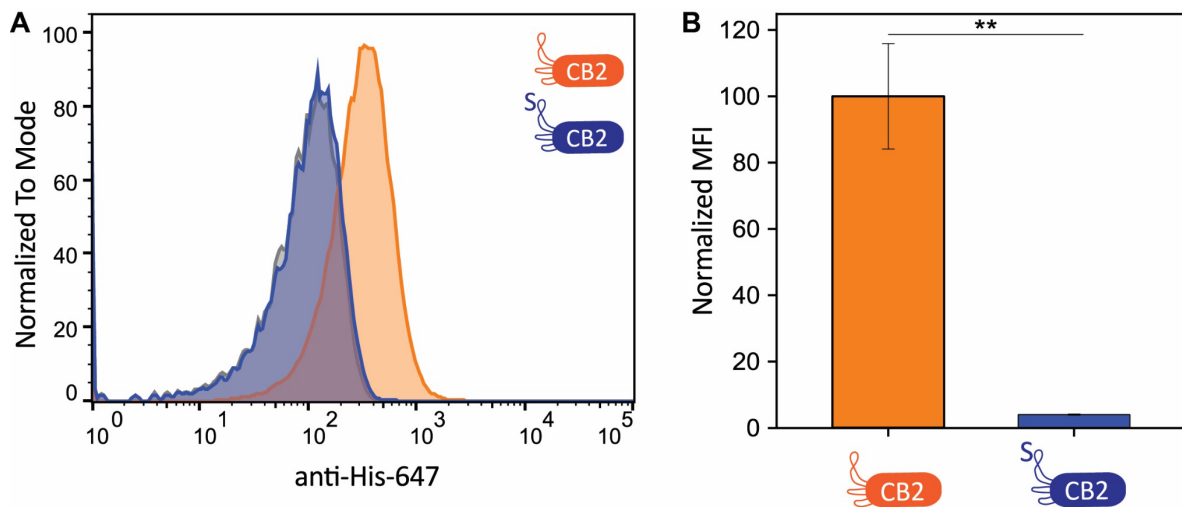


Figure 26 The C105S mutation completely abolishes SC-1 cell binding. (A) Flow cytometry histogram showing binding of CB2 to SC-1 cells (orange). No binding is observed for C^{105S}CB2 (blue) as fluorescence is the same as in the control stained only with secondary Ab anti-His-647 (grey). Y axis: cell count normalized to mode. X axis: fluorescence intensity. **(B)** Quantified MFI for SC-1 cell binding of CB2 (orange) or C^{105S}CB2 (blue) from three independent experiments. Values represent mean \pm SEM. Differences were tested for significance using one-way ANOVA followed by Tukey's *post-hoc* test with (**) $p < 0.01$.

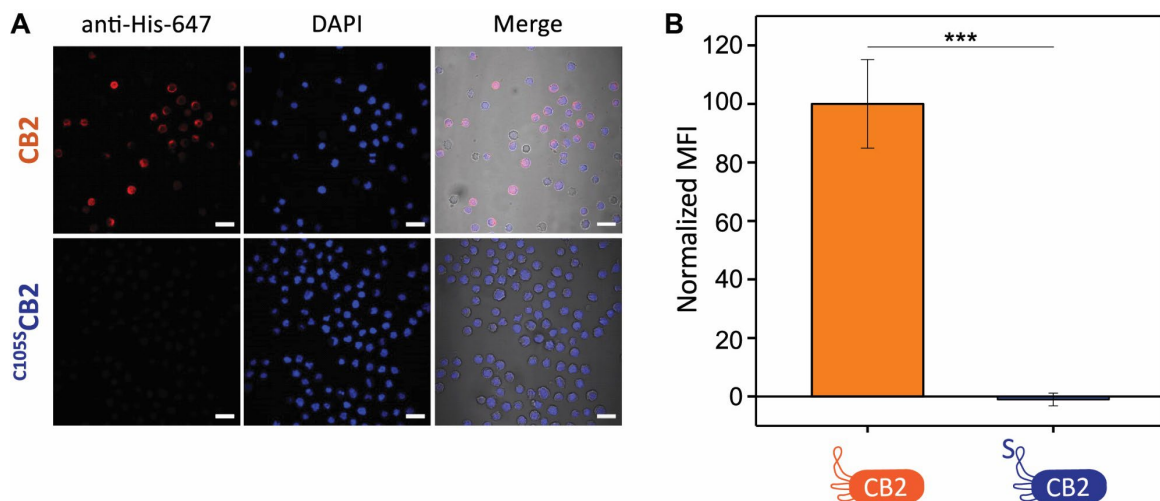


Figure 27 Loss-of-binding with C^{105S}CB2 is confirmed by confocal microscopy. (A) Representative images of SC-1 cells stained with either CB2 or C^{105S}CB2 followed by anti-His-647 detection Ab (red channel). Cells were co-stained with DAPI (blue channel). Greyscale = transmission light. Scale bar = 20 μ m. **(B)** Quantified MFI of > 170 cells selected from microscopy images from two independent experiments. Note that only CB2 recognizes lymphoma cells but not C^{105S}CB2. Values represent mean \pm SEM. Differences were tested for significance using one-way ANOVA followed by Tukey's *post-hoc* test with (***) $p < 0.001$.

3.3. Functionalizing CB2 for complement activation

3.3.1. Human serum shows higher Ab titers against Rha₃ than Rha

To enable the Nb to trigger a complement response against lymphoma cells, I decided to generate Rha-functionalized CB2. Rha-containing glycans are ARMs against which humans possess high levels of endogenous Abs. Previous studies successfully used Rha monomers to functionalize Abs or liposomes for Ab recruitment^{117,118}. However, small glycans generally exhibit low immunogenicity, and I speculated that a rhamnose trimer (Rha₃) might be recognized by more serum Abs. To test this hypothesis and to find the optimal Rha compound for Ab recruitment and complement activation, I compared the titers of Rha- and Rha₃-binding Abs isolated from pooled human serum by glycan array (Figure 28, Figure S 7). As a negative control, the Ab titer against mannose trimers (Man₃) was determined. In general, Ab titers (both IgG and IgM) were significantly higher for the rhamnose compounds compared to Man₃, emphasizing the suitability of rhamnose glycans as ARMs. Interestingly, while IgM titers for Rha and Rha₃ were very similar, IgG titers were approx. three times higher for Rha₃ than for Rha (Figure 28). These data suggest that more serum IgGs recognize Rha₃ than Rha, and I therefore chose Rha₃ for CB2 functionalization. This finding seems plausible as surface lipopolysaccharides of many bacteria contain rhamnose multimers, putatively triggering a robust Ab response in humans^{110,112}.

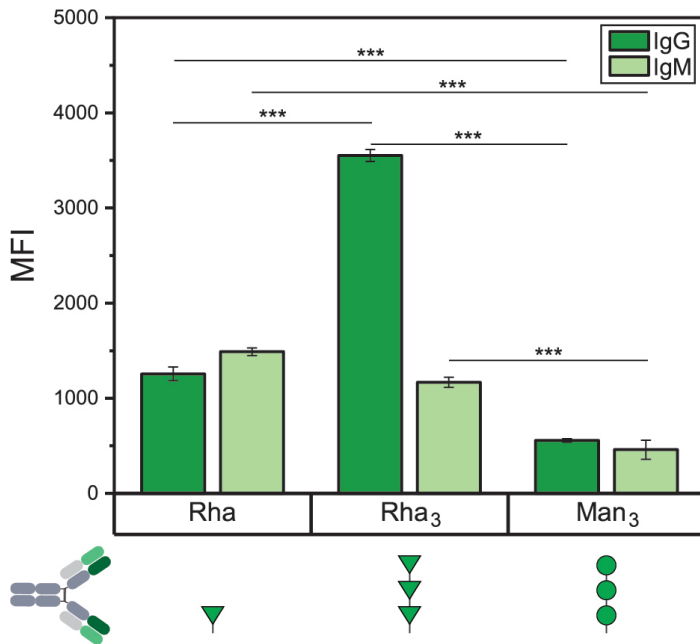


Figure 28 Rha₃-binding IgGs are significantly more abundant in human serum than Rha-binding IgGs. Abs isolated from pooled human serum were examined via glycan array, comparing binding to Rha, Rha₃ or Man₃ (negative control). Y axis: MFI. Values represent mean ± SEM from n = 6. Differences were tested for significance using one-way ANOVA followed by Tukey's *post-hoc* test with (***) p < 0.001.

3.3.2. Pure CB2-Rha₃ conjugates can be generated by srtA-mediated conjugation and fully retain binding activity

To generate Rha₃-functionalized CB2 (CB2-Rha₃), I employed srtA-mediated conjugation (Figure 8) because this allows site-specific attachment of the glycan to the Nb's C-terminus provided that the glycan is glycosylated and the C-terminus carries a sortag. After conjugation, I obtained pure CB2-Rha₃ by reverse-phase Ni-NTA affinity chromatography and tested its binding to lymphoma cells. Notably, CB2-Rha₃ caused a similar shift in flow cytometry compared to unconjugated CB2, indicating that Rha₃ conjugation does not interfere with CB2 binding (Figure 29).

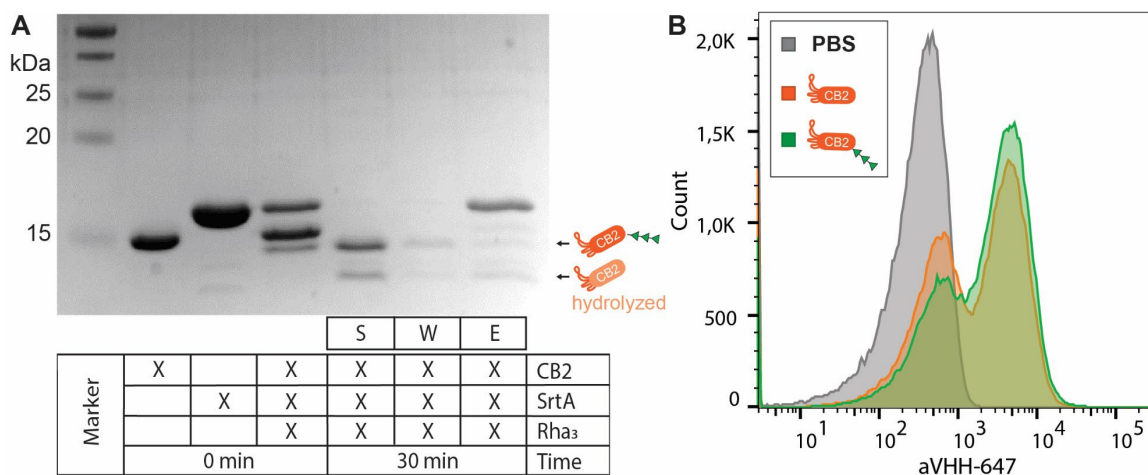


Figure 29 CB2-Rha₃ was successfully generated and still recognizes SC-1 cells. **(A)** The srtA-mediated conjugation of GG-Rha₃ to CB2 was monitored by SDS-PAGE. Fractions of the Ni-NTA affinity chromatography are S = supernatant, W = wash, E = eluate. Note that the desired product CB2-Rha₃ is found in the supernatant. Only minimal formation of the unwanted hydrolyzed side product is detected (discussed in more detail in 3.3.4). **(B)** The flow cytometry histogram confirms that CB2-Rha₃ (green) exhibits the same binding activity as unconjugated CB2 (orange). Cells incubated with PBS were included as a negative control (grey). Y axis: cell count, X axis: fluorescence of anti-VHH-647 detection Ab.

3.3.3. CB2-Rha₃ fails to activate complement against B cell lymphoma

Next, I examined CB2-Rha₃'s ability to induce a complement response against B cell lymphoma. Therefore, I incubated SC-1 cells with CB2-Rha₃ or unconjugated CB2 and Abs from human serum followed by rabbit complement, and then determined the percentage of dead cells as a measure of CDC by flow cytometry (Figure 30). Anti-human IgG Abs which recognize the B cell receptors on SC-1 cells were included as a positive control for complement activation. Heat-inactivated rabbit complement was used as one of the negative controls to measure the background of dead cells without complement activity. Strong complement-dependent cytotoxicity was induced with anti-human IgG Abs, validating the experimental setup. In contrast, both CB2 and CB2-Rha₃ failed to induce a complement response against SC-1 cells (Figure 30).

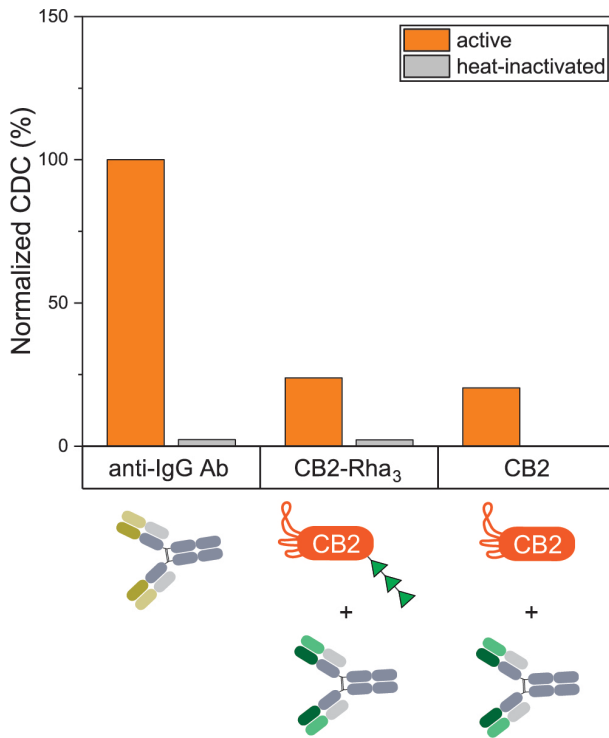


Figure 30 CB2-Rha₃ does not induce complement activity against SC-1 cells.

A comparison of CDC triggered by anti-IgG Ab (positive control), unconjugated CB2 (negative control) and CB2-Rha₃ reveals that only the anti-IgG Ab achieved complement activation. Y axis: normalized CDC (%), obtained by normalizing the % of dead cells to the positive and negative control (as described in 2.5.7). Orange: active complement, grey: heat-inactivated complement.

A problem on any level of the workflow could be responsible for the absence of CDC. In general, complement recruitment to SC-1 cells functions properly, indicated by the robust CDC response induced by the positive control anti-IgG Abs. I also ruled out that Rha₃ conjugation hampers CB2 binding as CB2-Rha₃ reliably recognized SC-1 cells in flow cytometry binding assays (see 3.3.2). To confirm that human Abs can bind the rhamnose moieties on CB2-Rha₃, a western blot with unconjugated and Rha₃-functionalized CB2 was performed (Figure S 5). Only CB2-Rha₃ but not CB2 was recognized by Abs from human serum, suggesting that, in principle, Rha₃-conjugated CB2 can recruit Abs.

The recruitment of complement factors depends on the distance between surface-bound Abs and generally requires multiple IgGs in close proximity to each other¹⁵¹. Notably, the single previous study describing rhamnosylated Nbs achieved CDC activation only when using serum of Rha-immunized rabbits as a source of anti-Rha Abs¹¹⁹. Hence, this study putatively compensated for the insufficient availability or recruitment of endogenous anti-Rha Abs by inducing Rha-targeting Abs through immunization. Considering these data, I hypothesized that CB2-Rha₃'s failure to induce

CDC might be the consequence of too few Abs being recruited to the cell surface or the recruited Abs being too far apart from each other. Since a requirement for non-endogenous, induced anti-Rha Abs would hamper a potential application of Nb-Rha conjugates in humans, I sought an alternative solution to address this problem. Previous studies have shown that the likelihood for complement recruitment and thus the level of CDC is strongly enhanced upon multivalent display of the ARM^{118,152}. Therefore, I generated a CB2 conjugate with multiple Rha3 moieties to examine whether such a construct would show enhanced Ab recruitment.

3.3.4. CB2-Rha-thFF03 can be generated in a two-step reaction and fully retains binding activity

To achieve site-specific attachment of multiple Rha3 moieties to CB2, I designed a two-step strategy, involving (1) the generation of a Rha3-functionalized glycopeptide and (2) the conjugation of the glycopeptide to CB2 by srtA. The synthetic peptide¹⁴⁶ thFF03 was chosen for the first step due to the presence of several lysines in its sequence, allowing chemical conjugation of multiple Rha3. After conjugation, several peaks could be discerned by MALDI-TOF, corresponding to the different DOLs of the peptide with an average DOL = 2.5 (Figure 31). Non-rhamnosylated thFF03 was removed by reverse-phase HPLC, yielding rhamnosylated thFF03 (Rha-thFF03). Next, I coupled Rha-thFF03 to the C-terminus of CB2 via srtA-mediated conjugation as described in 2.5.5. While the desired CB2-Rha-thFF03 was clearly detected by SDS-PAGE and MALDI-TOF at 17.9 kDa, I also noticed the formation of a side product at around 15.2 kDa (Figure 32).

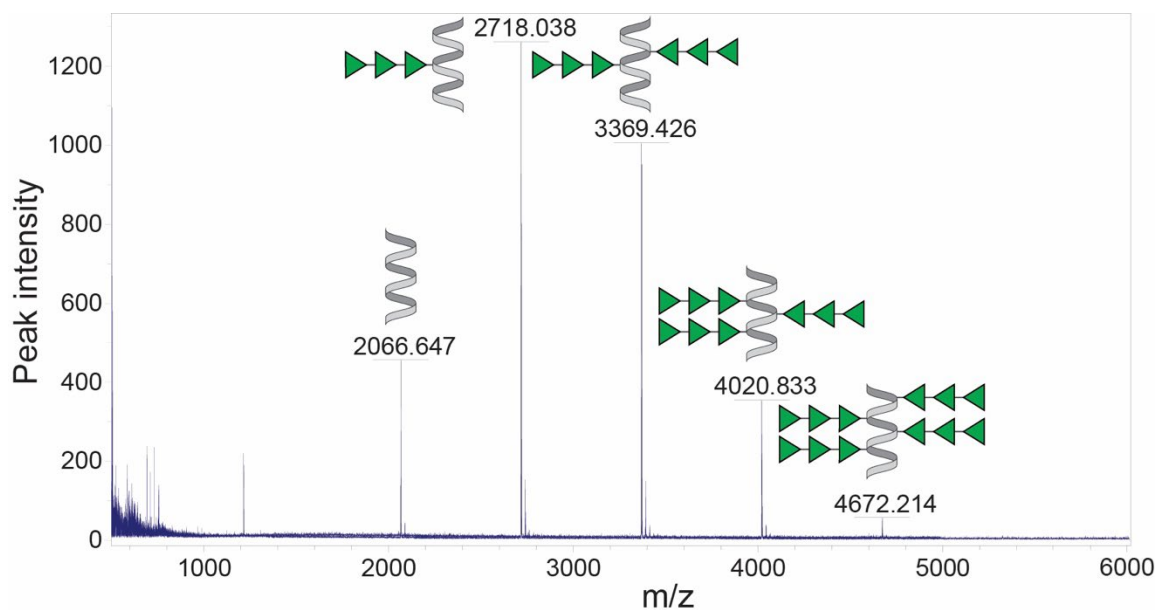


Figure 31 Chemical conjugation yields rhamnosylated thFF03 with varying DOLs. The MALDI-TOF spectrum contains several peaks, representing unconjugated thFF03 or Rha-thFF03 with loading between $1 < \text{DOL} < 4$. Y axis: peak intensity, X axis: m/z.

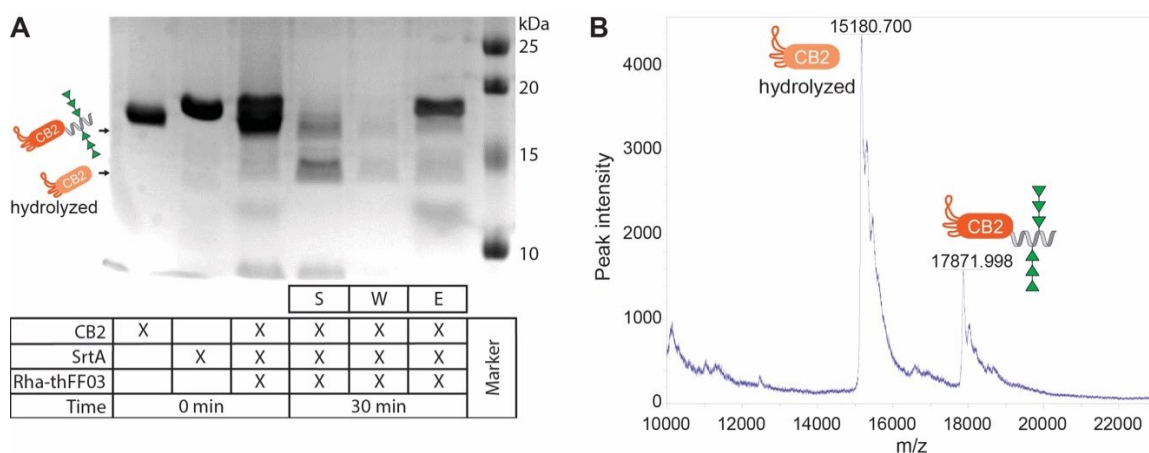


Figure 32 SrtA-mediated conjugation yields CB2-Rha-thFF03 but also hydrolyzed CB2. (A) SDS-PAGE was used to monitor the conjugation of CB2 and Rha-thFF03. Fractions of the Ni-NTA affinity chromatography are S = supernatant, W = wash, E = eluate. The desired product CB2-Rha-thFF03 is detected in the supernatant. However, another band is present at a lower molecular weight. (B) The supernatant from (A) was examined by MALDI-TOF and two main peaks were detected, representing CB2-Rha-thFF03 and hydrolyzed CB2. Y axis: peak intensity, X axis: m/z.

Most probably, the side product represents hydrolyzed CB2 as the detected mass matches the mass of CB2 without a sortag. Hydrolysis is a known side reaction during srtA-mediated conjugation which can usually be prevented by using an excess of substrate^{131,132}. Although the same excess of substrate was used for both Rha3 and Rha-thFF03 conjugation to CB2, I noticed substantially higher side product formation with Rha-thFF03. It is conceivable that during step (1), the generation of Rha-thFF03, Rha3 moieties were not only coupled to the ϵ -amino groups of the lysine side chains but also to the amino group at the N-terminus of the peptide. Considering the high level of side product formation in step (2), I assume that protection of the N-terminus with Rha3 interferes with the srtA reaction. This assumption is corroborated by the observation that substantially less side product is formed when conjugating CB2 to non-rhamnosylated thFF03 (Figure S 6). To circumvent this problem, it seems advisable to protect thFF03's N-terminus before Rha3 coupling followed by deprotection prior to srtA-mediated conjugation.

Due to the limited availability of synthetic peptide, I tested CB2-Rha-thFF03 on cells, despite the contamination with hydrolyzed CB2. Notably, Rha-thFF03 conjugation did not hamper CB2 binding to SC-1 cells as detected by flow cytometry (Figure 33), and I thus decided to probe CB2-Rha-thFF03's ability to induce CDC.

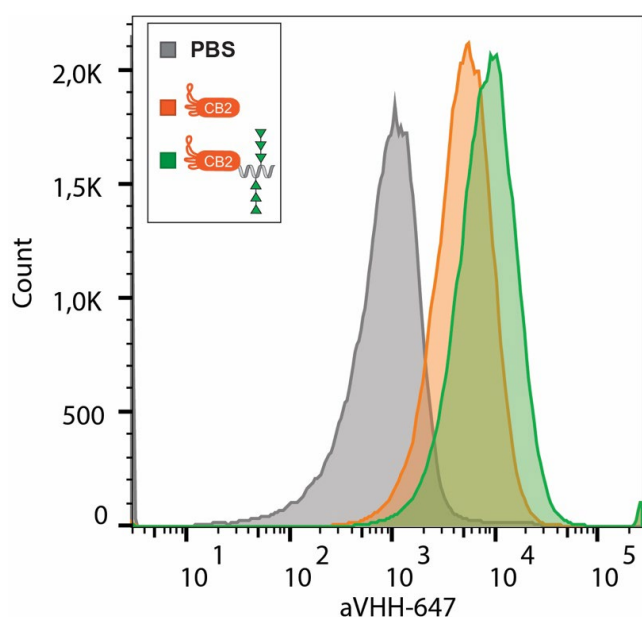


Figure 33 CB2-Rha-thFF03 retains full binding activity to SC-1 cells. The flow cytometry histogram compares binding of CB2 (orange) and CB2-Rha-thFF03 (green) to PBS (negative control, grey). Y axis: cell count, X axis: fluorescence of anti-VHH-647 detection Ab.

3.3.5. Multivalent Rha₃ display of CB2-Rha-thFF03 facilitates Ab recruitment and complement activation against cancer cells

To test complement activation, I incubated SC-1 lymphoma cells with CB2-Rha-thFF03 or unconjugated CB2 and Abs from human serum followed by rabbit complement. As a positive control, I again included anti-IgG Abs which reliably induced CDC (already shown in 3.3.3). Compared to 100 % CDC with the positive control, CB2-Rha-thFF03 achieved 76 % CDC (Figure 34). Cytotoxicity induced by unconjugated CB2 was significantly lower and corresponded to unspecific complement activity as no CDC effect was visible anymore after heat inactivation of the complement (Figure 34). These data suggest that CB2-Rha-thFF03 is able to recruit Abs and the complement cascade to SC-1 lymphoma cells (Figure 35).

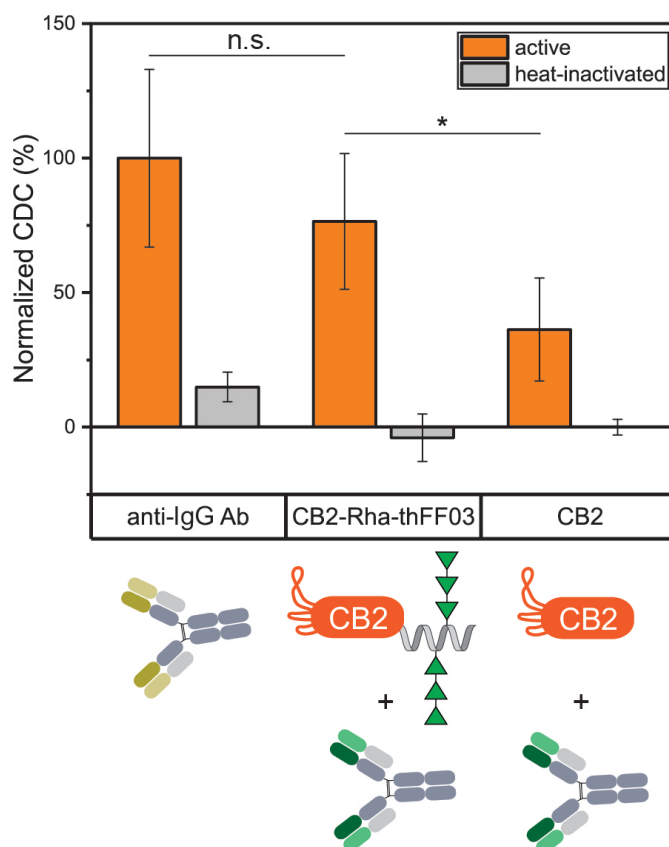


Figure 34 CB2-Rha-thFF03 induces complement activity against SC-1 cells. A comparison of CDC triggered by anti-IgG Ab (positive control), unconjugated CB2 (negative control) and CB2-Rha₃ reveals that complement activity is significantly increased in cells treated with anti-IgG Ab and CB2-Rha-thFF03. Y axis: Normalized CDC (%), obtained by normalizing the % of dead cells to the positive and negative control. Orange: active complement, grey: heat-inactivated complement. Values represent mean ± SEM from N = 3. Differences were tested for significance using student's t-test with (n.s.) p > 0.05, (*) p < 0.05.

Combining this observation with the failure of monovalent CB2-Rha₃ to induce CDC demonstrates the potential of displaying multiple rhamnose multimers for Ab and complement recruitment (Figure 35). The data clearly show that complement activation can be enhanced by conjugation of several Rha₃ moieties, and previous studies employing the attachment of only a single ARM might benefit from multivalent ARM display as well. Increasing the DOL of Rha₃ conjugated to CB2 seems also promising as a higher number of ARMs on the Nb might further enhance Ab recruitment and complement activation. A higher DOL could be achieved, for instance, by employing longer lysine-containing peptides or multivalent dendrimer structures, an approach which has been successfully used in the past¹⁵².

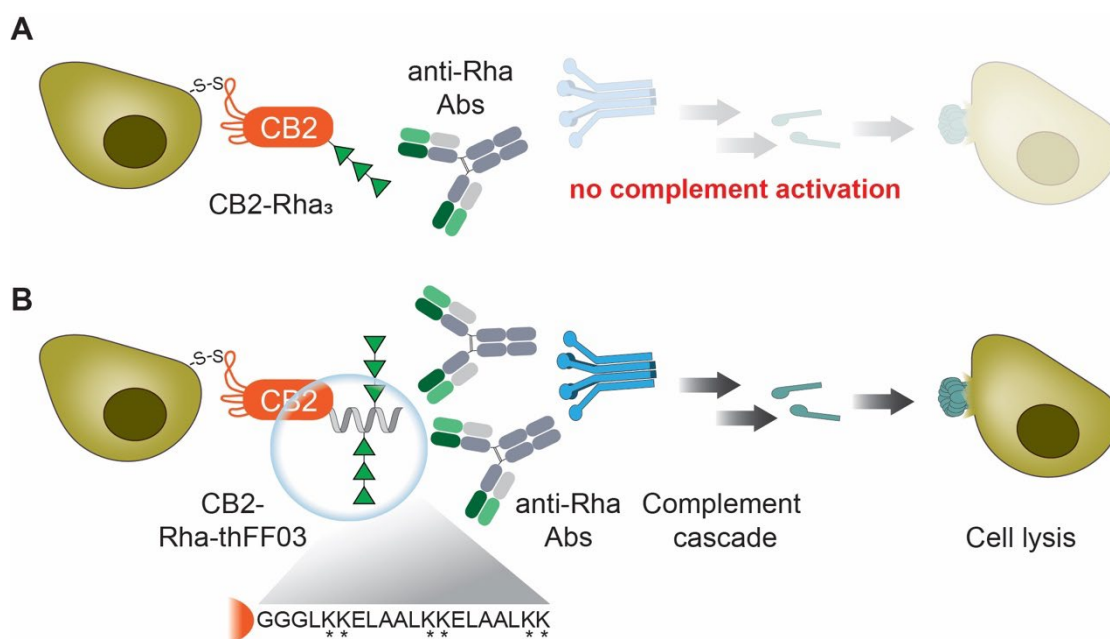


Figure 35 Proposed model for complement activation by CB2-Rha-thFF03. (A) CB2-Rha₃ binds to SC-1 cells via thiol-thiol interactions, but a single Rha₃ moiety does not recruit a sufficient number of anti-Rha Abs to trigger CDC. **(B)** CB2-Rha-thFF03 binds to SC-1 cells, and several anti-Rha Abs engage with the multiple Rha₃ moieties conjugated to thFF03. Anti-Rha Abs are recognized by the C1 complex (blue), activating the complement cascade and ultimately leading to cell lysis through the formation of membrane attack complexes (teal). Zoom-in: thFF03 sequence, asterisks indicate potential conjugation sites for Rha₃ attachment.

However, the considerable variation in CDC between individual complement activity assays (indicated by the error bars) and the substantial non-specific complement-induced cell killing with unconjugated CB2 also illustrate that further fine-tuning of the assay parameters is required to validate my current results. These issues should be addressed once the described obstacles in CB2-Rha-thFF03 conjugation (see 3.3.4) are solved and higher amounts of CB2-Rha-thFF03 are more readily available.

3.4. Examining and exploiting CB2 internalization for drug delivery

3.4.1. CB2-Cy3 and ^{C105S}CB2-Cy3 can be generated in a two-step reaction and directly detected on cells

Depending on the recognized surface protein, thiol-thiol interactions are often followed by cellular uptake⁶⁶⁻⁶⁹. Therefore, I set out to determine whether CB2 is also capable of internalization into B cell lymphoma. In order to address this question, I established a two-step strategy to generate fluorescent CB2 (Figure 17, Figure 36). First, I functionalized CB2's C-terminus with a DBCO group using srtA-mediated conjugation as previously published¹⁴⁷. This renders CB2 amenable to click chemistry that is employed to attach Cy3-azide in a second step. Both CB2-Cy3 and ^{C105S}CB2-Cy3 were successfully generated through this approach (Figure 36).

Next, I validated that the conjugates still maintain the same cell binding behavior. Only CB2-Cy3 bound to SC-1 cells but not ^{C105S}CB2-Cy3 when detected with anti-VHH-647 Ab, confirming that Cy3 conjugation does not interfere with binding (Figure 37). In addition, I directly detected Cy3 fluorescence on SC-1 cells and found again that only cells incubated with CB2-Cy3 showed a shift in fluorescence, whereas cell incubation with ^{C105S}CB2-Cy3 did not lead to a significant increase in Cy3 signal (Figure 37).

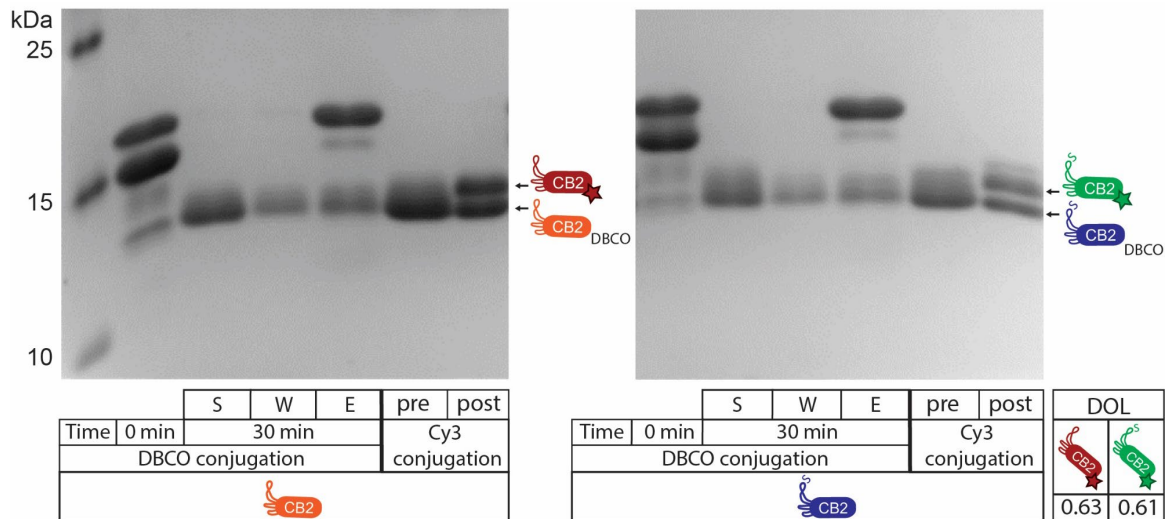


Figure 36 CB2-Cy3 and 105S CB2-Cy3 were successfully generated. SDS-PAGE was used to monitor the conjugation reactions with CB2 (left) and 105S CB2 (right). Conjugates were generated in two steps. First, Nbs were functionalized with DBCO, mixing Nbs with srtA and DBCO-NH₂. Nb-DBCO conjugates were purified via Ni-NTA affinity chromatography, and the fractions S = supernatant, W = wash, E = eluate are displayed. Second, Nb-DBCO was conjugated to Cy3 via click chemistry. The DOL was estimated based on band intensity of the Coomassie-stained gel.

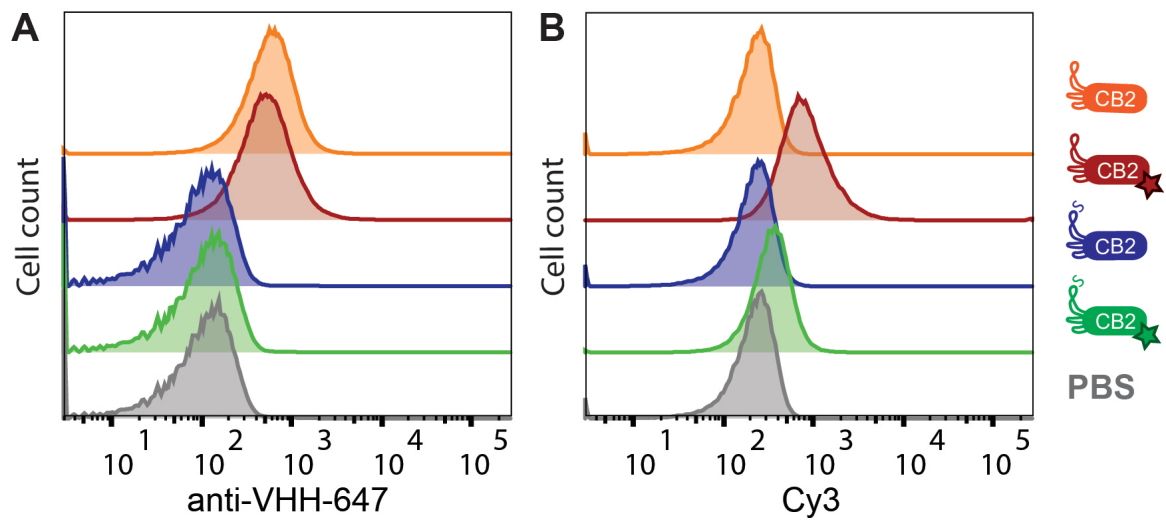


Figure 37 Cy3 conjugation does not affect the binding activity of CB2 and 105S CB2. Flow cytometry histograms compare SC-1 cell binding of CB2 (orange), CB2-Cy3 (red), 105S CB2 (blue), 105S CB2-Cy3 (green), and PBS (negative control, grey). **(A)** Nb binding is detected via anti-VHH-647 Ab. Note that CB2 and CB2-Cy3 show a similar level of binding. **(B)** Nb binding is directly detected via Cy3 fluorescence. Note that only CB2-Cy3 shows binding. Y axis: cell count, X axis: fluorescence intensity of anti-VHH-647 or Cy3.

While the SDS-PAGE of the conjugation reaction shows that parts of CB2-DBCO and ^{105}S CB2-DBCO remained without Cy3, the DOL was almost the same for CB2-Cy3 and ^{105}S CB2-Cy3. Since unconjugated Nb would not be detectable in internalization assays due to its non-fluorescent nature, I reasoned that potential internalization into cells could still be tested with the available Nb-Cy3 conjugates. However, if needed, additional purification steps could be employed to completely remove Nb without Cy3.

3.4.2. CB2-Cy3 is endocytosed by B cell lymphoma

To examine a putative thiol-mediated uptake of CB2-Cy3, I incubated SC-1 cells with CB2-Cy3 or ^{105}S CB2-Cy3, followed by extensive washing with acidic and neutral buffers to remove all surface-bound conjugates. Strikingly, I observed strong Cy3 fluorescence inside SC-1 cells incubated with CB2-Cy3 but not inside cells incubated with ^{105}S CB2-Cy3, indicating thiol-mediated uptake of CB2-Cy3 (Figure 38). To determine the mechanism of CB2-Cy3 uptake, I performed the same internalization experiment in the presence of clathrin-mediated endocytosis inhibitors dynasore and chlorpromazine. Transferrin-Alexa647 was included as positive control (Figure S 8) because it is predominantly internalized via clathrin-mediated endocytosis¹⁵³. Notably, CB2-Cy3 internalization was significantly reduced or completely abolished in cells treated with chlorpromazine or dynasore, respectively. Inhibition of internalization in the presence of dynasore was also observed for the transferrin control. These data suggest that CB2-Cy3 is predominantly internalized by clathrin-mediated endocytosis (Figure 38).

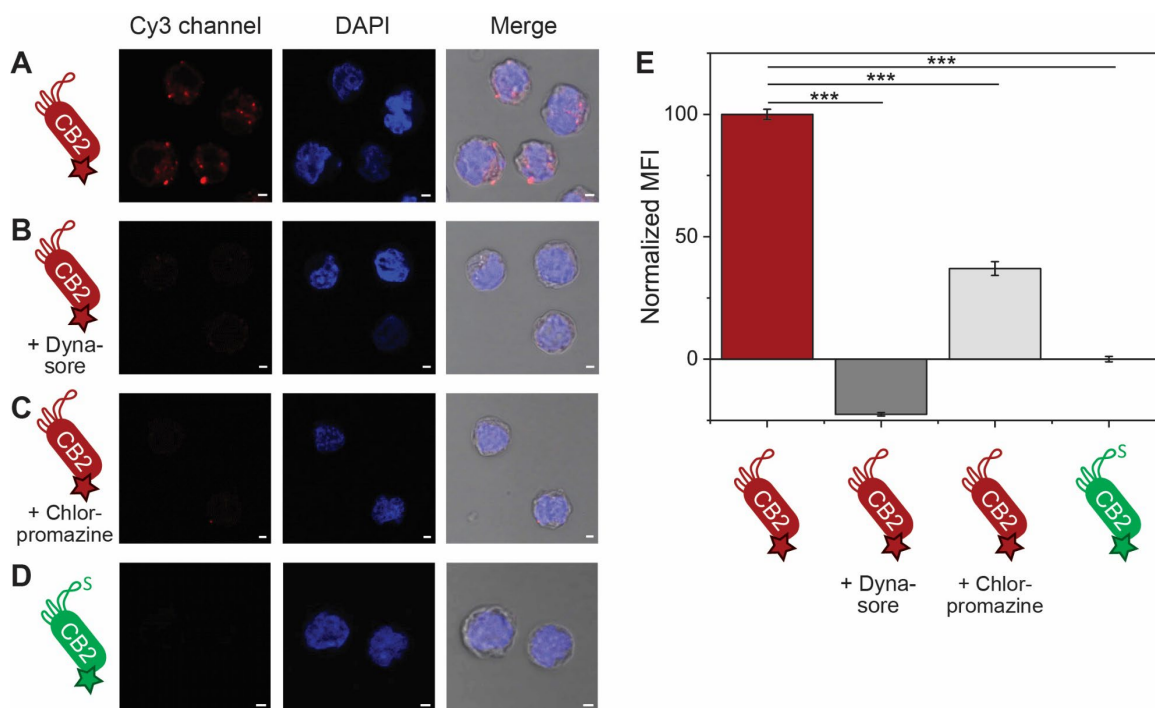


Figure 38 CB2-Cy3 is internalized by SC-1 cells, presumably via clathrin-mediated endocytosis.

Internalization in the absence and presence of clathrin-mediated endocytosis inhibitors dynasore and chlorpromazine was examined by confocal microscopy (A-D) and then quantified (E). Exemplary images of SC-1 cells incubated with (A) CB2-Cy3, (B) CB2-Cy3 + dynasore, (C) CB2-Cy3 + chlorpromazine, and (D) ^{C105S}CB2-Cy3. Note that only CB2-Cy3 is internalized by SC-1 cells. Scale bar = 2 μ m. Red: Cy3 fluorescence, blue: DAPI, greyscale: transmission light. (E) Quantification of internalization. Y axis: normalized MFI from N = 3 and n > 160 cells. Error bars represent SEM. Differences were tested for significance using one-way ANOVA followed by Tukey's *post-hoc* test with (***) p < 0.001.

To further corroborate this observation, it would be interesting to follow the process of CB2 internalization by staining different membrane compartments followed by examination of CB2 co-localization at multiple time points. In addition, clathrin-mediated endocytosis could be selectively inhibited by a clathrin knockdown, for instance via RNA interference. While additional validation of the uptake mechanism is of high relevance, examining possible applications of CB2 internalization was prioritized in this study. Therefore, I proceeded with testing CB2's potential as drug carrier.

3.4.3. CB2-MMAE and ^{C105S}CB2-MMAE can be generated by srtA-mediated conjugation and fully retain binding activity

Considering that CB2 internalizes into cells, I hypothesized that CB2 can be also employed for drug delivery and thus therapeutic application (Figure 39). To test this hypothesis, I conjugated CB2 and ^{C105S}CB2 to the antineoplastic agent monomethyl auristatin E (MMAE).

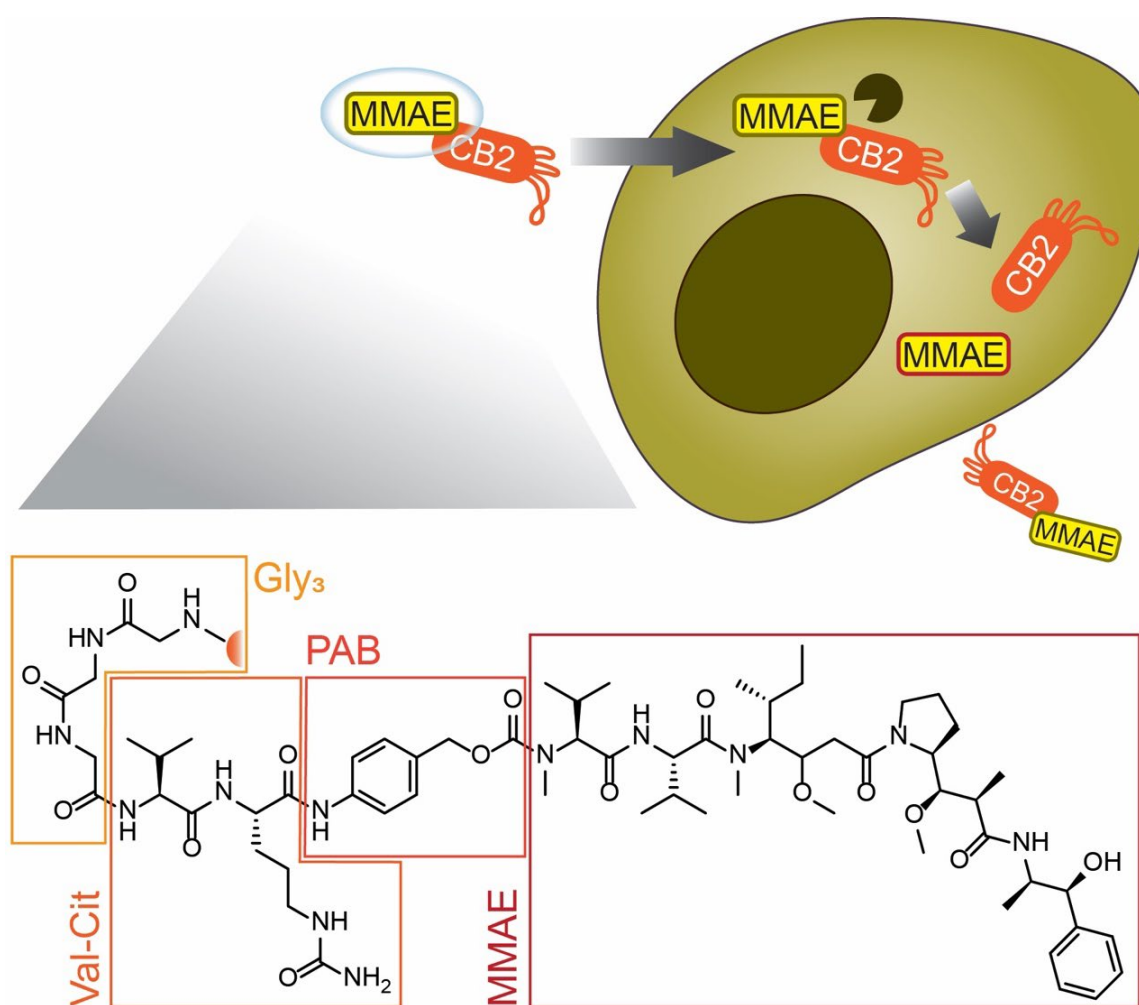


Figure 39 Structure and hypothesized mechanism of action of CB2-MMAE. Top: A part of the CB2-MMAE conjugates becomes internalized by SC-1 cells and intracellular enzymes such as cathepsin cleave off and release MMAE into the cytosol. Released MMAE inhibits tubulin, thereby blocking cell proliferation. Bottom: MMAE construct used in this study. Three terminal glycine are used for srtA-mediated conjugation to CB2. Glycines and the cytotoxic MMAE are connected via a cleavable valine-citrulline (Val-Cit) linker and a para-aminobenzylcarbamate (PAB) spacer.

MMAE is a widely used and approved payload for ADCs and NDCs as it cannot be administered in unconjugated form due to its high potency and resulting off-target toxicity¹⁵⁴. Furthermore, MMAE is already commercially available as glycyated version, amenable to srtA-mediated conjugation. Glycines and MMAE are connected by a para-aminobenzylcarbamate spacer and a valine-citrulline linker (Figure 39). The linker can be cleaved by intracellular cathepsins, ensuring that the drug is only released in the cytosol.

Using the srtA reaction, I successfully generated MMAE conjugates of CB2 and ^{C105S}CB2 (Figure 40). Next, I performed a cell binding assay with both conjugates to rule out that the presence of MMAE changes the binding activity. As expected, CB2-MMAE reliably recognized SC-1 cells, whereas no binding was detected with ^{C105S}CB2-MMAE, confirming that MMAE conjugation does not interfere with binding (Figure 41).

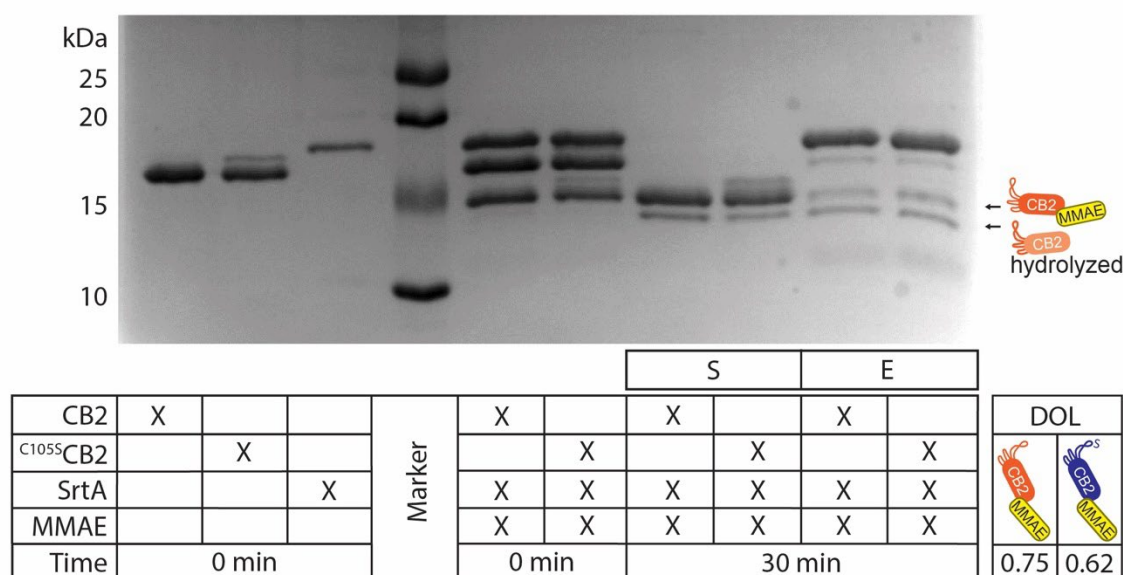


Figure 40 CB2 and ^{C105S}CB2 were successfully conjugated to MMAE. SDS-PAGE showing the different fractions of MMAE conjugation via srtA reaction (S = supernatant, E = eluate). The DOL was determined by quantification of the band intensity of the Coomassie-stained gel. Note that the desired products are detected in the supernatant and only minimal amounts of hydrolyzed Nb are formed.

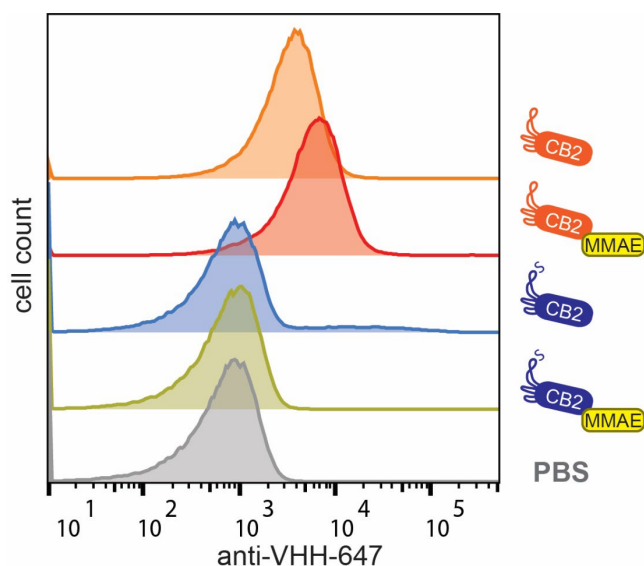


Figure 41 MMAE conjugation does not affect the binding activity of CB2 and C^{105S} CB2. Flow cytometry histogram comparing SC-1 cell binding of CB2 (orange), CB2-MMAE (red), C^{105S} CB2 (blue), C^{105S} CB2-MMAE (green), and PBS (negative control, grey). Note that only CB2 and CB2-MMAE bind SC-1 cells. Y axis: cell count, X axis: fluorescence of anti-VHH-647 Ab.

3.4.4. CB2-MMAE shows higher cytotoxicity against B cell lymphoma than C^{105S} CB2-MMAE

To test CB2's suitability for drug delivery to B cell lymphoma, I screened the cytotoxic effect of CB2-MMAE, C^{105S} CB2-MMAE or unconjugated MMAE at varying concentrations on SC-1 cells (Figure 42). I also included cells treated with Triton X-100 or unconjugated CB2 as positive and negative controls, respectively. Sigmoidal dose-response curves were obtained for all three compounds allowing the determination of IC₅₀ values and quantitative comparison.

While MMAE showed the highest cytotoxic effect as expected with an IC₅₀ in the subnanomolar range, CB2-MMAE still caused considerable cytotoxicity with an IC₅₀ of 3.7 nM. Cytotoxicity of C^{105S} CB2-MMAE was tenfold lower than of CB2-MMAE, suggesting that thiol-mediated uptake enhances drug efficacy (Figure 42). Next, I performed repeated cell viability measurements after treatment of SC-1 cells with CB2-MMAE, C^{105S} CB2-MMAE or unconjugated MMAE at a fixed MMAE concentration (10 nM) to ensure reproducibility. Unconjugated MMAE again showed the highest cytotoxicity (100 % dead cells), followed by CB2-MMAE with approx. 60 % dead cells. In contrast, C^{105S} CB2-MMAE killed only around 10 % of SC-1 cells (Figure 42).

These data suggest that thiol-mediated internalization of CB2 can be exploited to deliver antineoplastic agents into cancer cells and to decrease the high off-target toxicity of MMAE.

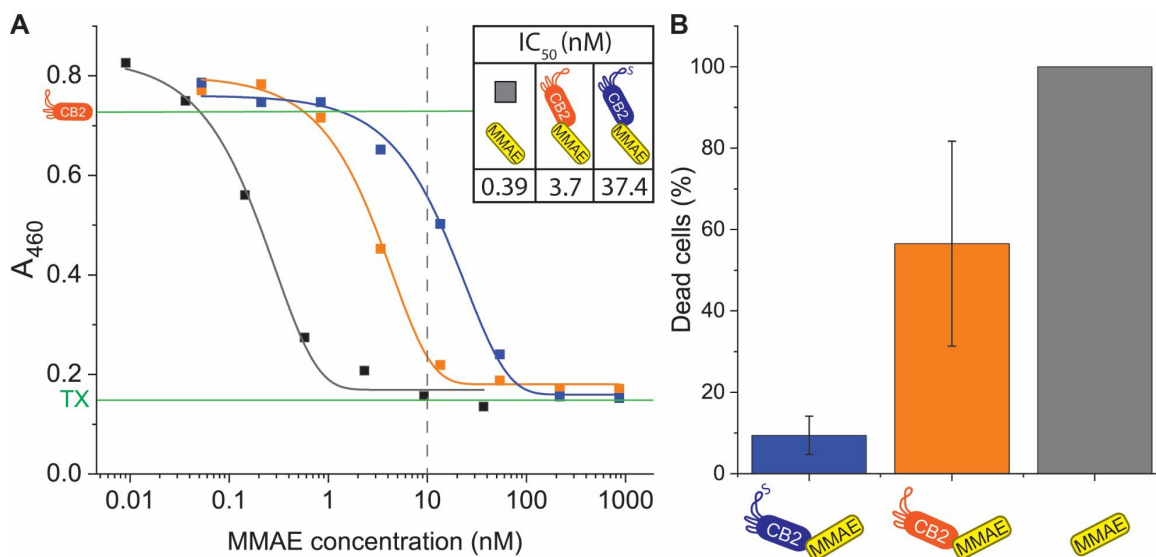


Figure 42 CB2-MMAE can be used for drug delivery to lymphoma cells. (A) Cytotoxicity measurement for various concentrations of MMAE (grey), CB2-MMAE (orange), and ^{C105S}CB2-MMAE (blue). Y axis: A₄₆₀, CCK8 assay read-out correlating to cell proliferation. X axis: MMAE concentration (nM). Sigmoidal dose-response curves were fitted to the measured values in OriginPro. Green lines indicate the measured values for positive (TX = Triton X100) and negative (unconjugated CB2) control. The dotted line indicates the MMAE concentration used for repetitions in (B). Inset: IC₅₀ values (nM) of the three different compounds calculated on the basis of sigmoidal fits. **(B)** Comparison of dead cells (%) induced by 10 nM ^{C105S}CB2-MMAE (blue), CB2-MMAE (orange), and MMAE (grey). Values represent mean ± SEM from N = 3.

However, I believe that two caveats need to be addressed before CB2-MMAE conjugates can be examined in an *in vivo* lymphoma model. First, ^{C105S}CB2-MMAE still caused substantial cell killing even though the IC₅₀ was approx. tenfold lower than the IC₅₀ of CB2-MMAE. Since I did not observe uptake of ^{C105S}CB2-Cy3 (as described in 3.4.2), it seemed unlikely that ^{C105S}CB2-MMAE would become internalized by SC-1 cells, and I assumed that free drug was present during cell incubation, causing non-specific cytotoxicity. While uncoupled MMAE was successfully removed after conjugation via extensive dialysis as confirmed by mass spectrometry, I could indeed detect increasing

amounts of free drug again over time (Figure 43). Since the srtA reaction is in principle reversible, it is conceivable that a small contamination of the Nb-drug conjugate with srtA would revert the conjugation over time, resulting in release of the free drug. For future studies, any remaining srtA should be quenched by chelators such as EDTA, and additional purification steps should be included, for instance hydrophobic interaction chromatography, to ensure sufficient purity of NDCs. In general, stability and purity are highly relevant parameters for any *in vivo* application of NDCs. While it has already become customary to provide evidence for purity and long-term stability for ADCs^{34,155,156}, many reports on NDCs lack convincing validation of their conjugates^{157,158}. With more NDCs entering *in vivo* trials, providing these data will hopefully become common practice.

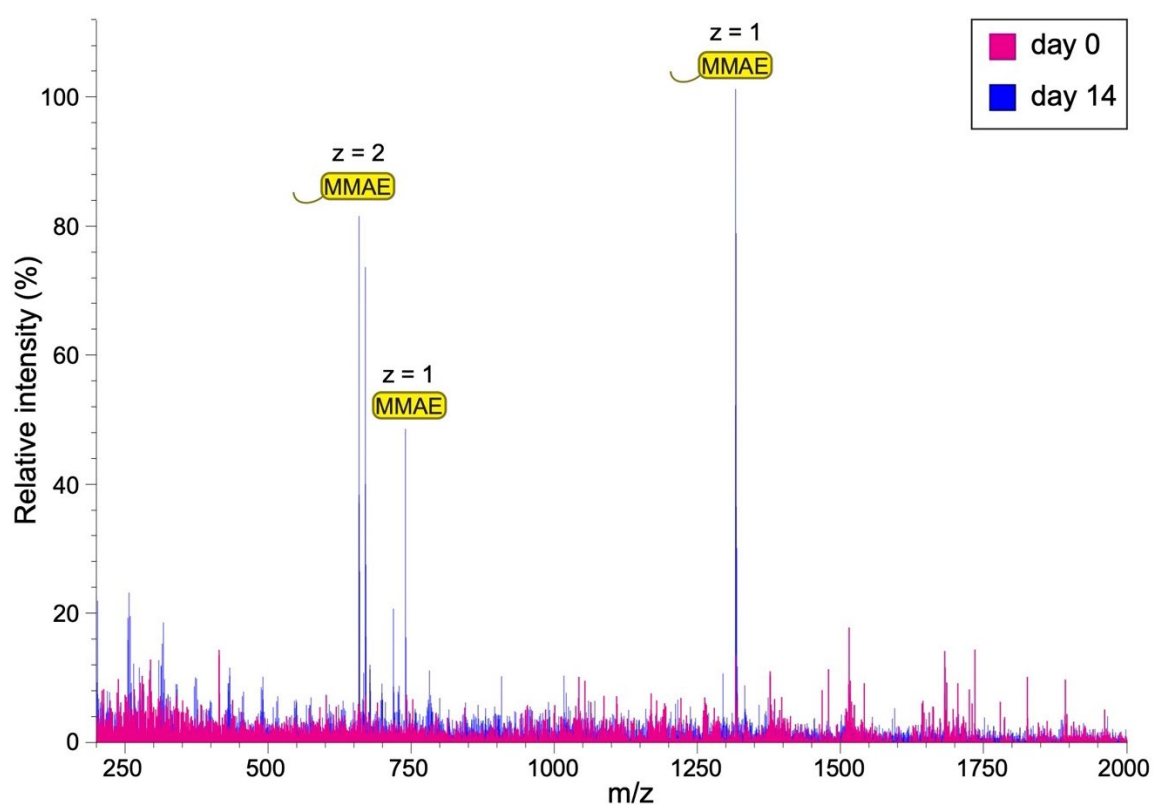


Figure 43 Time-dependent MMAE release from ^{C105S}CB2-MMAE in solution. Comparison of ^{C105S}CB2-MMAE mass spectra at day 0 (pink) and 14 (blue). Note that free MMAE with and without Gly-Gly-Val-Cit-PAB linker is substantially increased after two-week storage at 4 °C. Y axis: relative intensity (%), X axis: m/z with z = charge.

The second caveat is the lack of data on CB2-MMAE cytotoxicity on healthy lymphocytes and other cell types. While I showed that CB2 generally does not bind to healthy human PBMCs (see 3.2.1), even low off-target binding of MMAE conjugates to healthy lymphocytes or other human cell types would result in high off-target cytotoxicity due to the high potency of the drug. Therefore, additional drug delivery assays are required, testing the effect of CB2-MMAE on various control cell lines. However, this was not possible within the scope of this work, as non-tumorigenic lymphocyte cell lines were not available in our lab and healthy PBMCs as primary, non-proliferating cells are incompatible with my assay setup.

3.5. Exploring additional CB2 targets

3.5.1. CB2 specifically recognizes breast cancer cells

In breast cancer, cell attachment and migration during metastasis have been proven to be mediated by free thiol groups on the cancer cells⁶¹. Since CB2 binding correlates with increased surface thiols on B cell lymphoma, I reasoned that breast cancer cells would be potential CB2 targets as well. To test this hypothesis, CB2 binding assays with the two breast cancer cell lines MCF-7 and MDA-MB-231 were performed (Figure 44). As a control, I included the non-tumorigenic breast cell line MCF-10A. Interestingly, CB2 recognized both MCF-7 and MDA-MB-231 cells as detected by flow cytometry. In contrast, hardly any binding was observed with the non-tumorigenic MCF-10A control, indicating that CB2 binding is specific to tumor cells (Figure 44).

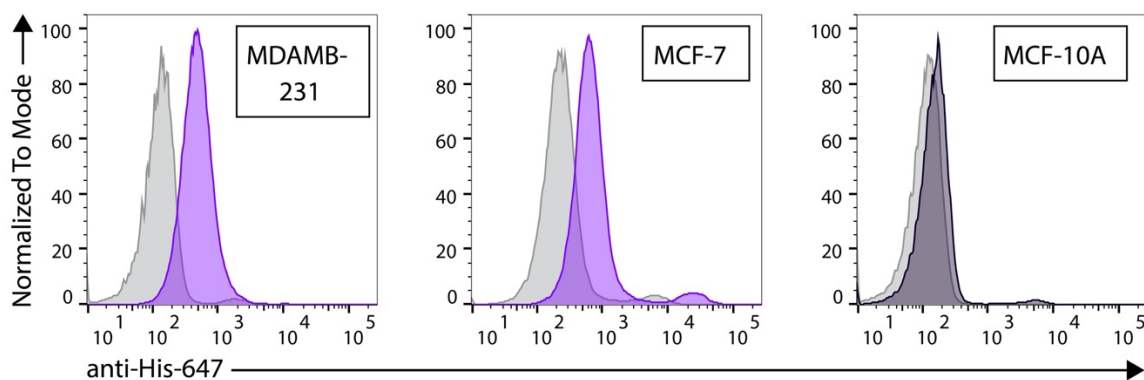


Figure 44 CB2 binds to different breast cancer cell lines but not to non-tumorigenic breast cells.

Flow cytometry histograms show a substantial shift upon CB2 incubation with breast cancer cell lines MDA-MB-231 (left) and MCF-7 (center). No CB2 binding to non-cancer breast cell line MCF-10A (right) was detected. Y axis: cell count normalized to mode, X axis: anti-His-647 fluorescence. Shades of purple = incubation with CB2, grey = incubation with PBS.

This finding is particularly interesting for therapeutic application as treatment of solid tumors highly benefits from the higher penetrability that Nbs can achieve^{88,89}. CB2 binding to the triple-negative breast cancer cell line MDA-MB-231 highlights the potential of surface thiol biomarkers for the therapy of triple-negative breast cancer whose treatment is generally challenging.

3.5.2. CB2 binds to the parasites *P. falciparum* and *L. major*

Cysteine-rich surface proteins are also abundantly found on the surface of the protozoan parasites *Plasmodium* and *Leishmania*, the causative agents of malaria and leishmaniasis, respectively¹⁵⁹⁻¹⁶⁴. They play a crucial role during *Plasmodium* invasion into host cells^{160,162}, and the parasite also induces expression of cysteine-rich proteins on the surface of infected erythrocytes after invading them¹⁶⁵. Previously, we already showed that surface thiols on *Plasmodium*-infected red blood cells can be targeted for drug delivery⁷⁴. Therefore, I speculated that CB2 might be able to bind to surface thiols on parasites as well, and tested CB2 on *Plasmodium falciparum* and *Leishmania major* parasites (Figure 45).

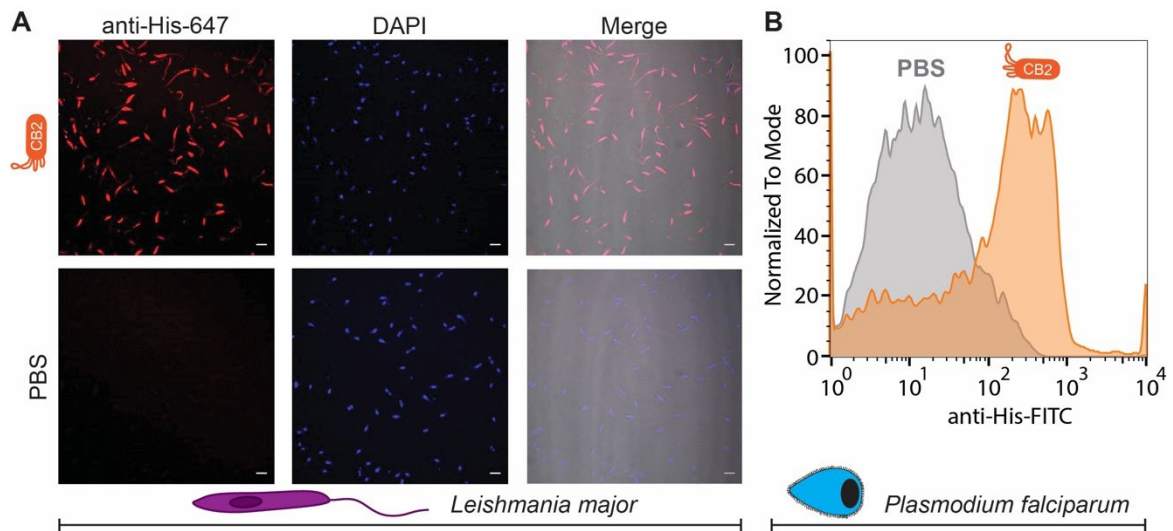


Figure 45 CB2 recognizes *L. major* and *P. falciparum*. (A) Immunostaining of *L. major* with CB2 or PBS (negative control) for confocal microscopy. Red: anti-His-647, blue: DAPI, greyscale: transmission light. Scale bar = 10 μ m. (B) Flow cytometry histogram of isolated *P. falciparum* incubated with CB2 (orange) or PBS (negative control, grey). Y axis: cell count normalized to mode, X axis: fluorescence of anti-His-FITC. Note that CB2 exhibits strong binding to both parasite species.

Incubation of *P. falciparum* with CB2 caused a marked shift in fluorescence detected by flow cytometry. Similarly, I observed a strong fluorescence signal on *L. major* parasites under the microscope after incubation with CB2 (Figure 45). These data suggest that CB2 can indeed be used to target protozoan parasites. Targeting parasite thiols is particularly attractive as overexpression of cysteine-rich proteins has been linked to drug resistance in *Leishmania*, highlighting the functional relevance of these proteins for the parasite's survival^{166,167}.

4. Conclusions and Outlook

Despite recent advances in cancer diagnostics and therapy, cancer remains the second-most common cause of death for humans, affecting millions of people worldwide every year. Both TACAs and surface thiols are tumor biomarkers with great potential as they are abundantly and specifically found on many cancer types, but the biological tools to target these biomarkers are sparse. With this thesis, I aimed to contribute to the toolbox of TACA- and thiol-binding biologicals in the fight against cancer.

By immunizing an alpaca with several TACA-CRM197 conjugates, I showed that the formation of TACA-targeting hcAbs can be reliably induced. Based on these hcAbs, my colleagues and I successfully developed Nbs with high-specificity for the TACA Globo-H, validated with the synthetic glycan in solution and the native glycan displayed on breast cancer cells¹⁴¹. The alpaca serum collected for this thesis also forms the basis for the development of additional Nbs targeting the other TACAs used for immunization, and a project aimed at generating anti-STn Nbs is already ongoing.

Taken together, these results prove that glycoconjugate immunization of alpacas is a feasible and suitable approach for the generation of anti-glycan Nbs. To my knowledge, this is the first report using synthetic glycans throughout the entire workflow of Nb development, from animal immunization till validation of binders¹⁴¹. The homogeneity and defined nature of synthetic glycans allows for the induction of glycan-specific hcAbs in the animal, and this work provides evidence for the potential of synthetic glycans for alpaca immunization.

With CB2, I introduced the first Nb with a binding mechanism based on thiol-thiol interactions, thereby contributing to the toolbox of thiol-binding probes. I demonstrated that CB2 specifically recognizes B cell lymphoma but not healthy lymphocytes, and I showed that the specificity is linked to elevated levels of surface thiols on lymphoma cells. CB2 binding strictly required the presence of cysteine 105 and was followed by thiol-mediated uptake into lymphoma cells, giving rise to a

plethora of potential diagnostic and therapeutic applications. In future studies, the precise uptake mechanism should be examined in more detail as internalizing Nbs are of great interest for the scientific community. For instance, binding to cell surface thiols and the proposed uptake via clathrin-mediated endocytosis could be further corroborated by knockdown experiments directed against PDI or clathrin which would also allow a step-by-step recapitulation of the whole process. The observation of Nb internalization via thiol-thiol interactions raises the question whether the internalization feature can be engineered into other Nb sequences as well. Even bispecific Nbs that retain target binding but also engage with cell surface cysteines are conceivable. Both internalization and target binding could be examined in parallel, for instance, by engineering a cysteine into different positions of the CDRs of a commonly used Nb with a known target. These questions are of particular importance in light of my results showing that thiol-mediated binding and uptake are highly applicable in combination with Nb functionalization.

On one hand, I demonstrated that fusions of CB2 and rhamnosylated glycopeptides are capable of recruiting Abs and activating the complement cascade against lymphoma cells. Conjugation of multiple Rha₃ moieties was the key to efficient Ab recruitment and complement activation, highlighting the importance of multivalent ARM display for triggering a robust immune response. On the other hand, CB2 internalization was exploited for drug delivery into lymphoma cells. My findings argue for a model where different populations of surface proteins are targeted by CB2, as Ab recruitment to the cell surface and internalization for drug delivery were observed within the same time scale. This suggests that some CB2 targets remain on the surface while others become internalized upon CB2 binding, and future work should focus on elucidating the different CB2 targets to validate this model.

Another layer of complexity is added by the observation that CB2 also binds to *Plasmodium/Leishmania* parasites and breast cancer cells but not to healthy breast cells. Again, this poses the question which proteins are targeted by CB2, and experiments

with additional control cell lines should be performed to characterize CB2's binding profile in more detail. This becomes particularly important for drug delivery where even low off-target binding can cause tremendous side effects. At the same time, the fact that thiol-binding Nbs are suitable for targeting such a diverse array of clinically relevant cell types emphasizes the great potential of surface thiols as disease biomarkers. In this context, quantitative data on surface thiol levels of various cancers is highly anticipated. I started filling this gap by comparing the accessible thiol groups on lymphoma cells and healthy lymphocytes, but additional cancer types should be examined to elucidate whether elevated surface thiol levels are a general feature of the tumor microenvironment.

Finally, *in vivo* examination of CB2 would be highly beneficial to assess the suitability of thiol-binding Nbs for diagnostic and therapeutic use. While surface thiols are present on any given cell, sufficient specificity could be achieved if the levels of free thiols are significantly higher on target cells than on healthy cells, similar to many protein and glycan antigens which are found at a basal level on healthy cells but appear highly elevated on cancer cells. To assess the applicability of CB2 for NHL diagnostics, a project examining blood samples from lymphoma patients is already ongoing in our lab.

While this work showcases applications of CB2 in Ab recruitment and drug delivery, my results will hopefully spark investigations of further applications. For instance, CB2-nuclide fusions could be generated for tumor tomography. Bispecific Nbs are also conceivable, combining the thiol specificity of CB2 with specificity for another lymphoma antigen, e.g. via fusion to an anti-CD19 Nb. Thereby, off-target binding could be further decreased, and desired therapeutic effects, such as receptor internalization leading to tumor inhibition, could be achieved. Finally, CB2 might be used for immunotherapy of B cell lymphoma by engineering CB2 into chimeric antigen receptors on genetically modified T cells (so-called CAR T cell therapy); work on this is already ongoing in our lab and initial results look promising. These examples illustrate the numerous potential applications of CB2, and I therefore envisage a bright future for thiol-binding, internalizing Nbs.

5. References

1. Sung, H. *et al.* Global Cancer Statistics 2020: GLOBOCAN Estimates of Incidence and Mortality Worldwide for 36 Cancers in 185 Countries. *CA. Cancer J. Clin.* **71**, (2021).
2. <https://www.who.int/news-room/fact-sheets/detail/cancer>. Cancer Fact Sheet. *World Heal. Organ. accessed 2022-08-10*.
3. Ferlay J *et al.* Global Cancer Observatory: Cancer Today. *Int. Agency Res. Cancer* **68**, (2020).
4. Shankland, K. R., Armitage, J. O. & Hancock, B. W. Non-Hodgkin lymphoma. *Lancet* **380**, 848–857 (2012).
5. <https://seer.cancer.gov/statfacts/html/nhl.html>. Cancer Stat Facts: Non-Hodgkin Lymphoma. *National Cancer Institute, accessed 2022-06-26*.
6. Denmeade, S. R. & Isaacs, J. T. A history of prostate cancer treatment. *Nature Reviews Cancer* vol. 2 (2002).
7. Waks, A. G. & Winer, E. P. Breast Cancer Treatment: A Review. *Journal of the American Medical Association* vol. 321 (2019).
8. Chabner, B. A. & Roberts, T. G. Chemotherapy and the war on cancer. *Nature Reviews Cancer* vol. 5 (2005).
9. Anderson, C. S., Quinones, R. & Olson, M. R. Determining efficacy and side effects from concurrent use of chemotherapy and radiation therapy for the management of adult solid tumors. *J. Clin. Oncol.* **32**, (2014).
10. Zugazagoitia, J. *et al.* Current Challenges in Cancer Treatment. *Clinical Therapeutics* vol. 38 (2016).
11. Schietinger, A., Philip, M. & Schreiber, H. Specificity in cancer immunotherapy. *Seminars in Immunology* vol. 20 (2008).

12. Mullard, A. FDA approves 100th monoclonal antibody product. *Nature reviews. Drug discovery* vol. 20 (2021).
13. Adler, M. J. & Dimitrov, D. S. Therapeutic Antibodies Against Cancer. *Hematology/Oncology Clinics of North America* vol. 26 (2012).
14. Piccart-Gebhart, M. J. *et al.* Trastuzumab after Adjuvant Chemotherapy in HER2-Positive Breast Cancer. *N. Engl. J. Med.* **353**, (2005).
15. <https://seer.cancer.gov/statfacts/html/breast-subtypes.html>. Cancer Stat Facts: Female Breast Cancer Subtypes. *National Cancer Institute, accessed 2022-06-29*.
16. An, Z., Aksoy, O., Zheng, T., Fan, Q. W. & Weiss, W. A. Epidermal growth factor receptor and EGFRvIII in glioblastoma: Signaling pathways and targeted therapies. *Oncogene* vol. 37 (2018).
17. Lampson, L. A. Monoclonal antibodies in neuro-oncology: Getting past the blood-brain barrier. *mAbs* vol. 3 (2011).
18. Sharma, P., Hu-Lieskovan, S., Wargo, J. A. & Ribas, A. Primary, Adaptive, and Acquired Resistance to Cancer Immunotherapy. *Cell* vol. 168 (2017).
19. Hakomori, S. I. Tumor-associated carbohydrate antigens defining tumor malignancy: Basis for development of anti-cancer vaccines. in *Advances in Experimental Medicine and Biology* vol. 491 (2001).
20. Taniguchi, N. & Kizuka, Y. Glycans and cancer: Role of N-Glycans in cancer biomarker, progression and metastasis, and therapeutics. in *Advances in Cancer Research* vol. 126 (2015).
21. Radhakrishnan, P. *et al.* Immature truncated O-glycophenotype of cancer directly induces oncogenic features. *Proc. Natl. Acad. Sci.* **111**, (2014).
22. Leivonen, M., Nordling, S., Lundin, J., Von Boguslawski, K. & Haglund, C. STn and prognosis in breast cancer. *Oncology* **61**, (2001).
23. Freitas, D. *et al.* O-glycans truncation modulates gastric cancer cell signaling and

- transcription leading to a more aggressive phenotype. *EBioMedicine* **40**, (2019).
24. Ferreira, J. A. *et al.* Overexpression of tumour-associated carbohydrate antigen sialyl-Tn in advanced bladder tumours. *Mol. Oncol.* **7**, (2013).
 25. Julien, S., Videira, P. A. & Delannoy, P. Sialyl-Tn in cancer: (How) did we miss the target? *Biomolecules* **2**, (2012).
 26. Kurtenkov, O. Profiling of Naturally Occurring Antibodies to the Thomsen-Friedenreich Antigen in Health and Cancer: The Diversity and Clinical Potential. *Biomed Res. Int.* **2020**, (2020).
 27. Chang, W. W. *et al.* Expression of Globo H and SSEA3 in breast cancer stem cells and the involvement of fucosyl transferases 1 and 2 in Globo H synthesis. *Proc. Natl. Acad. Sci.* **105**, (2008).
 28. Gottschling, S. *et al.* Stage-specific embryonic antigen-4 is expressed in basaloid lung cancer and associated with poor prognosis. *Eur. Respir. J.* **41**, (2013).
 29. Hung, T. C., Lin, C. W., Hsu, T. L., Wu, C. Y. & Wong, C. H. Investigation of SSEA-4 binding protein in breast cancer cells. *J. Am. Chem. Soc.* **135**, (2013).
 30. Sivasubramanian, K. *et al.* Expression of stage-specific embryonic antigen-4 (SSEA-4) defines spontaneous loss of epithelial phenotype in human solid tumor cells. *Glycobiology* **25**, (2015).
 31. Cheng, J. Y. *et al.* Globo-H ceramide shed from cancer cells triggers translin-Associated factor X-dependent angiogenesis. *Cancer Res.* **74**, (2014).
 32. Danishefsky, S. J., Shue, Y. K., Chang, M. N. & Wong, C. H. Development of Globo-H Cancer Vaccine. *Acc. Chem. Res.* **48**, (2015).
 33. Gilewski, T. *et al.* Immunization of metastatic breast cancer patients with a fully synthetic globo H conjugate: A phase I trial. *Proc. Natl. Acad. Sci.* **98**, (2001).
 34. Yang, M. C. *et al.* Preclinical studies of OBI-999: A novel globo h-targeting antibody-drug conjugate. *Mol. Cancer Ther.* **20**, (2021).

35. Huang, C. S. *et al.* Globo H-KLH vaccine adagloxad simolenin (OBI-822)/OBI-821 in patients with metastatic breast cancer: phase II randomized, placebo-controlled study. *J. Immunother. cancer* **8**, 342 (2020).
36. Huang, C.-S. *et al.* Randomized phase II/III trial of active immunotherapy with OPT-822/OPT-821 in patients with metastatic breast cancer. *J. Clin. Oncol.* **34**, (2016).
37. Rugo, H. S. *et al.* Phase III, randomized, double-blind, placebo-controlled study to evaluate the efficacy and safety of adagloxad simolenin (OBI-822) and OBI-821 treatment in patients with early-stage triple-negative breast cancer (TNBC) at high risk for recurrence. *J. Clin. Oncol.* **38**, (2020).
38. Feizi, T. Oligosaccharides that mediate mammalian cell-cell adhesion. *Curr. Opin. Struct. Biol.* **3**, (1993).
39. Hasegawa, A., Kiso, M. & Kannagi, R. Contribution of Carbohydrate Antigens Sialyl Lewis A and Sialyl Lewis X to Adhesion of Human Cancer Cells to Vascular Endothelium. *Cancer Res.* **53**, (1993).
40. Pendu, J. L. E. *et al.* ABH and Lewis histo-blood group antigens in cancer. *APMIS* vol. 109 (2001).
41. Luo, G. *et al.* Roles of CA19-9 in pancreatic cancer: Biomarker, predictor and promoter. *Biochimica et Biophysica Acta - Reviews on Cancer* vol. 1875 (2021).
42. Nudelman, E., Lavery, S. B., Kaizu, T. & Hakomori, S. Novel fucolipids of human adenocarcinoma: Characterization of the major Le(y) antigen of human adenocarcinoma as trifucosylnonaosyl Le(y) glycolipid (III3FucV3FucVI2FucnLc6). *J. Biol. Chem.* (1986).
43. Goonetilleke, K. S. & Siriwardena, A. K. Systematic review of carbohydrate antigen (CA 19-9) as a biochemical marker in the diagnosis of pancreatic cancer. *European Journal of Surgical Oncology* vol. 33 (2007).

44. Yip, G. W., Smollich, M. & Götte, M. Therapeutic value of glycosaminoglycans in cancer. *Molecular Cancer Therapeutics* vol. 5 (2006).
45. Wei, J., Hu, M., Huang, K., Lin, S. & Du, H. Roles of proteoglycans and glycosaminoglycans in cancer development and progression. *International Journal of Molecular Sciences* vol. 21 (2020).
46. Itzkowitz, S. H. *et al.* Expression of Tn, Sialosyl-Tn, and T Antigens in Human Colon Cancer. *Cancer Res.* **49**, (1989).
47. Sterner, E., Flanagan, N. & Gildersleeve, J. C. Perspectives on Anti-Glycan Antibodies Gleaned from Development of a Community Resource Database. *ACS Chem. Biol.* **11**, (2016).
48. Temme, J. S., Butler, D. L. & Gildersleeve, J. C. Anti-glycan antibodies: Roles in human disease. *Biochemical Journal* vol. 478 (2021).
49. Ballehaninna, U. K. & Chamberlain, R. S. The clinical utility of serum CA 19-9 in the diagnosis, prognosis and management of pancreatic adenocarcinoma: An evidence based appraisal. *J. Gastrointest. Oncol.* **3**, (2012).
50. Joseph, A. A., Pardo-Vargas, A. & Seeberger, P. H. Total Synthesis of Polysaccharides by Automated Glycan Assembly. *J. Am. Chem. Soc.* (2020) doi:10.1021/jacs.0c00751.
51. Danglad-Flores, J. *et al.* Microwave-Assisted Automated Glycan Assembly. *J. Am. Chem. Soc.* **143**, (2021).
52. Hahm, H. S. *et al.* Automated glycan assembly using the glyconeer 2.1 synthesizer. *Proc. Natl. Acad. Sci.* **114**, (2017).
53. Astronomo, R. D. & Burton, D. R. Carbohydrate vaccines: Developing sweet solutions to sticky situations? *Nature Reviews Drug Discovery* vol. 9 (2010).
54. Zasłona, M. E., Downey, A. M., Seeberger, P. H. & Moscovitz, O. Semi- And fully synthetic carbohydrate vaccines against pathogenic bacteria: recent

- developments. *Biochemical Society Transactions* vol. 49 (2021).
55. Avci, F. Y., Li, X., Tsuji, M. & Kasper, D. L. A mechanism for glycoconjugate vaccine activation of the adaptive immune system and its implications for vaccine design. *Nat. Med.* **17**, (2011).
 56. Ishioka, G. Y. *et al.* MHC interaction and T cell recognition of carbohydrates and glycopeptides. *J. Immunol.* **148**, (1992).
 57. Kaplonek, P. Improving the Immunoprotective Effect of Carbohydrate Vaccine Against Bacterial Pneumonia. (2020). doi:10.17169/refubium-27044.
 58. Giannini, G., Rappuoli, R. & Ratti, G. The amino-acid sequence of two non-toxic mutants of diphtheria toxin: CRM45 and CRM197. *Nucleic Acids Res.* **12**, (1984).
 59. Gruber, W. C., Scott, D. A. & Emini, E. A. Development and clinical evaluation of Prevnar 13, a 13-valent pneumococcal CRM197 conjugate vaccine. *Ann. N. Y. Acad. Sci.* **1263**, (2012).
 60. Arnér, E. S. J. & Holmgren, A. The thioredoxin system in cancer. *Semin. Cancer Biol.* **16**, 420–426 (2006).
 61. Popielarski, M., Ponamarczuk, H., Stasiak, M., Watała, C. & Świątkowska, M. Modifications of disulfide bonds in breast cancer cell migration and invasiveness. *Am. J. Cancer Res.* **9**, 1554 (2019).
 62. Sahaf, B., Heydari, K., Herzenberg, L. A. & Herzenberg, L. A. Lymphocyte surface thiol levels. *Proc. Natl. Acad. Sci.* **100**, (2003).
 63. Robinson, R. M. *et al.* Inhibitors of the protein disulfide isomerase family for the treatment of multiple myeloma. *Leukemia* **33**, 1011–1022 (2019).
 64. Kuo, T. F. *et al.* Protein disulfide isomerase a4 acts as a novel regulator of cancer growth through the procaspase pathway. *Oncogene* **36**, 5484–5496 (2017).
 65. Tufo, G. *et al.* The protein disulfide isomerases PDIA4 and PDIA6 mediate resistance to cisplatin-induced cell death in lung adenocarcinoma. *Cell Death*

- Differ.* **21**, 685–695 (2014).
66. Aubry, S. *et al.* Cell-surface thiols affect cell entry of disulfide-conjugated peptides. *FASEB J.* **23**, 2956–2967 (2009).
 67. Gasparini, G., Sargsyan, G., Bang, E. K., Sakai, N. & Matile, S. Ring Tension Applied to Thiol-Mediated Cellular Uptake. *Angew. Chemie - Int. Ed.* **54**, 7328–7331 (2015).
 68. Li, T. & Takeoka, S. Enhanced cellular uptake of maleimide-modified liposomes via thiol-mediated transport. *Int. J. Nanomedicine* **9**, 2849–2861 (2014).
 69. Torres, A. G. & Gait, M. J. Exploiting cell surface thiols to enhance cellular uptake. *Trends in Biotechnology* vol. 30 (2012).
 70. Laurent, Q. *et al.* Thiol-Mediated Uptake. *JACS Au* **1**, 710–728 (2021).
 71. Okamoto, Y. *et al.* A cell-penetrating artificial metalloenzyme regulates a gene switch in a designer mammalian cell. *Nat. Commun.* **9**, (2018).
 72. Derivery, E., Bartolami, E., Matile, S. & Gonzalez-Gaitan, M. Efficient Delivery of Quantum Dots into the Cytosol of Cells Using Cell-Penetrating Poly(disulfide)s. *J. Am. Chem. Soc.* **139**, (2017).
 73. Digilio, G. *et al.* Exofacial protein thiols as a route for the internalization of Gd(III)-based complexes for magnetic resonance imaging cell labeling. *J. Med. Chem.* **53**, (2010).
 74. Varela-Aramburu, S. *et al.* Targeting and inhibiting Plasmodium falciparum using ultra-small gold nanoparticles. *ACS Appl. Mater. Interfaces* **9**, (2020).
 75. Zhang, Q. *et al.* Functionalized mesoporous silica nanoparticles with mucoadhesive and sustained drug release properties for potential bladder cancer therapy. *Langmuir* **30**, (2014).
 76. Hamers-Casterman, C. *et al.* Naturally occurring antibodies devoid of light chains. *Nature* **363**, 446–448 (1993).

77. Maass, D. R., Sepulveda, J., Pernthaner, A. & Shoemaker, C. B. Alpaca (Lama pacos) as a convenient source of recombinant camelid heavy chain antibodies (VHHs). *J. Immunol. Methods* **324**, (2007).
78. Hassanzadeh-Ghassabeh, G., Devoogdt, N., De Pauw, P., Vincke, C. & Muyldermans, S. Nanobodies and their potential applications. *Nanomedicine* **8**, 1013–1026 (2013).
79. Muyldermans, S. Nanobodies: Natural Single-Domain Antibodies. *Annu. Rev. Biochem.* **82**, 775–797 (2013).
80. Vu, K. B., Ghahroudi, M. A., Wyns, L. & Muyldermans, S. Comparison of llama V(H) sequences from conventional and heavy chain antibodies. *Mol. Immunol.* **34**, (1997).
81. Wu, T. Te, Johnson, G. & Kabat, E. A. Length distribution of CDRH3 in antibodies. *Proteins: Structure, Function, and Bioinformatics* vol. 16 (1993).
82. Stijlemans, B. *et al.* Efficient targeting of conserved cryptic epitopes of infectious agents by single domain antibodies: African trypanosomes as paradigm. *J. Biol. Chem.* **279**, 1256–1261 (2004).
83. Chen, X., Gentili, M., Hacoheh, N. & Regev, A. A cell-free nanobody engineering platform rapidly generates SARS-CoV-2 neutralizing nanobodies. *Nat. Commun.* **12**, (2021).
84. Vincke, C. *et al.* General strategy to humanize a camelid single-domain antibody and identification of a universal humanized nanobody scaffold. *J. Biol. Chem.* **284**, (2009).
85. Govaert, J. *et al.* Dual beneficial effect of interloop disulfide bond for single domain antibody fragments. *J. Biol. Chem.* **287**, 1970–9 (2012).
86. Hoefman, S., Ottevaere, I., Baumeister, J. & Sargentini-Maier, M. L. Pre-clinical intravenous serum pharmacokinetics of albumin binding and non-half-life

- extended nanobodies®. *Antibodies* **4**, (2015).
87. Ackaert, C. *et al.* Immunogenicity Risk Profile of Nanobodies. *Front. Immunol.* **12**, (2021).
 88. Debie, P. *et al.* Size and affinity kinetics of nanobodies influence targeting and penetration of solid tumours. *J. Control. Release* **317**, (2020).
 89. Li, Z. *et al.* Influence of molecular size on tissue distribution of antibody fragments. *MAbs* **8**, (2016).
 90. Holzlöhner, P. & Hanack, K. Generation of murine monoclonal antibodies by hybridoma technology. *J. Vis. Exp.* **2017**, (2017).
 91. Monegal, A. *et al.* Immunological applications of single-domain llama recombinant antibodies isolated from a naïve library. *Protein Eng. Des. Sel.* **22**, (2009).
 92. Yan, J., Li, G., Hu, Y., Ou, W. & Wan, Y. Construction of a synthetic phage-displayed Nanobody library with CDR3 regions randomized by trinucleotide cassettes for diagnostic applications. *J. Transl. Med.* **12**, (2014).
 93. Yau, K. Y. F. *et al.* Selection of hapten-specific single-domain antibodies from a non-immunized llama ribosome display library. *J. Immunol. Methods* **281**, (2003).
 94. Pellis, M. *et al.* A bacterial-two-hybrid selection system for one-step isolation of intracellularly functional Nanobodies. *Arch. Biochem. Biophys.* **526**, (2012).
 95. McMahon, C. *et al.* Yeast surface display platform for rapid discovery of conformationally selective nanobodies. *Nat. Struct. Mol. Biol.* **25**, (2018).
 96. Fridy, P. C. *et al.* A robust pipeline for rapid production of versatile nanobody repertoires. *Nat. Methods* **11**, 1253–1260 (2014).
 97. Ebrahimizadeh, W. *et al.* Isolation and characterization of protective anti-LPS nanobody against *V. cholerae* O1 recognizing Inaba and Ogawa serotypes. *Appl.*

- Microbiol. Biotechnol.* **97**, (2013).
98. Behar, G. *et al.* Llama single-domain antibodies directed against nonconventional epitopes of tumor-associated carcinoembryonic antigen absent from nonspecific cross-reacting antigen. *FEBS J.* **276**, (2009).
 99. Beirnaert, E. *et al.* Bivalent llama single-domain antibody fragments against tumor necrosis factor have picomolar potencies due to intramolecular interactions. *Front. Immunol.* **8**, (2017).
 100. Bannas, P., Hambach, J. & Koch-Nolte, F. Nanobodies and nanobody-based human heavy chain antibodies as antitumor therapeutics. *Frontiers in Immunology* vol. 8 (2017).
 101. Ding, L. *et al.* Small sized EGFR1 and HER2 specific bifunctional antibody for targeted cancer therapy. *Theranostics* **5**, (2015).
 102. Ries, J., Kaplan, C., Platonova, E., Eghlidi, H. & Ewers, H. A simple, versatile method for GFP-based super-resolution microscopy via nanobodies. *Nat. Methods* **9**, 582–584 (2012).
 103. Maier, J., Traenkle, B. & Rothbauer, U. Visualizing epithelial-mesenchymal transition using the chromobody technology. *Cancer Research* vol. 76 (2016).
 104. Oliveira, S. *et al.* Rapid visualization of human tumor xenografts through optical imaging with a near-infrared fluorescent anti-epidermal growth factor receptor nanobody. *Mol. Imaging* **11**, (2012).
 105. Kijanka, M. *et al.* Rapid optical imaging of human breast tumour xenografts using anti-HER2 VHHs site-directly conjugated to IRDye 800CW for image-guided surgery. *Eur. J. Nucl. Med. Mol. Imaging* **40**, (2013).
 106. Sheridan, R. T. C., Hudon, J., Hank, J. A., Sondel, P. M. & Kiessling, L. L. Rhamnose glycoconjugates for the recruitment of endogenous anti-carbohydrate antibodies to tumor cells. *ChemBioChem* **15**, 1393–1398 (2014).

107. Farah, F. S. Natural Antibodies Specific to the 2,4-Dinitrophenyl Group*. *Immunology* **25**, (1973).
108. Macher, B. A. & Galili, U. The Gal α 1,3Gal β 1,4GlcNAc-R (α -Gal) epitope: A carbohydrate of unique evolution and clinical relevance. *Biochim. Biophys. Acta - Gen. Subj.* **1780**, (2008).
109. Galili, U., Rachmilewitz, E. A., Peleg, A. & Flechner, I. A unique natural human IgG antibody with anti- α -galactosyl specificity. *J. Exp. Med.* **160**, (1984).
110. van der Beek, S. L. *et al.* Streptococcal dTDP-L-rhamnose biosynthesis enzymes: functional characterization and lead compound identification. *Mol. Microbiol.* **111**, (2019).
111. Crispell, G. *et al.* Discovery of alpha-gal-containing antigens in North American tick species believed to induce red meat allergy. *Front. Immunol.* **10**, (2019).
112. Kovacs, C. J., Faustoferri, R. C., Bischer, A. P. & Quivey, R. G. Streptococcus mutans requires mature rhamnose-glucose polysaccharides for proper pathophysiology, morphogenesis and cellular division. *Mol. Microbiol.* **112**, (2019).
113. Galili, U. & Swanson, K. Gene sequences suggest inactivation of alpha-1,3-galactosyltransferase in catarrhines after the divergence of apes from monkeys. *Proc. Natl. Acad. Sci.* **88**, 7401–7404 (1991).
114. Oyelaran, O., McShane, L. M., Dodd, L. & Gildersleeve, J. C. Profiling human serum antibodies with a carbohydrate antigen microarray. *J. Proteome Res.* **8**, (2009).
115. Wang, S. Y. & Weiner, G. Complement and cellular cytotoxicity in antibody therapy of cancer. *Expert Opinion on Biological Therapy* vol. 8 (2008).
116. Hong, H. *et al.* Site-specific C-terminal dinitrophenylation to reconstitute the antibody Fc functions for nanobodies. *Chem. Sci.* **10**, 9331–9338 (2019).

117. Zhou, K. *et al.* Chemical Synthesis of Antibody–Hapten Conjugates Capable of Recruiting the Endogenous Antibody to Magnify the Fc Effector Immunity of Antibody for Cancer Immunotherapy. *J. Med. Chem.* **65**, (2022).
118. Li, X. *et al.* Targeting Tumor Cells by Natural Anti-Carbohydrate Antibodies Using Rhamnose-Functionalized Liposomes. *ACS Chem. Biol.* **11**, 1205–1209 (2016).
119. Hong, H. *et al.* Chemoenzymatic Synthesis of a Rhamnose-Functionalized Bispecific Nanobody as a Bispecific Antibody Mimic for Cancer Immunotherapy. *Angew. Chemie Int. Ed.* (2022) doi:10.1002/anie.202208773.
120. Schumacher, D., Helma, J., Schneider, A. F. L., Leonhardt, H. & Hackenberger, C. P. R. Nanobodies: Chemical Functionalization Strategies and Intracellular Applications. *Angew. Chemie Int. Ed.* **57**, 2314–2333 (2018).
121. Heukers, R. *et al.* Endocytosis of EGFR requires its kinase activity and N-terminal transmembrane dimerization motif. *J. Cell Sci.* **126**, (2013).
122. Bruce, V. J., Lopez-Islas, M. & McNaughton, B. R. Resurfaced cell-penetrating nanobodies: A potentially general scaffold for intracellularly targeted protein discovery. *Protein Sci.* **25**, 1129–1137 (2016).
123. Herce, H. D. *et al.* Cell-permeable nanobodies for targeted immunolabelling and antigen manipulation in living cells. *Nat. Chem.* **9**, 762–771 (2017).
124. Khongorzul, P., Ling, C. J., Khan, F. U., Ihsan, A. U. & Zhang, J. Antibody-drug conjugates: A comprehensive review. *Molecular Cancer Research* vol. 18 (2020).
125. Panikar, S. S. *et al.* Nanobodies as efficient drug-carriers: Progress and trends in chemotherapy. *Journal of Controlled Release* vol. 334 (2021).
126. Massa, S. *et al.* Site-specific labeling of cysteine-tagged camelid single-domain antibody-fragments for use in molecular imaging. *Bioconjug. Chem.* **25**, (2014).
127. Mao, H., Hart, S. A., Schink, A. & Pollok, B. A. Sortase-Mediated Protein

- Ligation: A New Method for Protein Engineering. *J. Am. Chem. Soc.* **126**, (2004).
128. Popp, M. W., Antos, J. M., Grotenbreg, G. M., Spooner, E. & Ploegh, H. L. Sortagging: A versatile method for protein labeling. *Nat. Chem. Biol.* **3**, (2007).
129. Mazmanian, S. K., Liu, G., Ton-That, H. & Schneewind, O. Staphylococcus aureus sortase, an enzyme that anchors surface proteins to the cell wall. *Science* (80-.). **285**, (1999).
130. Massa, S. *et al.* Sortase A-mediated site-specific labeling of camelid single-domain antibody-fragments: a versatile strategy for multiple molecular imaging modalities. *Contrast Media Mol. Imaging* **11**, (2016).
131. Möhlmann, S., Mahlert, C., Greven, S., Scholz, P. & Harrenga, A. In vitro Sortagging of an Antibody Fab Fragment: Overcoming Unproductive Reactions of Sortase with Water and Lysine Side Chains. *ChemBioChem* **12**, (2011).
132. Ton-That, H., Mazmanian, S. K., Faull, K. F. & Schneewind, O. Anchoring of Surface Proteins to the Cell Wall of Staphylococcus aureus. *J. Biol. Chem.* **275**, (2000).
133. Guberman, M., Bräutigam, M. & Seeberger, P. H. Automated glycan assembly of Lewis type I and II oligosaccharide antigens. *Chem. Sci.* **10**, 5634–5640 (2019).
134. Lai, C. H., Hahm, H. S., Liang, C. F. & Seeberger, P. H. Automated solid-phase synthesis of oligosaccharides containing sialic acids. *Beilstein J. Org. Chem.* **11**, 617–621 (2015).
135. Werz, D. B., Castagner, B. & Seeberger, P. H. Automated synthesis of the tumor-associated carbohydrate antigens Gb-3 and Globo-H: Incorporation of α -galactosidic linkages. *J. Am. Chem. Soc.* **129**, (2007).
136. Broecker, F. *et al.* Multivalent display of minimal Clostridium difficile glycan epitopes mimics antigenic properties of larger glycans. *Nat. Commun.* **7**, (2016).
137. Wu, X., Ling, C. C. & Bundle, D. R. A new homobifunctional p-nitro phenyl ester

- coupling reagent for the preparation of neoglycoproteins. *Org. Lett.* **6**, (2004).
138. Hamers-Casterman, C. *et al.* Naturally occurring antibodies devoid of light chains. *Nature* **363**, 446–448 (1993).
 139. Laemmli, U. K. Cleavage of Structural Proteins during the Assembly of the Head of Bacteriophage T4. *Nature* **227**, (1970).
 140. Disney, M. D. & Seeberger, P. H. The use of carbohydrate microarrays to study carbohydrate–cell interactions and to detect pathogens. *Chem. Biol.* **11**, (2004).
 141. Khilji, S. K. *et al.* Generation of glycan-specific nanobodies. *Cell Chem. Biol.* **29**, 1–9 (2022).
 142. Fuss, I. J., Kanof, M. E., Smith, P. D. & Zola, H. Isolation of whole mononuclear Cells from peripheral blood and cord blood. *Curr. Protoc. Immunol.* **85**, (2009).
 143. Radfar, A. *et al.* Synchronous culture of Plasmodium falciparum at high parasitemia levels. *Nat. Protoc.* **4**, 1828–1844 (2009).
 144. Heckman, K. L. & Pease, L. R. Gene splicing and mutagenesis by PCR-driven overlap extension. *Nat. Protoc.* **2**, (2007).
 145. Cheng, X., Zhu, T., Hong, H., Zhou, Z. & Wu, Z. Sortase A-mediated on-resin peptide cleavage and: In situ ligation: An efficient one-pot strategy for the synthesis of functional peptides and proteins. *Org. Chem. Front.* **4**, (2017).
 146. Hellmund, K. S. *et al.* Functionalized peptide hydrogels as tunable extracellular matrix mimics for biological applications. *Pept. Sci.* **113**, 1–13 (2021).
 147. Fabricius, V., Lefèbre, J., Geertsema, H., Marino, S. F. & Ewers, H. Rapid and efficient C-terminal labeling of nanobodies for DNA-PAINT. *J. Phys. D. Appl. Phys.* **51**, 474005 (2018).
 148. Varki, A. *et al.* Symbol nomenclature for graphical representations of glycans. *Glycobiology* **25**, (2015).

149. Sun, X., Stefanetti, G., Berti, F. & Kasper, D. L. Polysaccharide structure dictates mechanism of adaptive immune response to glycoconjugate vaccines. *Proc. Natl. Acad. Sci.* **116**, (2019).
150. Jegatheeswaran, S. *et al.* Recognition of dimeric lewis X by anti-dimeric LeX antibody SH2. *Vaccines* **8**, (2020).
151. Merle, N. S., Church, S. E., Fremeaux-Bacchi, V. & Roumenina, L. T. Complement system part I - molecular mechanisms of activation and regulation. *Frontiers in Immunology* vol. 6 (2015).
152. Sianturi, J. *et al.* Development of α -Gal–Antibody Conjugates to Increase Immune Response by Recruiting Natural Antibodies. *Angewandte Chemie - International Edition* vol. 58 4526–4530 (2019).
153. Motley, A., Bright, N. A., Seaman, M. N. J. & Robinson, M. S. Clathrin-mediated endocytosis in AP-2-depleted cells. *J. Cell Biol.* **162**, (2003).
154. Beck, A., Goetsch, L., Dumontet, C. & Corvaia, N. Strategies and challenges for the next generation of antibody-drug conjugates. *Nature Reviews Drug Discovery* vol. 16 (2017).
155. Li, D. *et al.* DCDT2980S, an anti-CD22-monomethyl auristatin E antibody-drug conjugate, is a potential treatment for non-hodgkin lymphoma. *Mol. Cancer Ther.* **12**, (2013).
156. Doronina, S. O. *et al.* Development of potent monoclonal antibody auristatin conjugates for cancer therapy. *Nat. Biotechnol.* **21**, (2003).
157. Wu, T. *et al.* Clustered nanobody-drug conjugates for targeted cancer therapy. *Chem. Commun.* **56**, 9344–9347 (2020).
158. Huang, H. *et al.* Modular design of nanobody-drug conjugates for targeted-delivery of platinum anticancer drugs with an MRI contrast agent. *Chem. Commun.* **55**, 5175–5178 (2019).

159. Sanders, P. R. *et al.* Distinct protein classes including novel merozoite surface antigens in raft-like membranes of *Plasmodium falciparum*. *J. Biol. Chem.* **280**, (2005).
160. Michon, P., Stevens, J. R., Kaneko, O. & Adams, J. H. Evolutionary relationships of conserved cysteine-rich motifs in adhesive molecules of malaria parasites. *Mol. Biol. Evol.* **19**, (2002).
161. Thompson, J. *et al.* Plasmodium cysteine repeat modular proteins 1-4: Complex proteins with roles throughout the malaria parasite life cycle. *Cell. Microbiol.* **9**, (2007).
162. Ishino, T., Chinzei, Y. & Yuda, M. Two proteins with 6-cys motifs are required for malarial parasites to commit to infection of the hepatocyte. *Mol. Microbiol.* **58**, (2005).
163. Murray, P. J. & Spithill, T. W. Variants of a *Leishmania* surface antigen derived from a multigenic family. *J. Biol. Chem.* **266**, (1991).
164. Devault, A. & Bãuls, A. L. The promastigote surface antigen gene family of the *Leishmania* parasite: Differential evolution by positive selection and recombination. *BMC Evol. Biol.* **8**, (2008).
165. Su, X. zhuan *et al.* The large diverse gene family var encodes proteins involved in cytoadherence and antigenic variation of plasmodium falciparum-infected erythrocytes. *Cell* **82**, (1995).
166. Mandal, G. *et al.* Increased levels of thiols protect antimony unresponsive *Leishmania donovani* field isolates against reactive oxygen species generated by trivalent antimony. *Parasitology* **134**, 1679–1687 (2007).
167. Das, S. *et al.* Over-expression of cysteine leucine rich protein is related to SAG resistance in clinical isolates of *leishmania donovani*. *PLoS Negl. Trop. Dis.* **9**, (2015).

6. Scientific Publications

1. Goerdeler F, Reuber EE, Lühle J, Lechnitz S, Freitag A, Nedielkov R, Möller HM, Seeberger PH, Moscovitz O. *Thiol-mediated Uptake of a Cysteine-containing Nanobody for Anti-Cancer Drug Delivery*. Preprint available on bioRxiv (2022). [doi:10.1101/2022.07.12.497993](https://doi.org/10.1101/2022.07.12.497993)
2. Khilji SK*, Goerdeler F*, Frensemeier K, Warschkau D, Lühle J, Fandi Z, Schirmeister F, Chen ZA, Turak O, Mallagaray A, Boerno S, Timmermann B, Rappsilber J, Seeberger PH, Moscovitz O. *Generation of glycan-specific nanobodies*. Cell Chem. Biol. **29** (2022). [doi:10.1016/j.chembiol.2022.05.007](https://doi.org/10.1016/j.chembiol.2022.05.007)
(*equal contribution)
3. Midha A, Goyette-Desjardins G, Goerdeler F, Moscovitz O, Seeberger PH, Tedin K, Bertzbach LD, Lepenies B, Hartmann S. *Lectin-Mediated Bacterial Modulation by the Intestinal Nematode *Ascaris suum**. Int. J. Mol. Sci. **22** (2021). [doi:10.3390/ijms22168739](https://doi.org/10.3390/ijms22168739)
4. Goerdeler F, Seeberger PH, Moscovitz O. *Unveiling the Sugary Secrets of *Plasmodium Parasites**. Front. Microbiol. **12** (2021). [doi:10.3389/fmicb.2021.712538](https://doi.org/10.3389/fmicb.2021.712538)
5. Varela-Aramburu S, Ghosh C, Goerdeler F, Priegue P, Moscovitz O, Seeberger PH. *Targeting and inhibiting *Plasmodium falciparum* using ultra-small gold nanoparticles*. ACS Appl. Mater. Interfaces **12** (2020). [doi:10.1021/acsami.0c09075](https://doi.org/10.1021/acsami.0c09075)
6. Budde S, Goerdeler F, Floß J, Kreitmeier P, Hicks EF, Moscovitz O, Seeberger PH, Davies HML, Reiser O. *Visible-light mediated oxidative ring expansion of anellated cyclopropanes to fused endoperoxides with antimalarial activity*. Org. Chem. Front. **7** (2020). [doi:10.1039/d0qo00168f](https://doi.org/10.1039/d0qo00168f)

7. Scientific Conferences and Prizes

Conferences

1. GIF-Leibniz Young Scientists' Meeting *Post Corona: Smart photonic and molecular technologies to combat infectious diseases*. Ma'ale HaHamisha, Israel, 2022 (oral presentation).
2. Biomolecular Systems Symposium of the Max Planck Institute of Colloids and Interfaces. Ringberg, Germany, 2021 (oral presentation).
3. Conference *Nanobodies*. Virtual, 2021 (poster).
4. Conference *29th Annual Meeting of the German Society for Parasitology*. Virtual, 2021 (poster).
5. Conference *Antibody Engineering and Therapeutics*. Virtual, 2020 (oral presentation + poster).

Prizes

1. Mobility grant for the GIF-Leibniz Young Scientists' Meeting *Post Corona: Smart photonic and molecular technologies to combat infectious diseases*. Ma'ale HaHamisha, Israel, 2022.
2. Best poster award by The Antibody Society at the conference *Antibody Engineering and Therapeutics*. Virtual, 2020.

8. Appendix

8.1. Spectroscopic characterization of rhamnose compounds

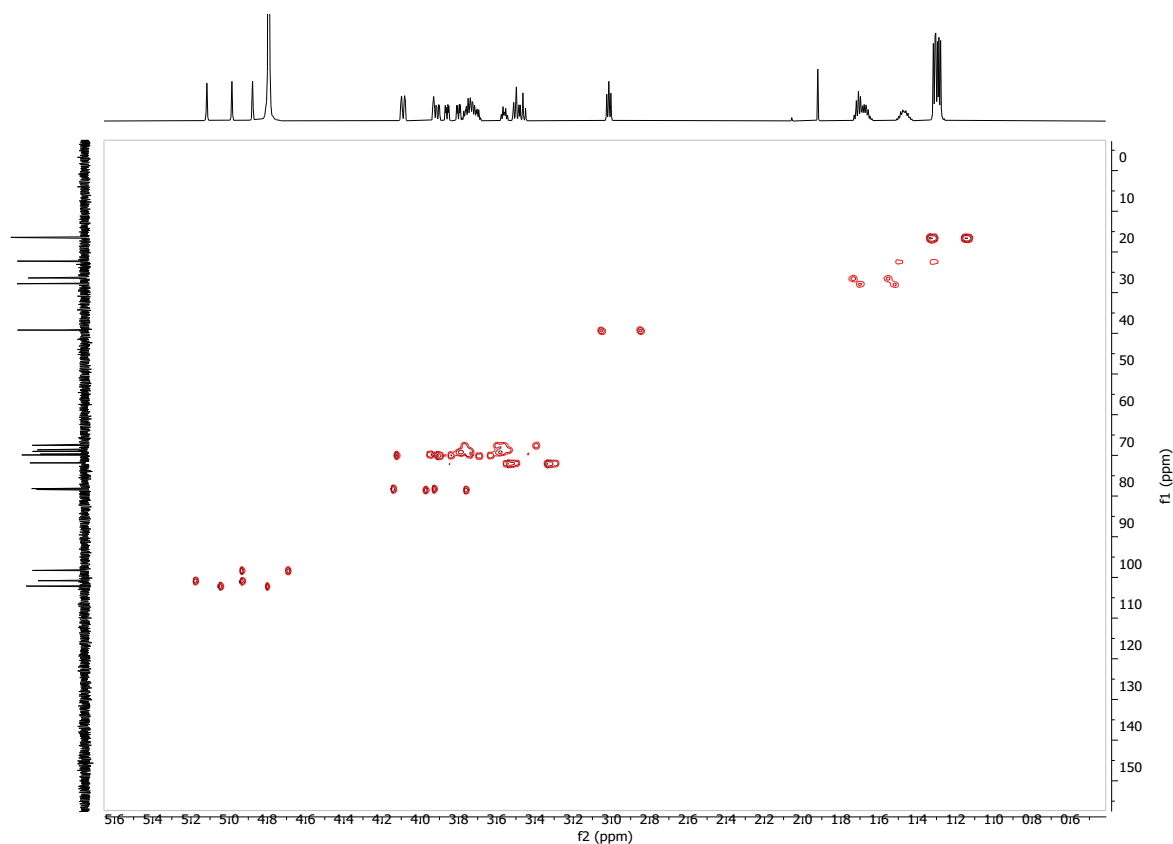


Figure S 1 ^{13}C - ^1H HSQC spectrum of Rha₃. ^1H NMR (700 MHz, D₂O): δ 5.11 (s, 1H), 4.99 (s, 1H), 4.87 (s, 1H), 4.09 (ddd, J = 11.5, 3.4, 1.7 Hz, 2H), 3.95 – 3.83 (m, 3H), 3.82 – 3.67 (m, 5H), 3.56 (dt, J = 10.0, 6.1 Hz, 1H), 3.53 – 3.43 (m, 3H), 3.01 (t, J = 7.6 Hz, 2H), 1.76 – 1.61 (m, 4H), 1.52 – 1.41 (m, 2H), 1.31 (d, J = 6.3 Hz, 3H), 1.30 (d, J = 6.2 Hz, 3H), 1.28 (d, J = 6.2 Hz, 3H) ppm. ^{13}C NMR (176 MHz, D₂O): δ 102.2, 100.9, 98.4, 78.5, 78.3, 72.1, 72.1, 72.0, 70.2, 70.1, 70.0, 69.8, 69.3, 69.2, 68.8, 67.7, 39.4, 28.0, 26.6, 22.5, 16.7, 16.6, 16.6 ppm. HRMS (QToF): Calcd for C₂₃H₄₄NO₁₃ [M + H]⁺ 542.2807; found 542.2813. Spectrum provided by Sabrina Lechnitz.

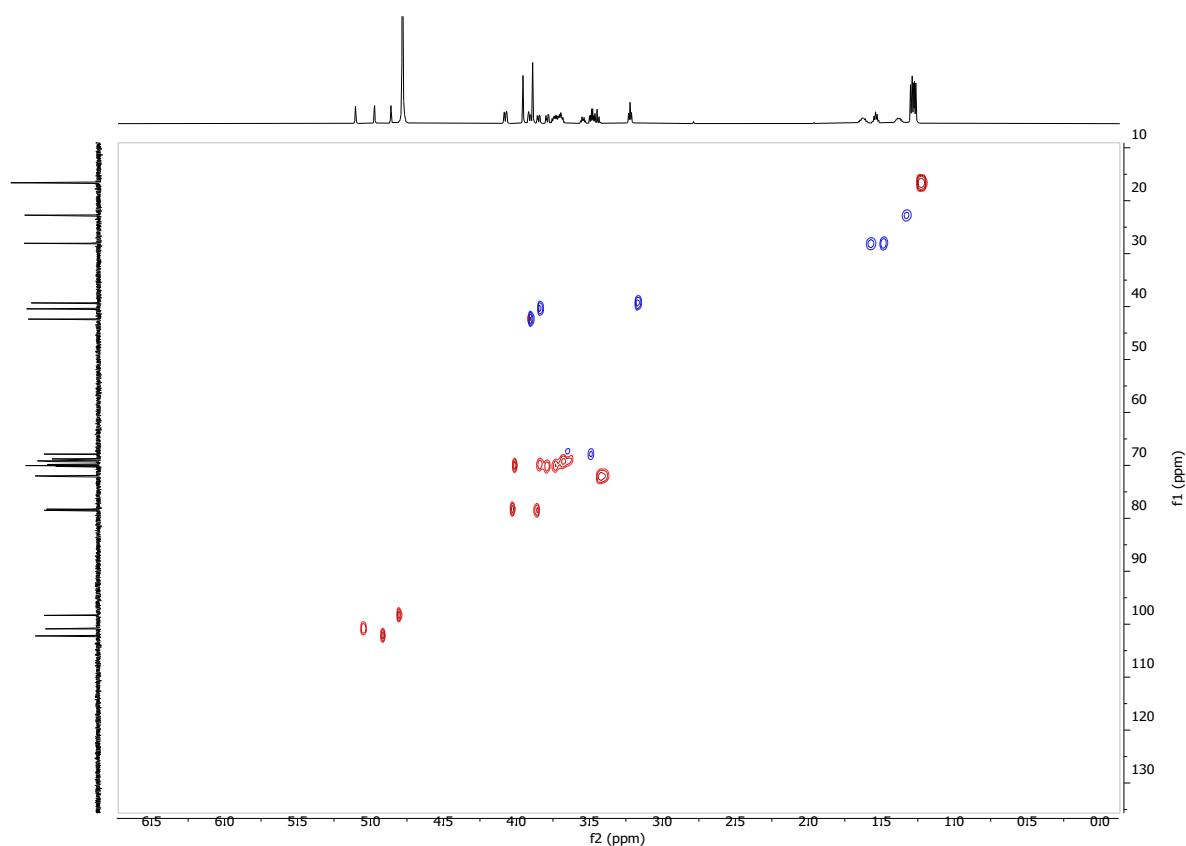


Figure S 2 ^{13}C - ^1H HSQC spectrum of GG-Rha₃. ^1H NMR (700 MHz, D₂O): δ 5.11 (d, J = 1.9 Hz, 1H), 4.98 (d, J = 1.9 Hz, 1H), 4.87 (d, J = 1.8 Hz, 1H), 4.09 (ddd, J = 10.5, 3.4, 1.8 Hz, 2H), 3.96 (s, 2H), 3.94 – 3.91 (m, 2H), 3.90 (s, 2H), 3.86 (dd, J = 9.7, 3.4 Hz, 1H), 3.80 (dd, J = 9.8, 3.3 Hz, 1H), 3.77 – 3.67 (m, 4H), 3.55 (dt, J = 9.9, 6.1 Hz, 1H), 3.52 – 3.41 (m, 3H), 3.23 (t, J = 7.0 Hz, 2H), 1.69 – 1.58 (m, 2H), 1.58 – 1.50 (m, 2H), 1.44 – 1.35 (m, 2H), 1.30 (d, J = 6.2 Hz, 3H), 1.29 (d, J = 6.2 Hz, 3H), 1.28 (d, J = 6.2 Hz, 3H) ppm. ^{13}C NMR (176 MHz, D₂O): δ 169.0, 167.7, 102.2, 100.9, 98.3, 78.5, 78.3, 72.1, 72.1, 72.0, 70.2, 70.0, 70.0, 69.8, 69.3, 69.2, 68.8, 67.9, 42.4, 40.4, 39.3, 28.1, 28.1, 22.7, 16.7, 16.6, 16.6 ppm. **HRMS** (QToF): Calcd for C₂₇H₅₀N₃O₁₅ [M + H]⁺ 656.3236; found 656.3261. Spectrum provided by Sabrina Lechnitz.

8.2. Biochemical characterization of CB2 and ^{C105S}CB2

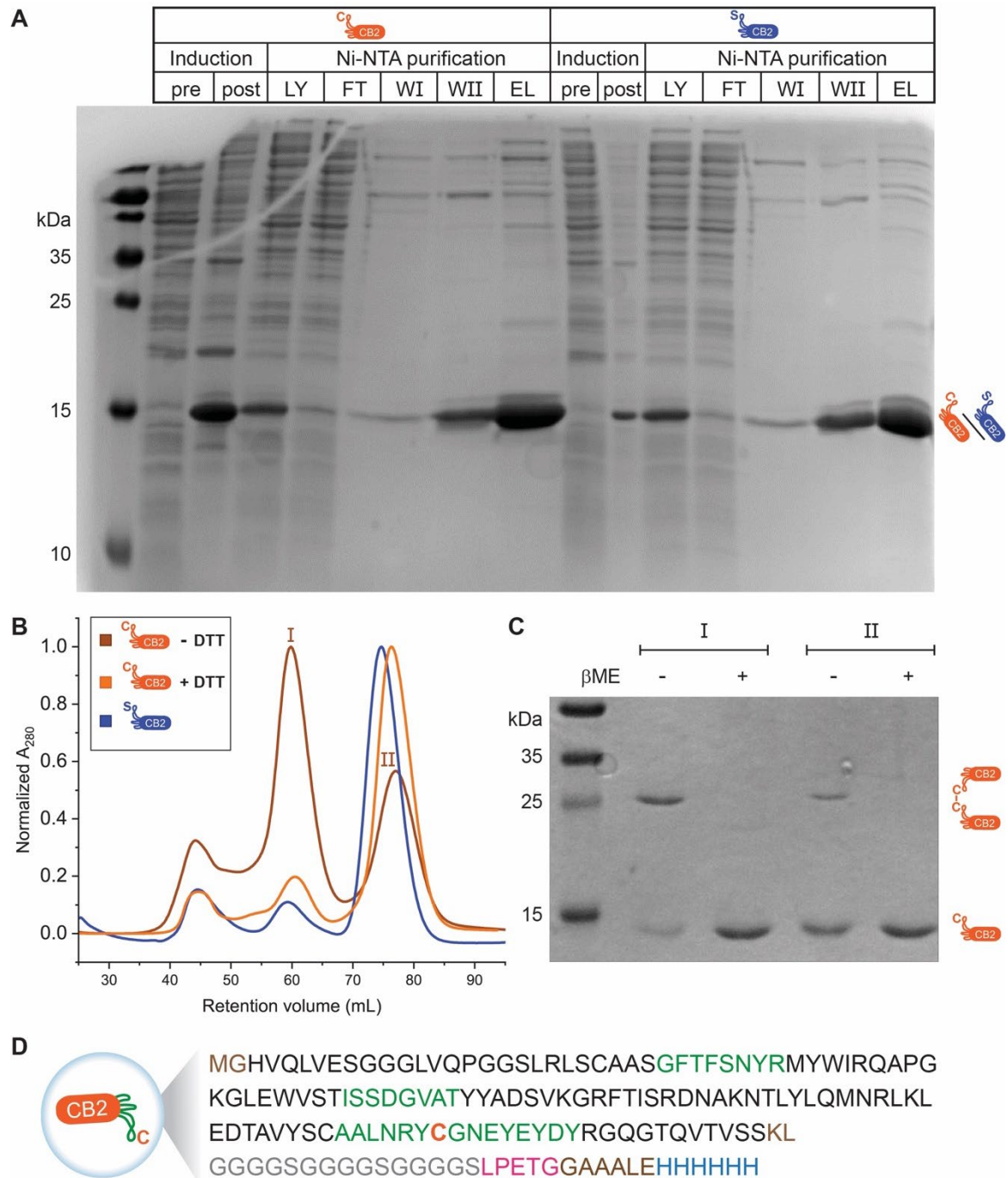


Figure S 3 Purification of CB2 and ^{C105S}CB2. **(A)** Protein expression and Ni-NTA affinity chromatography were monitored by reducing SDS-PAGE. LY = lysate, FT = flow-through, WI = first wash, WII = second wash, EL = eluate. The most intense band corresponds to the Nb. **(B)** Remaining contaminants were removed by SEC. Notably, when purifying CB2 in the absence of DTT (brown curve), a substantial part of the protein is present as dimers (peak I). When 0.75 mM DTT is present during purification, almost all CB2 is monomeric (peak II). **(C)** Dimer formation was confirmed by

SDS-PAGE (performed by Jost Lühle). 5 μg protein from each of the two peaks from (B) were treated with 60 mM β -mercaptoethanol (β ME) or PBS for 1.5 h at 37 $^{\circ}\text{C}$. Note that β ME leads to a complete reduction of dimers to monomers. **(D)** CB2 amino acid sequence. Black: FRs, green: CDRs, orange: cysteine 105, brown: translated restriction sites for cloning, grey: glycine-serine linker, pink: sortag, blue: 6xHis-tag.

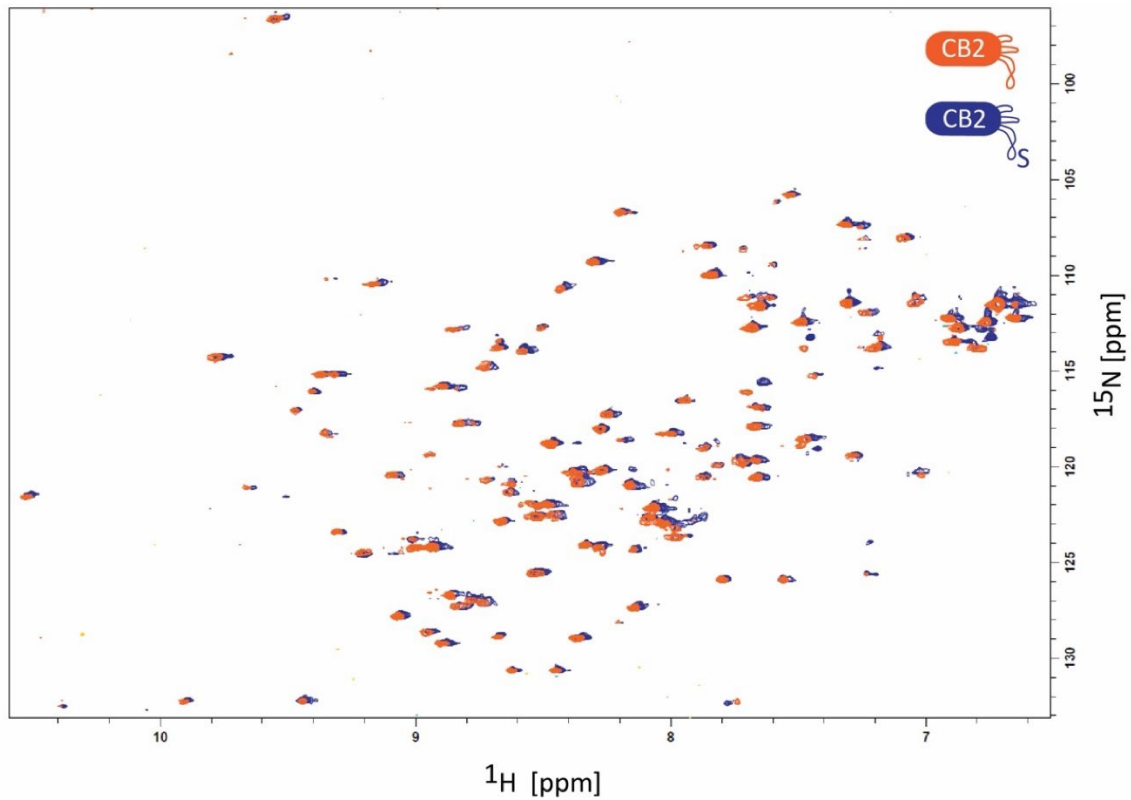


Figure S 4 Comparison of ^{15}N - ^1H HSQC spectra of CB2 and $\text{C}^{105\text{S}}$ CB2. Orange: CB2, blue: $\text{C}^{105\text{S}}$ CB2. Note that only minimal differences in chemical shifts are detected between the two spectra. Spectra provided by Anika Freitag and Dr. Ruslan Nediolkov.

8.4. Control experiments for CB2 conjugation to Rha₃ and Rha-thFF03

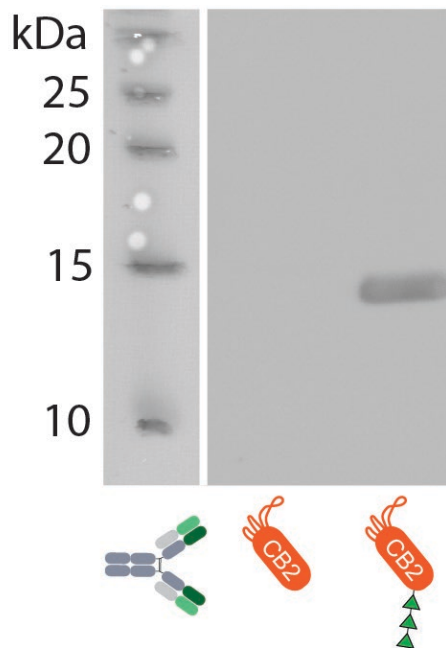


Figure S 5 Western blot of CB2 and CB2-Rha₃ with Abs from human serum. Human Abs were detected with anti-human IgG HRP (1:2000). Note that CB2-Rha₃ is reliably recognized by human Abs while unconjugated CB2 is not.

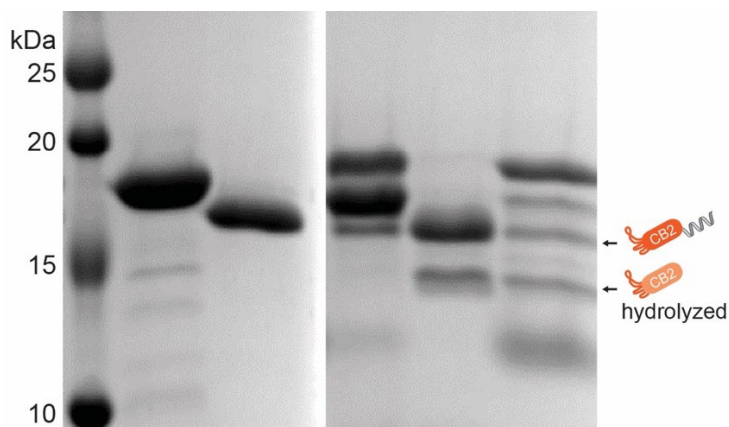


Figure S 6 Conjugation of CB2 and non-rhamnosylated thFF03. SDS-PAGE was used to monitor the conjugation reaction and Ni-NTA affinity chromatography with fractions S = supernatant, E = eluate. Note that less hydrolyzed CB2 is formed than for the conjugation reaction with Rha-thFF03.

				S	E
CB2	X		X	X	X
SrtA		X	X	X	X
thFF03			X	X	X
Time	0 min			30 min	

8.5. Purification of human Abs

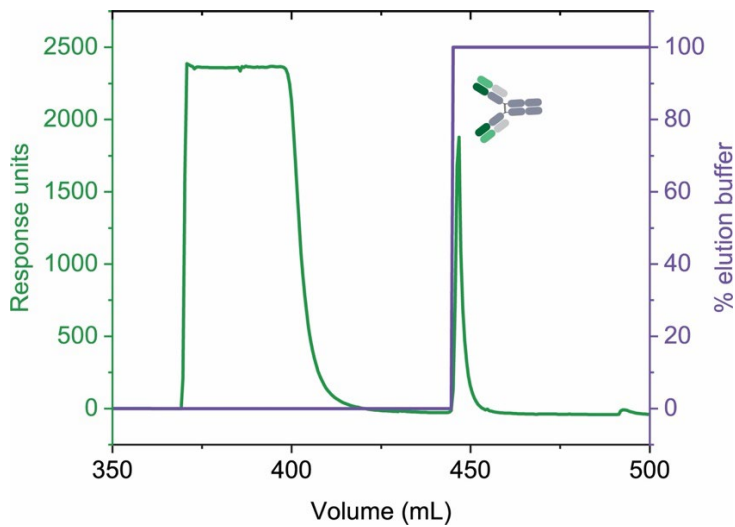


Figure S 7 Ab purification from human serum. Chromatogram of Protein A/G affinity purification. Y axis (green): A_{280} , Y axis (purple): % elution buffer, X axis: retention volume (mL). Non-Ab serum components are not retained on the column and directly flow through. Abs elute in the second peak at the low pH of the elution buffer.

8.6. Control experiment for endocytosis inhibition

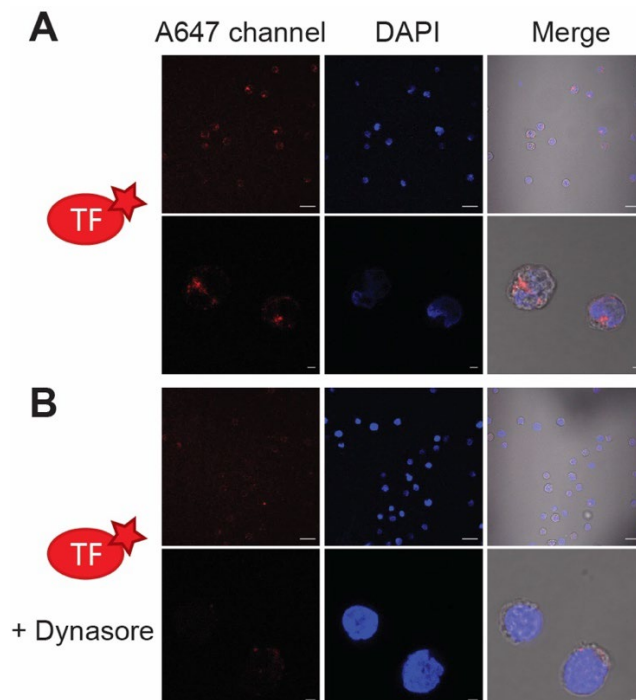


Figure S 8 Inhibition of transferrin endocytosis. Uptake of transferrin-Alexa647 was examined by confocal microscopy (A) in the absence and (B) presence of clathrin-mediated endocytosis inhibitor dynasore. Red: Alexa647, blue: DAPI, greyscale: transmission light. Upper row: zoom-out, scale bar = 10 μm . Lower row: zoom-in, scale bar = 2 μm .